Chemical and physical drivers of the evolution of organic aerosols over forests

Ruud H. H. Janssen

Thesis committee

Thesis supervisor

Prof. dr. P. Kabat

Director/CEO, International Institute for Applied Systems Analysis, Laxenburg, Austria
Professor of Earth System Science, Wageningen University

Thesis co-supervisors

Dr. J. Vilà-Guerau de Arellano

Associate professor, Meteorology and Air Quality Group
Wageningen University

Dr. L. N. Ganzeveld

Assistant professor, Earth System Science Group
Wageningen University

Other members

Prof. dr. M. Kulmala, University of Helsinki, Helsinki, Finland
Prof. dr. J. Lelieveld, Max-Planck-Institute for Chemistry, Mainz, Germany
Prof. dr. T. Röckmann, Utrecht University
Prof. dr. M. Scheffer, Wageningen University

This research was conducted under the auspices of the SENSE Research School

Chemical and physical drivers of the evolution of organic aerosols over forests

Ruud H. H. Janssen

Thesis
submitted in fulfilment of the requirements for the degree of doctor
at Wageningen University
by the authority of the Rector Magnificus
Prof. dr. M.J. Kropff,
in the presence of the
Thesis Committee appointed by the Academic Board
to be defended in public
on Friday 1 March 2013
at 1:30 p.m. in the Aula.

Ruud H. H. Janssen
Chemical and physical drivers of the evolution of organic aerosols over forests
152 pages

Thesis, Wageningen University, Wageningen, NL (2013)
With references, with summaries in Dutch and English

ISBN 978-94-6173-510-2

Contents

1 Introduction **9**

1.1 Research definition and context 9
1.2 Research strategy 11
1.3 Concepts and state of the art 13
1.3.1 Biogenic secondary organic aerosols 14
1.3.2 Diurnal dynamics of the boundary layer 16
1.4 Outline of this thesis 17

2 Physics and chemistry of the modeling system MXLCH-SOA **19**

2.1 The coupled system 19
2.2 Governing equations for the heat budget 20
2.3 Governing equations for the moisture budget 22
2.4 Governing equations for chemical species 25
2.5 SOA formation: gas/particle partitioning 26

3 Combined effects of surface conditions, boundary layer dynamics and chemistry on diurnal SOA evolution **31**

3.1 Introduction 32
3.2 Methods 34
3.2.1 Dynamics of the boundary layer: mixed layer approach 34
3.2.2 Gas-phase chemistry 35
3.2.3 Organic aerosol formation: gas/particle partitioning 37
3.2.4 Observational evaluation: case study 38
3.2.5 Numerical strategy 40
3.3 Results 41
3.3.1 Model evaluation 41
3.3.2 Diurnal evolution of organic aerosol 44
3.3.3 Budgets 47
3.3.4 Sensitivity analysis 49

3.4 Conclusions 55

4 Influence of meteorological forcings and isoprene chemistry on the organic aerosol budget in a tropical forest 59
4.1 Introduction 60
4.2 Methods 63
4.2.1 Observations of the diurnal variability during OP3 63
4.2.2 Description of MXLCH-SOA 66
4.2.3 Initialization of MXLCH-SOA 68
4.2.4 Numerical experiments 70
4.3 Interpretation of observations by modeling 73
4.4 Budget analysis of VOCs, SVOCs and OA 77
4.5 Sensitivity analyses 81
4.5.1 Large scale meteorological forcings 81
4.5.2 OH recycling 82
4.5.3 SOA formation from MPAN: effect of NO_2/NO ratio 83
4.5.4 SOA formation from IEPOX 84
4.6 Conclusions 86

5 Estimating seasonal variations in cloud droplet number concentration over the boreal forest from satellite observations 89
5.1 Introduction 90
5.2 Data and methods 92
5.2.1 Satellite data selection 92
5.2.2 Ground-based measurements 94
5.2.3 Cloud model 94
5.2.4 Uncertainty analysis 96
5.3 Results 100
5.3.1 Seasonal cycle in $N_{\mathbf{CD}}$ 100
5.3.2 Relation to surface aerosol concentrations and meteorology 101
5.4 Discussion and conclusions 107

6 Conclusions 111
6.1 Diurnal evolution of organic aerosol over boreal and tropical forests 111
6.2 Satellite observations of cloud droplet concentration over the boreal forest . . 114

7 Synthesis and outlook 115
7.1 From aerosol mass to number concentration 116
7.2 Macrophysics of cloud formation 119

7.3 Outlook 120

References **123**

Samenvatting **143**

Dankwoord / Acknowledgments **145**

List of journal publications **149**

SENSE certificate **151**

1 Introduction

1.1 Research definition and context

This thesis deals with the formation of secondary organic aerosols from biogenic emissions in boreal and tropical forests, their evolution in the atmosphere and how they may influence clouds by acting as condensation nuclei. This topic is related to one of the fundamental issues in climate science: how the interaction of the biosphere with the physical and chemical components of the earth system regulates the climate. Many links between biosphere and atmosphere have been investigated, mainly focusing on the energy, water and carbon cycles. Lately, there has been a growing interest in the role of the terrestrial biosphere in modulating climate by its effect on atmospheric chemistry, as reviewed by Arneth et al. (2010), and several feedback mechanisms involving aerosols formed from the volatile organic compounds (VOCs) emitted by vegetation have been proposed. Kulmala et al. (2004a) suggested, based on observations made in the boreal forest, a coupling between forests and the climate by the production of organic aerosols which may directly or indirectly (through clouds) affect the surface energy balance, which in turn feeds back on vegetation growth and VOC emissions. More in general, Barth et al. (2005) hypothesized on the existence of feedbacks linking emissions from vegetation with the hydrological cycle through the formation of aerosols and their impact on clouds. For the tropical forest, Pöschl et al. (2010) proposed that biogenic aerosols

are important to sustain the hydrological cycle by their influence on clouds and precipitation, which in turn drives biological activity and emissions thereby stabilizing the Amazonian rain forest ecosystem.

The fact that the proposed mechanisms mainly concern boreal and tropical forests has a reason: they are both ecosystems that are characterized by high emissions of biogenic VOCs and are both environments that experience relatively little anthropogenic pollution and cover large regions of the earth. Therefore, these ecosystems are the most appropriate ones for studying the biogenic pathways leading to aerosol formation with likely a significant impact on the climate. It should be noted, however, that there are several mechanisms by which anthropogenic emissions enhance the formation of secondary organic aerosol (SOA) from biogenic emissions (Hoyle et al., 2010) and that even the most remote rain forest shows signs of human pollution aerosols (Andreae, 2007).

Conceptually, the proposed feedback mechanisms may be clear, but the level of understanding of the underlying processes is low (Barth et al., 2005; Stevens and Feingold, 2009; Riipinen et al., 2012). Before the influence of these interactions on the climate system can be quantified, a fundamental understanding of the underlying physical, chemical and biological processes, how they interact with each other and on which temporal and spatial scales is needed. Especially when the typical time scales on which biochemical and physical processes act are similar, it is necessary to study them as an integrated system. Relevant in this research is, for example, the fact that the time scales of the emission and oxidation of VOCs and the formation of SOA are similar as those of the atmospheric boundary layer (BL) dynamics (Karl et al., 2007; Vilà-Guerau de Arellano et al., 2011). These processes have typical time scales of minutes to hours and their interactions should therefore be studied on the diurnal time scale. Another important argument to study these interactions on diurnal time scales is that the diurnal tendencies of certain variables can be used to gain understanding of the processes that drive them. For instance, the growth of the boundary layer in the morning or photochemistry peaking around noon cause typical patterns in the diurnal evolution of boundary layer dynamics and chemistry. Understanding the coupling between these physical and chemical processes is an essential first step to scale up from diurnal to longer time scales since it gives insight in which processes operating at short time scales deserve most consideration in studies over longer time scales. In the first part of this thesis I therefore study the diurnal cycle of the coupled land surface - VOC chemistry - boundary layer dynamics system in case studies for both a boreal and a tropical forest based on local scale observations.

While the diurnal time scale is useful to gain process understanding, the effect of a certain mechanism should be evaluated at longer time scales and larger spatial scales to eventually assess its climatic significance. Therefore, the second part of this thesis is a first step in this direction as I study the effects of the boreal forest on cloud properties through aerosol formation on seasonal time scale and regional spatial scale.

In summary, I focus on how forests drive organic aerosol production and its evolution in the atmosphere. To this end, I combine two fundamental aspects of biosphere-atmosphere interaction: aerosol formation from organic vapors and surface energy budget partitioning, which drives the dynamics of the boundary layer and cloud formation. In addition, I will also evaluate the influence of large-scale meteorological forcings on the observed phenomena, since the forest - aerosol - boundary layer dynamics system is not a closed system.

In view of the complexity and the multi-disciplinary and multi-scale character of the subject, I have defined the following research questions:

- What are the contributions of land surface and large-scale meteorological forcings and boundary layer processes to the organic aerosol budget over boreal and tropical forests?
- Are recently discovered pathways of isoprene chemistry the key to closing the gap between measured and modeled organic aerosol concentrations in tropical forests?
- How do aerosols and meteorological factors influence cloud droplet number concentration over the boreal forest?

1.2 Research strategy

We design a methodology that enables us to break down the complexity of the forest - aerosol - boundary layer dynamics system. The system that we study and the tools that we use to this end are shown in Fig. 1.1. It includes the development of our model in Chapter 2, the formation and diurnal evolution of SOA in a boreal and a tropical forest as described in Chapters 3 and 4, respectively, and the use of satellite observations to infer cloud droplet number concentration over the boreal forest in Chapter 5.

In order to answer the first two research questions, we combine measurements and modeling of the coupled land surface - VOC chemistry - boundary layer (BL) dynamics system. This system has many degrees of freedom, due to the complexity of atmospheric flows and chemistry. The former is due to land-atmosphere interactions and the turbulent character of the BL and the latter due to the many compounds involved at low concentrations, especially in the organic chemistry involved in SOA formation. In our research strategy, we therefore seek for a balanced approach in which the complexity of the representation of physical and chemical processes is kept to a minimum, while keeping enough realism in the model to reproduce the main interactions among the processes. We have put special effort in guiding and constraining our numerical experiments by complete data sets in terms of surface characteristics, boundary layer dynamics and chemistry. In this way, we aim to keep the model

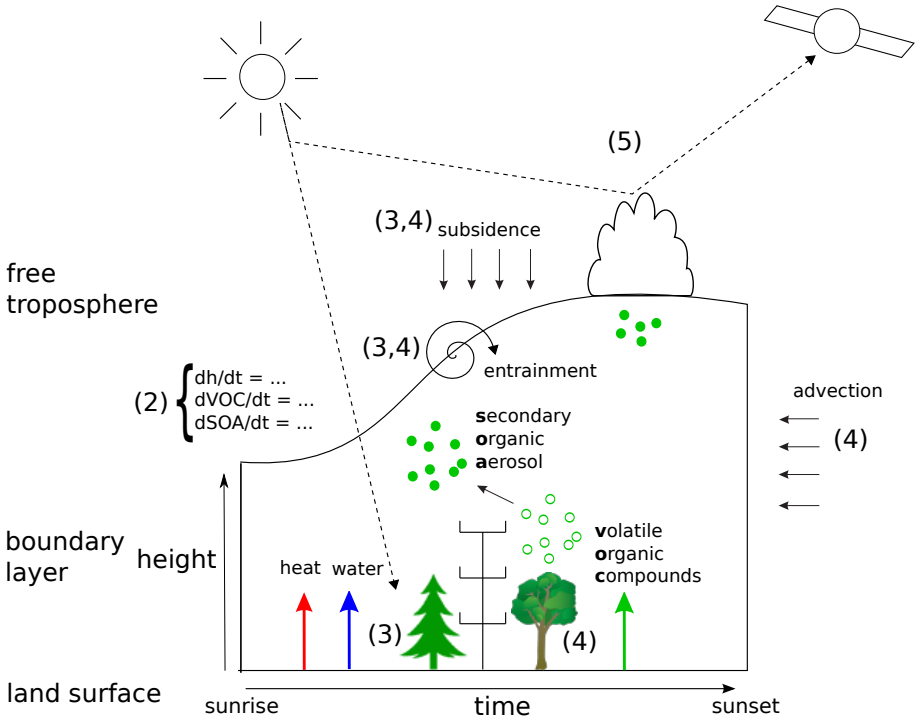

Figure 1.1: Conceptual representation of the main studied processes in the boreal and tropical forest and the modeling and observational methods with which they are studied. The numbers indicate the chapters of this thesis in which the different aspects are treated.

comprehensible while at the same time assuring that we are representing the essentials of the system that we are studying.

To study the diurnal variability, we develop a model in which the essentials of the dynamics of a convective BL during day time are coupled with a chemical mechanism that represents the main chemical pathways through which biogenic VOCs are oxidized and with a module for calculating the gas/particle partitioning of the VOC oxidation products. The vegetated land surface is not an interactive part of the model. Instead, we have prescribed its impact on diurnal time scales by applying surface heat fluxes and VOC emission fluxes as constrained by observations. In addition, all other relevant emission and deposition terms of reactive species are prescribed.

Our model allows us to dissect the total tendency of chemical species like VOCs and SOA into the contributions of the individual processes that drive their evolution during the day. In this way we can quantify the dominant processes at diurnal time scales, which can guide upscaling to longer time scales. In turn, BL dynamics are driven by the underlying

land surface and the free troposphere on top of it, which connects it to regional and global scale meteorological phenomena. This may be important in interpreting the observations. Moreover, by confronting our model with data, we are able to identify if processes are missing in the description of an observed phenomenon. In the field of atmospheric chemistry, new pathways in both gas-phase and aerosol phase chemistry that drive SOA formation are being discovered in laboratory or smog chamber studies. Our modeling approach combined with a complete data set allows for the evaluation of these new mechanisms under atmospheric conditions. Finally, our modeling tool can easily be used for sensitivity analyses, since it is computationally efficient. Scanning the parameter space can give insight in the possible effect of a parameter that is not well constrained by observations or it can give information on which processes are important under specific forcings.

As such, our newly developed modeling system is an efficient tool for interpreting data sets obtained during atmospheric chemistry measurement campaigns. These campaigns are essential to translate the knowledge of fundamental chemical processes as obtained from theoretical and laboratory studies to the atmosphere. Intensive measurement campaigns typically last several weeks and are often comprised of point measurements taken at a single site, occasionally supported by aircraft observations. Fortunately, complete data sets are becoming more available since recent field campaigns in boreal (HUMPPA-COPEC, Williams et al., 2011), tropical (OP3, Hewitt et al., 2010) and temperate (BEACHON-RoMBAS, `http://tinyurl.com/BEACHON-RoMBAS`) forests are starting to include measurements of BL and land surface characteristics as well.

In order to answer the third research question, we employ observations of cloud properties from several years of satellite observations combined with a cloud model to obtain seasonally averaged cloud droplet number concentrations over the boreal forest. The averaging over multiple years assures us that we have a statistically robust data set. These satellite data are supported by point measurements of cloud active aerosol concentrations at the surface and reanalysis data of meteorological fields over the same period.

1.3 Concepts and state of the art

We introduce the key concepts of the subject of this thesis: biogenic secondary organic aerosol and the diurnal dynamics of the atmospheric boundary layer. First, we explain how they are linked and why they should be studied simultaneously.

The formation of SOA from a VOC depends on both its chemical transformation by means of oxidation to a semi-volatile VOC (SVOC) and on the partitioning of the SVOC between the gas and the aerosol phase. For both the former and the latter, meteorological factors are

important. First, dilution in the atmosphere will determine the mixing ratio of VOCs and their oxidants and therewith their reaction rate and, consequently, the amount of oxidation products formed. Besides, the rate of many chemical reactions is temperature and/or moisture dependent. Both variables are characterized by a strong diurnal variability. Second, the semi-volatile character of the first or higher generation oxidation products of biogenic VOCs is essential for understanding meteorological effects on the fraction of the oxidized VOCs that enters the aerosol phase. Its semi-volatile character means that only a fraction of an SVOC will partition into the aerosol phase with the other part remaining in the gas phase (Pankow, 1994; Donahue et al., 2006). The partitioning between gas and aerosol phase depends on the saturation concentration of the SVOC, which in turn depends on the atmospheric temperature due to its effect on the saturation vapor pressure following the Clausius-Clapeyron relation. Further, the gas/particle partitioning depends on the mass concentration of the organic aerosol already present in the atmosphere, hereinafter referred to as the background organic aerosol, which is governed by its dilution in the atmosphere and the exchange with the residual layer/free troposphere on top of the BL. In addition, there is a possible effect of the relative humidity on SOA mass, because water can be taken up in the aerosol. This effect is not treated in this thesis.

To provide the reader with the fundamental concepts, in the following we give a general overview of basic concepts and the state of the art on the formation of biogenic secondary organic aerosols and the diurnal dynamics of the boundary layer.

1.3.1 Biogenic secondary organic aerosols

Aerosols are tiny particles dispersed in gases (Seinfeld and Pandis, 2006). They can be liquid or solid, primary or secondary, the latter meaning that they are formed in the atmosphere from gas-phase precursors. They are important in air quality, weather and climate. This may be due to their direct effect on radiative forcing by scattering incoming solar radiation (Haywood and Boucher, 2000) or indirectly by modulating cloud properties when functioning as cloud condensation nuclei (Twomey, 1977; Albrecht, 1989; Lohmann and Feichter, 2005). The role of organic aerosols, specifically, is likely globally significant, but difficult to assess. They constitute 20-90% of the submicron aerosol mass (Jimenez et al., 2009) and a substantial fraction is of biogenic origin (Spracklen et al., 2011). However, the sources and formation mechanisms of organic aerosols and consequently their effects on air quality and climate are not well understood (Jimenez et al., 2009).

Biogenic SOA originates from the oxidation of biogenic VOCs in the atmosphere (Fuentes et al., 2000; Goldstein and Galbally, 2007). VOCs emitted by natural vegetation are known since decades to play an important role in atmospheric chemistry by regulating oxidant con-

centrations and fueling organic aerosol production (Fehsenfeld et al., 1992). Among the different classes of VOCs emitted by vegetation, isoprene (C_5H_8) and monoterpenes ($C_{10}H_{16}$) are the most abundant (together they account for about 50% of the global emissions (Guenther et al., 1995)) and are the only biogenic VOCs considered in this thesis. Sesquiterpenes ($C_{15}H_{24}$) have high SOA yields upon oxidation (Griffin et al., 1999), but since they are highly reactive and therefore difficult to measure, little is known about their contribution to ambient SOA.

More than 50 years ago, Went (1960) was the first to hypothesize on the aerosol forming potential of monoterpenes (hereinafter referred to as terpenes) and suggested that these aerosols were responsible for the blue haze observed in many forested areas. He also proposed that these particles may directly influence on the surface energy budget by reflecting incoming solar radiation and indirectly by providing condensation nuclei for cloud droplets to form on. Numerous smog chamber studies have confirmed the aerosol-forming potential of terpenes afterwards (e.g. Griffin et al., 1999). The importance of terpene oxidation products in the atmosphere was confirmed by Tunved et al. (2006), who found that they are the main contributor to aerosol mass over the boreal forest.

The oxidation of isoprene, the globally most abundant biogenic VOC (Guenther et al., 1995), on the other hand, has long been considered not to lead to substantial formation of semi-volatile products that may enter the aerosol phase, until Claeys et al. (2004) found tracers of isoprene oxidation products in Amazonian aerosols. The aerosol yields of isoprene were thereafter found to be low (Kroll et al., 2006), but isoprene as SOA precursor was thought to be significant at global scales, due to its high emission flux of an estimated 600 Tg/yr (Guenther et al., 2006). However, the mechanisms leading to isoprene formation are not well understood (Carlton et al., 2009) and isoprene SOA yields are very much dependent on the exact chemical pathways leading to its formation (Surratt et al., 2010). For example, recent experimental studies have indicated that acid seed aerosol (Lin et al., 2012b) and elevated NO_x levels (Chan et al., 2010) lead to unexpected high yields. Moreover, Robinson et al. (2011a) found that isoprene SOA forms a substantial fraction of the organic mass loading in a tropical forest and possibly also in other isoprene dominated environments.

The formation of biogenic SOA starts with the emission of a VOC from a plant. This emission is governed by a combination of biochemical and physical drivers (Guenther et al., 1995; Arneth et al., 2007). At the level of an individual plant, temperature, light intensity and CO_2 concentration are known to be important factors governing the emission on short temporal scales. At ecosystem level, factors like species composition and vegetation productivity become important.

In the atmosphere, VOCs are subject to oxidation by ozone (O_3), the hydroxyl radical (OH) and, during night time, the nitrate radical (NO_3). Reaction with either of these oxidants

results in the addition of polar oxygenated functional groups to the VOC or in the breaking of its carbon skeleton. Since the vapor pressure, or its reciprocal the saturation concentration, of a molecule is determined by both its polarity and size, the change in volatility of the VOC upon oxidation depends on the competition between these two effects (Kroll and Seinfeld, 2008). In general, the first-step oxidation products have lower volatilities than the parent VOC. In that way, oxidation results in the formation of species that have low enough volatilities to be condensable and thus to be present as liquids or solids in aerosols. The distribution of products formed from a specific VOC, and therewith the amount of SOA formed from the specific precursor, depends on environmental conditions, such as the oxidant that initiates the oxidation, NO_x-concentration, temperature and humidity. Oxidized VOCs may undergo further oxygenation in the atmosphere, which can further reduce their volatility and enhance SOA formation (Jimenez et al., 2009). The final fate of all reactive carbon in the atmosphere is either to oxidize down to CO_2 or CO, or to end up in aerosols, which are eventually removed from the atmosphere by dry or wet deposition. In our investigations, we will focus on the first-step oxidation of monoterpenes, several pathways of isoprene oxidation and the resulting aerosol formation.

1.3.2 Diurnal dynamics of the boundary layer

To quantify the importance of meteorological processes on the formation and evolution of SOA, it is necessary to take the diurnal behavior of the BL into account. Here, we focus on a special case (prototype) of the atmospheric boundary layer, the convective boundary layer. This is formed during daytime when the introduction of heat and moisture by the sensible and latent heat fluxes drives atmospheric convection and turbulence, which in turn drive the diurnal cycle in atmospheric chemistry (Fig. 1.1). During day time, the sun heats the land surface. Most of this energy is used to evaporate water from the land surface and to warm the air above it. As an air parcel is warmed and moistened at the surface, it becomes less dense than its environment and therefore rises. These motions are organized in turbulent plumes which move upwards since they have a higher buoyancy (capacity to float) than their surroundings, a process called convection. Their rising motion continues until they reach the top of the BL which is capped by a potential temperature inversion: a sudden increase of the potential temperature over a thin layer of air (typically ten to hundred meter) called the entrainment zone, which marks the transition to the free troposphere (FT). As a consequence of this potential temperature increase, the parcel becomes denser than its environment, will loose its buoyancy and it will start to return to the surface. However, since it has penetrated the warmer layer during its ascent, some warmer (and drier) air has been mixed into the parcel, in a process called entrainment, so when the parcel sinks back towards the surface it introduces heat into the BL. This process of mixing in warm and dry air from the FT into

the BL causes the latter to grow during day time, since the BL temperature increases which enables the rising parcels to rise higher up and to entrain even more warm air. After sunset the surface heat fluxes are no longer positive, the convective motions are no longer sustained and the convective BL collapses.

The important point for the atmospheric chemistry occurring in the BL is not only that it grows, which increases the mixing volume into which chemical species are emitted and in which they react, but also that in the FT species often have different mixing ratios than in the BL. Consequently, when the parcels entrain air from the FT and sink back into the BL, the concentrations of chemical species is altered, which affects their subsequent chemical transformations. In summary, there are two effects of a growing BL on the chemistry occurring in it: 1) an increased mixing volume and 2) entrainment of air with a different reactant mixing ratio. Both are treated in the simulations with the land surface - VOC chemistry - BL dynamics model.

1.4 Outline of this thesis

The model that I employ to analyze the diurnal evolution of organic aerosol as a function of land surface conditions, meteorology and chemistry is a mixed layer model for the convective boundary layer. It is coupled with a reduced mechanism for the gas-phase chemistry of VOC oxidation and a module for gas/particle partitioning. The basics of the model are described in Chapter 2 and its updates for the individual case studies in further chapters. In Chapter 3, I study the diurnal cycle of organic aerosol and how the land surface drives this diurnal cycle, guided by observations from a boreal forest in Hyytiälä, Finland. Then, I apply it to a case study for a tropical forest at Borneo (Chapter 4). To this end, the model is updated with mechanisms through which SOA from isoprene is formed and the sensitivity of modeled OA concentrations to large-scale meteorological forcings is studied. A step to seasonal time scales is taken in Chapter 5, in which I investigate how the cloud droplet number concentration of clouds over the boreal forest is related to the concentrations of cloud active aerosols in the forest and meteorological factors. Finally, in Chapter 6 the most important findings of this thesis are summarized and in Chapter 7 recommendations for future research on the coupled land surface - VOC chemistry - boundary layer dynamics system are given.

2

Physics and chemistry of the modeling system MXLCH-SOA

2.1 The coupled system

In this chapter, we will introduce the basic equations of MXLCH-SOA, a coupled model of boundary layer dynamics, O_3-NO_x-HO_x-VOC chemistry and SOA formation through gas/particle-partitioning. In short, the mixed-layer (MXL) model for the convective boundary layer (BL) that forms the representation of the BL dynamics was developed by Lilly (1968) and Tennekes (1973). It is based on the assumption that mixing throughout the convective BL is vigorous, and as a result the state variables and atmospheric compounds are constant with height. Consequently, we can describe the evolution of these variables by a slab or mixed-layer value that solely depends on time. It was expanded for use in atmospheric chemistry studies by including a chemical module by Vilà-Guerau de Arellano et al. (2009, 2011). For the work in this thesis, a module for gas/particle-partitioning of semi-volatile organic species (Donahue et al., 2006) has been included.

2.2 Governing equations for the heat budget

The leading role in the structure and evolution of the diurnal BL is played by the potential temperature, which represents the heat budget of the BL. The reason is that the intensity and characteristics of convective turbulence, the main process that drives the convective BL, are strongly dependent on the energy available at the surface, expressed by the sensible heat flux, and the heat exchange between the BL and the free troposphere (FT).

Therefore, we begin with the analysis of the heat budget and which processes and variables are controlling it. We first explain the equations for the potential temperature θ, which is depicted here between brackets as $\langle\theta\rangle$ to indicate mixed-layer values. Subsequently, we show the equations that govern the moisture budget and therewith we complete the set of equations that represent the BL dynamics.

If we consider a horizontally homogeneous dry convective BL, the evolution of the potential temperature is driven by the surface and entrainment sensible heat flux:

$$\frac{\partial\langle\theta\rangle}{\partial t} = \frac{\left(\overline{w'\theta'}\right)_s - \left(\overline{w'\theta'}\right)_e}{h} \tag{2.1}$$

Equation 2.1 is the result of a vertical integration of the 1-dimensional equation of the heat budget and we have assumed that the vertical profile of θ is in quasi-steady state (Lilly, 1968). In this equation, $\overline{w'\theta'}_s$ is the kinematic heat flux at the surface, which is related to the sensible heat flux (H) as: $\overline{w'\theta'}_s = \mathrm{H}/(\rho \cdot c_p)$, with ρ the density of air and c_p the specific heat of air. The entrainment process, represented by $\left(\overline{w'\theta'}\right)_e$, is defined as the process whereby air with heat properties from the FT is mixed in into the mixed layer, and it is therefore related to the θ jump at the inversion. The evolution of $\langle\theta\rangle$ thus equals the input of heat into the BL at the surface and due to entrainment over the BL height h.

When calculating the entrainment flux, we assume that the transition from the BL to the FT, the inversion, is represented by a sharp discontinuity, namely the zero-order jump closure (ZOJ, Tennekes, 1973). ZOJ closure defines this jump as $\Delta\theta = \theta_{FT} - \langle\theta\rangle$ over an infinitely thin inversion layer. In this ZOJ approach, the entrainment flux is the product of the entrainment velocity w_e (defined positive in the upward direction) and the potential temperature jump $\Delta\theta$ at the inversion. The equation for the potential temperature entrainment flux reads:

$$\left(\overline{w'\theta'}\right)_e = -\left(\frac{\partial h}{\partial t} - w_s\right)\Delta\theta = -w_e \cdot \Delta\theta \tag{2.2}$$

In our model, we calculate the subsidence velocity as:

$$w_s = -\omega\, h \tag{2.3}$$

where ω represents the large scale vertical velocity that is a function of the horizontal wind

divergence in s^{-1}, *i.e.* $\omega = -Div\left(\vec{U_h}\right)$; where $\vec{U_h}$ is the horizontal wind. It can be thought of as the fraction with which the BL is pushed down every second, due to large-scale subsiding air motions. Therefore, w_s is per definition negative.

By rewriting Eq. 2.2, we obtain an expression of the boundary layer growth ($\frac{\partial h}{\partial t}$) as a function of the entrainment flux $\left(\overline{w'\theta'}\right)_e$, the potential temperature inversion jump ($\Delta\theta$) and the subsidence velocity (w_s). It reads:

$$\frac{\partial h}{\partial t} = -\frac{\left(\overline{w'\theta'}\right)_e}{\Delta\theta} + w_s = w_e + w_s \tag{2.4}$$

This equation states that the mixed layer grows by entrainment of warm air from the free atmosphere ($w_e > 0$) and that it is opposed by the vertical subsidence velocity ($w_s < 0$) driven by high pressure situations. This growth is limited by the presence of a stably stratified layer defined by a potential temperature jump on top of the convective BL. This jump at the inversion, represented by $\Delta\theta$, changes during the growth of the mixed-layer. Consequently, depending on a positive or negative tendency of $\Delta\theta$, the BL growth increases or decreases.

As Eq. 2.2 shows, the entrainment flux for heat depends on the entrainment velocity and the potential temperature jump at the inversion. It is therefore necessary to obtain a prognostic equation for the potential temperature jump. This equation reads:

$$\frac{\partial \Delta\theta}{\partial t} = \frac{\partial \theta_{FT}}{\partial t} - \frac{\partial \langle\theta\rangle}{\partial t} = \gamma_\theta \left(\frac{\partial h}{\partial t} - w_s\right) - \frac{\partial \langle\theta\rangle}{\partial t} \tag{2.5}$$

where γ_θ is the lapse rate (change with height) of θ in the FT. The final set of equations, which describes the heat budget in the diurnal atmospheric boundary layer, is therefore composed by Eqs. 2.1, 2.4 and 2.5. The three prognostic variables are $\langle\theta\rangle$, $\Delta\theta$ and h.

In this set of equations, four variables still remain as unknowns. The surface heat flux $\left(\overline{w'\theta'}\right)_s$ is the result of land-atmosphere interactions, but here we prescribe it according to observations. The external variables w_s and γ_θ represent the influence of the free tropospheric conditions on the BL development and their values are imposed on the mixed-layer model. Finally, the entrainment heat flux $\left(\overline{w'\theta'}\right)_e$ remains. Here, we assume an important closure and we relate the entrainment flux to the surface heat flux as:

$$\left(\overline{w'\theta'}\right)_e = -\beta\left(\overline{w'\theta'}\right)_s \tag{2.6}$$

where the coefficient β can be imposed as a constant or as a parameter depending on the thermodynamic characteristics at the inversion, for instance the presence of shear. In our research, we assume a value of β equal to 0.2 which physically means that 20% of the heat contribution to the diurnal boundary layer is due to the entrainment of heat at the inversion layer. The potential temperature is normally underestimated if this contribution is neglected.

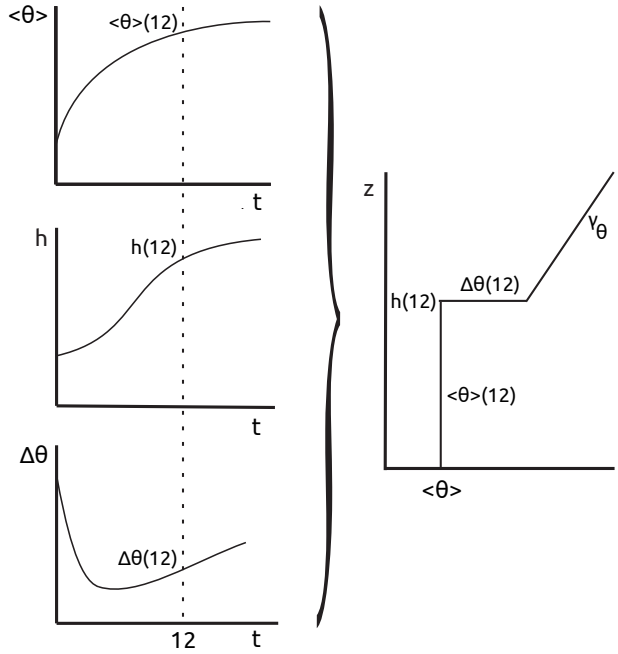

Figure 2.1: Construction of the vertical profile of potential temperature from the evolution of the mixed-layer potential temperature ($\langle\theta\rangle$), the BL height (h) and the potential temperature jump across the BL-FT interface ($\Delta\theta$). It is particularized at 12 local time.

As we will show later on when introducing the moisture budget, Eq. 2.6 needs to be modified to make entrainment depending on the buoyancy flux.

An illustration of a typical diurnal evolution of $\langle\theta\rangle$, h and $\Delta\theta$ in the mixed-layer model and how a vertical profile of θ can be constructed from these evolutions is shown in Fig. 2.1. It shows that the BL is represented by a bulk value of θ and capped by a infinitesimally thin layer over which θ strongly increases, represented by $\Delta\theta$. Above this inversion layer lies the free troposphere, which is characterized by a θ, which increases with height.

2.3 Governing equations for the moisture budget

By adding the moisture budget to the heat budget, we complete the configuration of the thermodynamic variables in the BL. To understand the role of moisture in the BL dynamics, the concept of buoyancy is essential. Buoyancy is the upward force exerted by a denser atmospheric flow on less dense air parcels, or in other words, it is the capacity of an air parcel to float in the surrounding air. In order to calculate it, we have to take the evolution of

both the heat and moisture budget into account, since both determine the density of air. The inclusion of the moisture effects on the dynamics of the BL requires the introduction of two new equations. The first one (similar to Eq. 2.1) is the evolution of the mixed-layer specific humidity $\langle q \rangle$:

$$\frac{\partial \langle q \rangle}{\partial t} = \frac{\left(\overline{w'q'}\right)_s - \left(\overline{w'q'}\right)_e}{h} \tag{2.7}$$

where $\left(\overline{w'q'}\right)_s$ represents the surface specific moisture flux and $\left(\overline{w'q'}\right)_e$ the entrainment flux of moisture. The specific moisture flux is related to the latent heat flux (LE) following $\left(\overline{w'q'}\right)_s = \mathrm{LE}/(\rho \cdot L_\mathrm{v})$, with L_v the latent heat of vaporization. Similarly to Eq. 2.2, we represent the entrainment flux as:

$$\left(\overline{w'q'}\right)_e = -\left(\frac{\partial h}{\partial t} - w_s\right)\Delta q = -w_e \cdot \Delta q. \tag{2.8}$$

This is an important equation since it relates the dynamics of the boundary layer growth, represented by the entrainment velocity with the specific conditions at the interface between the BL and the FT.

Eq. 2.8 requires an additional equation for the temporal evolution of the jump of q at the BL-FT interface (Δq). It reads:

$$\frac{\partial \Delta q}{\partial t} = \frac{\partial q_{FT}}{\partial t} - \frac{\partial \langle q \rangle}{\partial t} = \gamma_q \left(\frac{\partial h}{\partial t} - w_s\right) - \frac{\partial \langle q \rangle}{\partial t} \tag{2.9}$$

where γ_q is the lapse rate of q in the FT.

At this point, we need to introduce a new variable, the virtual potential temperature, which accounts for the changes in the heat and moisture budgets and is used to quantify buoyancy. It is defined as:

$$\theta_v = \theta(1 + 0.61q) \tag{2.10}$$

The virtual potential temperature is the potential temperature that dry air would need to attain in order to have the same density as the moist air at the same pressure. Since moist air is less dense than dry air at the same conditions of temperature and pressure, θ_v is always greater than the actual temperature, but only by a few degrees. The turbulent transport of this variable, namely the buoyancy flux, combines in one quantity the information of the potential temperature flux and the specific moisture flux. It reads:

$$\overline{w'\theta'_v} = w'\theta' + 0.61(\langle\theta\rangle w'q' + \langle q\rangle w'\theta' + w'\theta'q') \approx w'\theta' + 0.61(\langle\theta\rangle w'q'). \tag{2.11}$$

This buoyancy flux expresses the production of turbulent kinetic energy in the BL due to density differences in diurnal convective boundary layers. Turbulence driven by shear (mechanical turbulence) on the mixed-layer thermodynamic equations is not dealt with in our research.

The buoyancy flux directly enters in the BL growth formulated in Eq. 2.2. Therefore, we rewrite Eq. 2.2 in the definitive form as:

$$\left(\overline{w'\theta'_v}\right)_e = -\left(\frac{\partial h}{\partial t} - w_s\right)\Delta\theta_v = -w_e \cdot \Delta\theta_v, \tag{2.12}$$

where $\Delta\theta_v$ is expressed in terms of the characteristics of the θ- and q-budgets:

$$\Delta\theta_v = \Delta\theta + 0.61\,(\langle q\rangle\Delta\theta + \langle\theta\rangle\Delta q + \Delta\theta\Delta q) \tag{2.13}$$

By introducing the buoyancy flux as the driver of the turbulent process in the determination of the boundary layer growth, we complete the main framework of our model formulation based on mixed-layer theory.

In summary, the combined heat and moisture system is composed by the following 5 equations:

1. Budget prognostic equation for θ and q (Eqs. 2.1 and 2.7)
2. Boundary layer growth evolution (Eq. 2.12) rewritten as:

$$\frac{\partial h}{\partial t} = -\frac{\left(\overline{w'\theta'_v}\right)_e}{\Delta\theta_v} + w_s \tag{2.14}$$

3. Prognostic equation for $\Delta\theta$ and Δq (Eqs. 2.5 and 2.9)
4. Closure assumption relating the surface buoyancy flux to the entrainment buoyancy flux $\left(\overline{w'\theta'_v}\right)_e = -\beta\left(\overline{w'\theta'_v}\right)_s$.

2.4 Governing equations for chemical species

The mixed-layer model allows us to investigate the influence of the boundary layer dynamics on reactive atmospheric compounds during daytime. Our aim is to show that in order to explain the diurnal evolution of a chemical species, we need, besides accounting for chemical transformations, to understand the influence of the boundary layer growth on the species concentration and its emission from and deposition to the land surface. It is important to remark that in mixed-layer theory we assume that species are mixed instantaneously as soon as they are chemically produced, emitted or entrained from the free troposphere. In other words, the mixed-layer model acts as a reactive chamber with the additional advantage of accounting for boundary layer growth and BL-FT exchange.

Like our analysis of the heat and moisture budget, mixed-layer theory enables us to determine how chemically reactive species are modified during the day. This challenge can be met by increasing the complexity of the atmospheric system since, in addition to the dynamics, we have to account for radiation effects on photo-dissociated species and chemical transformation. To the main governing equations of the heat and moisture, therefore, we add the governing equations for reactive species. These species are transformed according to a chemical mechanism that reproduces the essential components of the O_3-NO_x-HO_x-VOC system. The chemical mechanism that reproduces the diurnal variability of these reactants is slightly different for the different applications in this thesis and the applied versions are shown in Chapters 3 and 4.

We begin by explaining the governing equation of a generic chemical species C. We emphasize the advantages of using this dynamics-chemistry framework and the similarity of the governing equations for chemical species, heat and moisture equations, paying particular attention to explaining the source and sink terms related to the chemical transformations.

Like scalars (for instance moisture), the inclusion of reactive species requires the introduction of two additional equations for each species. The expression for the evolution of the generic species is similar as that for potential temperature (Eq. 2.1) and moisture (Eq. 2.7), but includes a term for the chemical transformation:

$$\frac{\partial C}{\partial t} = \frac{\left(\overline{w'C'}\right)_s - \left(\overline{w'C'}\right)_e}{h} + S_C \tag{2.15}$$

By solving Eq. 2.15, we determine how C varies over time as a function of emission/deposition processes at the surface (represented by the term $\left(\overline{w'C'}\right)_s$), the dynamic effects ($h$ and $\left(\overline{w'C'}\right)_e$) and the chemical transformation (S_C).

Since the surface processes are prescribed throughout the research in this thesis, we focus here on the explanation of the dynamic and chemical terms. The flux at the top of the boundary layer is represented in the same way as the entrainment flux for buoyancy and moisture.

For C it reads:

$$\left(\overline{w'C'}\right)_e = -\left(\frac{\partial h}{\partial t} - w_s\right)\Delta C = -w_e \cdot \Delta C. \tag{2.16}$$

By representing the exchange of C as the product of the entrainment velocity and the jump of C, we account for both the dynamics and chemistry, which together determine the exchange between the BL and FT.

Eq. 2.16 requires an additional prognostic equation to solve the evolution of ΔC:

$$\frac{\partial \Delta C}{\partial t} = \frac{\partial C_{FT}}{\partial t} - \frac{\partial \langle C \rangle}{\partial t} = \gamma_C \left(\frac{\partial h}{\partial t} - w_s\right) - \frac{\partial \langle C \rangle}{\partial t} + S_{C_{FT}}, \tag{2.17}$$

where γ_C represents the free tropospheric lapse rate of C. Notice that we introduce here an extra term to account for the chemical transformation of the reactive species in the free troposphere ($S_{C_{FT}}$).

As mentioned above, there is a new term in Eqs. 2.15 and 2.17 describing the sources and sinks due to the reactivity of individual species. This term can be illustrated using the following generic set of reactions describing the production and destruction of C with rate constants k_{AB} and k_{CD}, respectively:

$$A + B \rightarrow C \tag{2.18}$$

$$C + D \rightarrow A \tag{2.19}$$

From this reaction scheme, we can specify the rates of production and loss of C, P_C and L_C respectively. S_C (or $S_{C_{FT}}$) thus reads:

$$S_C = P_C - L_C = \begin{cases} P_C = k_{AB} \langle A \rangle \langle B \rangle \\ L_C = k_{CD} \langle C \rangle \langle D \rangle \end{cases} \tag{2.20}$$

The same method can be applied to more complex reaction schemes to determine the individual source and sinks terms of any reactant, for instance those of the reaction schemes in Chapters 3 and 4.

2.5 SOA formation: gas/particle partitioning

To describe the diurnal variability of organic aerosol, a new component is added to the coupled dynamics-chemistry modeling system. By including a formulation for gas/particle partitioning leading to SOA formation we complete the development of MXLCH-SOA.

Atmospheric aerosol usually consists of a mixture of organic and inorganic species, like sulfate and nitrate. Gas/particle partitioning of semi-volatile organic species is dominated by absorption of these species into the organic aerosol phase (Pankow, 1994). In that way, more organic mass present in the aerosol leads to a more efficient partitioning of semi-volatile organics into the aerosol phase. Several modeling frameworks exist for modeling SOA formation. The simplest modeling approach calculates SOA as a fixed fraction of the emissions. This approach can lead to large errors in the calculation of SOA formation as it does not account for the semi-volatile character of SOA and consequently for the dependence of its formation on the pre-existing OA mass or the role of temperature and humidity (Pankow, 1994; Donahue et al., 2009). On the other hand, the most thorough approach would be to explicitly treat the gas-phase oxidation of SOA precursors and to determine which species attain a saturation concentration low enough to partition to the aerosol phase. However, since the number of individual organic species in the atmosphere is vast (Goldstein and Galbally, 2007) and only a small fraction of SOA forming species has been identified, this approach is not considered practical for atmospheric modeling purposes (Donahue et al., 2006).

Therefore in the mostly applied methods, SOA forming species are treated as surrogate species and lumped according to their volatility. The so called 2-product model (Odum et al., 1996) uses two surrogate species with different saturation concentrations to represent SOA yields from smog chamber experiments. The yields of these species are obtained by fitting the model to measured SOA concentrations in the lab. This approach treats the semi-volatile nature of SOA and can therefore explain the chamber observations of increasing SOA yields with increasing organic aerosol concentrations (Odum et al., 1996). A disadvantage of this method is that it does not capture the wide range of OA concentrations in the atmosphere since lab studies are generally done at a single OA mass. Besides, the further chemical evolution (aging) in the atmosphere of the semi-volatile organics in the gas and aerosol phase can not be accounted for in this approach.

To solve these issues, Donahue et al. (2006) developed a unified framework for treating semi-volatile species in the atmosphere, called the Volatility Basis Set (VBS). This approach lumps the numerous semi-volatile products that are formed after VOC oxidation into several bins with logarithmically spaced effective saturation concentrations. The mass yields for the different bins are obtained by fitting results from laboratory studies of SOA formation to a prescribed distribution of saturation concentrations. Further oxidation in the gas or aerosol phase that changes the volatility of organic species can be accounted for by redistributing of these species over the bins.

In MXLCH-SOA, we account for gas/particle partitioning by implementing the VBS approach. We use 4 bins with effective saturation concentrations (C_i^*) of 1, 10, 100 and 1000 $\mu g\, m^{-3}$ at 298 K, encompassing a relevant range of product vapor pressures (Lane et al., 2008a). Consequently, a generic reaction for the formation of semi-volatile VOC (SVOC)

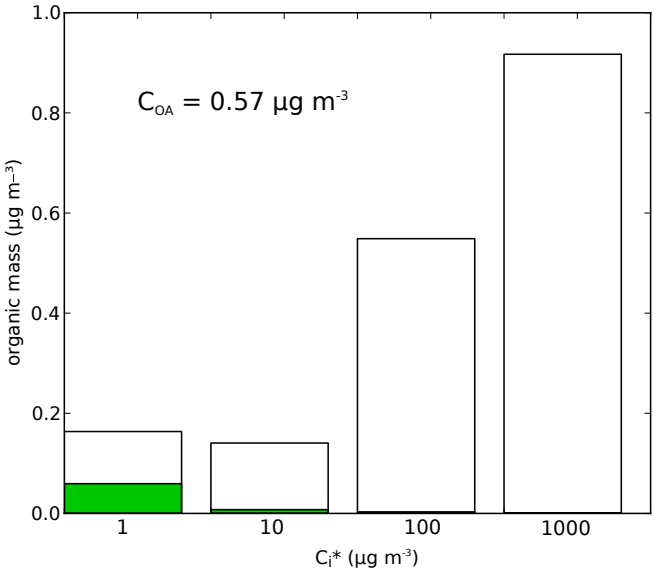

Figure 2.2: Partitioning of semi-volatile organic compounds (SVOCs) with total concentrations (in $\mu g\, m^{-3}$) shown with full bars and the aerosol phase fraction with filled (green) bars at OA_{BG} = 0.5 $\mu g\, m^{-3}$ and T = 298 K. The SVOCs are distributed over the volatility bins according to the yields α_1-α_4 in Eq. 2.21 and the aerosol phase fraction of each SVOC is calculated using Eq. 2.22.

species from the reaction of a VOC with an oxidant OX can be formulated:

$$VOC + OX \rightarrow \alpha_1 C_1 + \alpha_2 C_2 + \alpha_3 C_3 + \alpha_3 C_3 + \alpha_4 C_4 \tag{2.21}$$

where $\alpha_1 - \alpha_4$ are stoichiometric yields and $C_1 - C_4$ the 4 lumped SVOC species characterized by different saturation concentrations. We apply this generic reaction to calculate SVOC formation from terpenes after reaction with O_3 and OH (see Table 3.1 and Table 4.1, respectively) and isoprene with OH (Table 4.1). The SVOC yields are strongly dependent on the gas-phase chemistry that leads to the formation of the SVOC species (Kroll and Seinfeld, 2008). Therefore, in Chapter 4, we account for their dependence on the NO_x regime.

In addition, we represent the OA mass already present in the atmosphere by including a background OA term (OA_{BG}) that is assumed to be strongly aged and consequently non-volatile, so it will not repartition into the gas phase (Cappa and Jimenez, 2010).

At each time step, the total organic aerosol concentration C_{OA} is diagnosed by iteratively

solving the following equations:

$$C_{\mathrm{OA}} = \sum_i (X_{p,i} C_i) + \mathrm{OA_{BG}}\,; \quad X_{p,i} = \left(1 + \frac{C_i^*}{C_{\mathrm{OA}}}\right)^{-1} \tag{2.22}$$

where C_{OA} is the total organic aerosol mass concentration (μg m^{-3}), $\mathrm{OA_{BG}}$ the background organic aerosol concentration (μg m^{-3}), $X_{p,i}$ is the fraction of compound i in the aerosol phase (dimensionless). Partitioning occurs instantaneously, as it is assumed that the SVOCs are in thermodynamic equilibrium with the aerosol phase. Since partitioning is instantaneous, the assumption of a well-mixed C_{OA} throughout the boundary layer is valid.

Temperature dependence of the saturation concentrations follows Clausius-Clapeyron (Sheehan and Bowman, 2001):

$$C_i^* = C_{i,0}^* \frac{T_0}{T} \exp\left[\frac{\Delta H_{\mathrm{vap}}}{R}\left(\frac{1}{T_0} - \frac{1}{T}\right)\right] \tag{2.23}$$

in which $C_{i,0}^*$ is the effective saturation concentration of compound i at reference temperature T_0 (here 298 K), T is the atmospheric temperature (K), ΔH_{vap} is the enthalpy of vaporization (kJ mol^{-1}), and R is the ideal gas constant (J mol^{-1} K^{-1}).

As Eq. 3.2 requires the absolute temperature T, we approximate it in MXLCH-SOA following $T \simeq \theta - \frac{g}{c_p} \cdot z$ at half of the BL height, so at $z = 0.5\,h$. The error resulting of not accounting for the change of T with height is small.

To close this section, we show an example from this thesis of the performance of the VBS approach. The approach is illustrated in Fig. 2.2 for typical conditions for the case study in Chapter 3: the distribution of the SVOCs resulting from the oxidation of a generic terpene TERP is shown and their partitioning at OA_{BG} = 0.5 μg m^{-3} and T = 298 K. It shows that for bins with $\mathrm{C}_i^* >> C_{\mathrm{OA}}$, only a small fraction of the organics will partition to the aerosol phase. Another important feature of Eq. 2.22 is that when C_{OA}=1, 50% of the organics in the bin with C_i^*=1 is in aerosol phase and the other 50% in the gas phase.

3

Combined effects of surface conditions, boundary layer dynamics and chemistry on diurnal SOA evolution

We study the combined effects of land surface conditions, atmospheric boundary layer dynamics and chemistry on the diurnal evolution of biogenic secondary organic aerosol in the atmospheric boundary layer, using a model that contains the essentials of all these components. First, we evaluate the model for a case study in Hyytiälä, Finland, and find that it is able to satisfactorily reproduce the observed dynamics and gas-phase chemistry. We show that the exchange of organic aerosol between the free troposphere and the boundary layer (entrainment) must be taken into account in order to explain the observed diurnal cycle in organic aerosol (OA) concentration. An examination of the budgets of organic aerosol and terpene concentrations show that the former is dominated by entrainment, while the latter is mainly driven by emission and chemical transformation. We systematically investigate the role of the land surface, which governs both the surface energy balance partitioning and terpene emissions, and the large-scale atmospheric process of vertical subsidence. Entrainment is especially important for the dilution of organic aerosol concentrations under conditions of dry soils and low terpene emissions.

This chapter is published as Janssen et al. (2012).

Subsidence suppresses boundary layer growth while enhancing entrainment. Therefore, it influences the relationship between organic aerosol and terpene concentrations. Our findings indicate that the diurnal evolution of secondary organic aerosols (SOA) in the boundary layer is the result of coupled effects of the land surface, dynamics of the atmospheric boundary layer, chemistry, and free troposphere conditions. This has potentially some consequences for the design of both field campaigns and large-scale modeling studies.

3.1 Introduction

A large part of submicron atmospheric particulate material is organic (Hallquist et al., 2009; Jimenez et al., 2009). Secondary organic aerosols (SOA) which are formed in the atmosphere from oxidation of high-volatility precursors are an important contributor to the total organic aerosol budget. The importance of SOA in new particle formation (Metzger et al., 2010; Laaksonen et al., 2008; O'Dowd et al., 2002) and the growth of atmospheric particles to cloud condensation nuclei (Riipinen et al., 2011; Slowik et al., 2010; Tunved et al., 2006) is well established. Formation of SOA from gas-phase species depends on the emissions of these species and their processing in the atmosphere. When emitted at the land surface, they enter into the atmospheric boundary layer (BL), the lowest part of the atmosphere, which is characterized by strong turbulent motions that are largely influenced by the underlying land surface and the free troposphere (FT) on top of it (de Bruin, 1983; van Heerwaarden et al., 2009). Acting as a buffer between the surface processes and the FT, the BL dynamics affect the processing of aerosol precursor species and the partitioning into the aerosol phase of their low-volatility reaction products.

Here we aim to systematically study the role of the diurnal variability of dynamics and chemical transformation on the evolution of organic aerosol. We do this by modeling a case study and conducting a set of sensitivity analyses using MXLCH-SOA, a coupled model of BL dynamics, land surface, gas-phase chemistry and gas/particle partitioning, aiming to determine the role of different processes in controlling the diurnal variability in OA. A schematic overview of the studied system is given in Fig. 3.1. It is important to note that we strive for a balance between all relevant components of the system and therefore include the land surface, BL dynamics, chemistry and gas/particle partitioning in a way that keeps the essentials of all components. This allows us to systematically study the whole system in a coupled approach while avoiding excessive complexity. Thus, we expand upon modeling studies that take the diurnal variability of BL characteristics on SOA formation into account using box models with prescribed diurnal cycles of temperature, humidity, boundary layer height, and oxidants (Sheehan and Bowman, 2001; Bowman and Karamalegos, 2002; Dzepina et al., 2009), or applying a fixed BL height, thereby neglecting the effects of entrain-

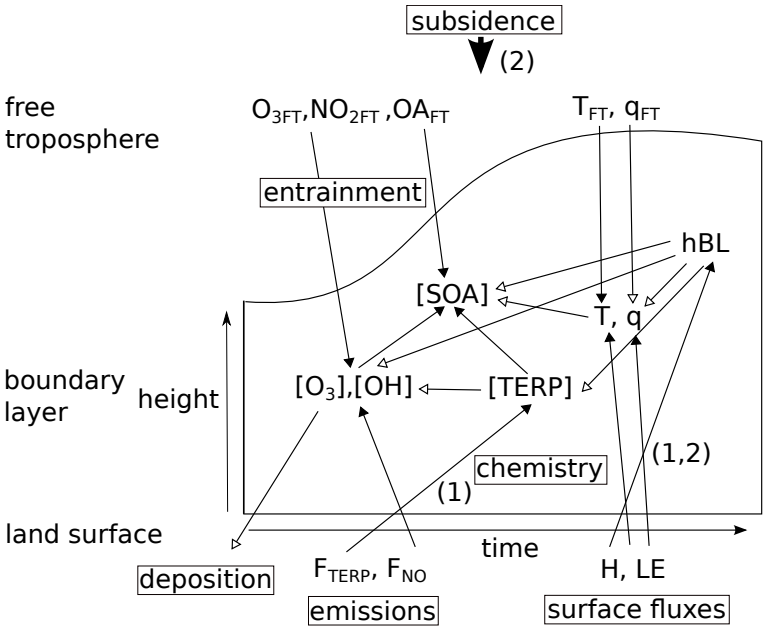

Figure 3.1: Scheme of the interactions in and the boundaries of the system studied in this work. The numbers relate to the forcings of the system that are varied in the sensitivity analysis. Closed arrows indicate a positive relation, open arrows a negative relation, and circles relations which can be either positive or negative. Processes are indicated in the boxes.

ment on BL growth and reactant concentrations (Tunved et al., 2006; Riipinen et al., 2011). Besides, regional and global chemical transport models used for simulating SOA formation are usually forced by offline meteorology (Lane et al., 2008a; Slowik et al., 2010; Riipinen et al., 2011), which hinders the ability to study their sensitivity to meteorological and land surface boundary conditions. In contrast, in our approach the dynamics and chemistry are solved simultaneously, which allows for an analysis of different cases in which BL growth and entrainment are driven by varying land surface and FT conditions. Moreover, in our approach we are able to explicitly calculate the contributions of the different processes to the budgets of reactants, since MXLCH-SOA contains basic parametrizations of the relevant processes based on sound physical and chemical assumptions.

As a first step we validate MXLCH-SOA with observations of BL dynamics and gas-phase chemistry collected at the SMEAR II measurement station at Hyytiälä, Finland. It is located in the boreal forest which is an important source of SOA, mainly from terpene oxidation (e.g. Tunved et al., 2006). Then we perform a budget analysis of the main contributions to terpene and organic aerosol mass in time, including emissions, entrainment, chemistry and

partitioning. Finally, we analyze the sensitivity of BL organic aerosol evolution to (1) the land surface conditions, in terms of surface heat flux partitioning which drives the exchange between the FT and the BL, and terpene emissions and (2) land surface conditions (heat flux partitioning), entrainment and the large-scale atmospheric process of vertical subsidence associated with the presence of a high pressure system. The experiments are based on a case study for the boreal forest region. However, since our focus is on understanding the processes that occur in each BL in which SOA formation occurs, we will discuss the general applicability of the findings for this case study and their implications for field campaigns and large-scale modeling.

3.2 Methods

In this section we briefly introduce the methods used to represent the BL dynamics and gas-phase chemistry, including SOA formation through oxidation of volatile organic compounds (VOCs), in MXLCH-SOA. Furthermore, we describe the case study and the numerical experiments that we performed.

3.2.1 Dynamics of the boundary layer: mixed layer approach

Mixed layer theory (Lilly, 1968; Tennekes, 1973) is an approximation for mixing in the BL under convective conditions. Under this approximation scalars and chemical species are instantaneously and perfectly mixed throughout the BL due to the high turbulent intensity (Vilà-Guerau de Arellano et al., 2011). In this way, the mixed layer approach is comparable to a homogeneous reactive box in which chemical transformations take place. Within this approach, the BL grows due to the entrainment of dry air at the interface between the FT and the BL, which is induced by the buoyancy flux at the surface. These processes influence the concentrations of reactive species due to the fact that the BL becomes higher, which increases the mixing volume, and because the air that is entrained from the FT typically contains different concentrations of reactive species. The importance of FT–BL exchange for the diurnal variability of reactants in the Amazon was already suggested by Martin et al. (1988) and Ganzeveld et al. (2008).

With respect to the surface conditions, the vegetated land surface forms the source of biogenic VOCs that are oxidized in the BL to form SOA. NO emissions from the soil influence atmospheric NO_x levels and consequently the formation of the oxidants ozone (O_3) and the hydroxyl radical (OH). In this study, we prescribe surface fluxes of sensible (H) and latent heat (LE), VOCs and NO. The FT conditions for temperature, moisture and reactants are also imposed, both in terms of their initial value and, in the case of temperature and moisture, their lapse rate. Reactive species in the FT are affected by chemical transformations, but have

an assumed constant concentration profile. More complex assumptions could be made (e.g. modification of the lapse rate of the reactants due to chemical transformations), but these would not take away the existing uncertainties, yet would increase the degrees of freedom of the model. Initial and boundary conditions are obtained from fitting MXLCH-SOA to the case study observations.

3.2.2 Gas-phase chemistry

The chemical mechanism used to represent the essentials of the O_3–NO_x–VOC–HO_x chemistry is given by reactions (R1)–(R19) in Table 3.1. It is based on and further extends the simplified reaction schemes used by Krol et al. (2000) and Vilà-Guerau de Arellano et al. (2011) with reaction rate coefficients from the International Union of Pure and Applied Chemistry (IUPAC) Subcommittee for Gas Kinetic Data Evaluation (`http://www.iupac-kinetic.ch.cam.ac.uk/`). It is able to capture the essential photochemistry of the main reactive species in rural and remote areas with low anthropogenic influence. O_3 deposition follows a sinusoidal profile during the day (Table 4.4). In this way, the deposition velocity of O_3 scales with stomatal resistance and LE (e.g. Ganzeveld et al., 2008).

A simple reaction mechanism to simulate SOA formation is introduced in MXLCH. In this mechanism, semi-volatile compounds that are able to partition into the aerosol phase are generated by the first step oxidation of terpenes by O_3 and OH. Further chemical ageing is not represented. The SOA-forming reactions are shown in Table 3.1 (Reactions R20 and R21) and the stoichiometric coefficients in Table 3.2. For all simulations we assumed low NO_x conditions, i.e. that organic peroxy radicals react predominantly with HO_2 or RO_2 and not NO, which is a reasonable approximation for the conditions of our study.

All terpenes in our model are assumed to behave as α-pinene with reaction rate coefficients from Atkinson and Arey (2003). The total terpene concentration is the sum of the measured concentrations of 8 terpenes by Spirig et al. (2004). In the experiments, we used TERP, a generic terpene with the properties of α-pinene, but with emissions scaled up to reproduce the total terpene concentration. Hao et al. (2011) showed that for low VOC concentrations ($<5\,\mu g\,m^{-3}$) the assumption that SOA yields for α-pinene and real plant emissions are similar is justified. Furthermore, we assumed that aerosol yields from α-pinene with OH are equal to the better documented yields for ozonolysis of α-pinene. The information on OH initiated oxidation in the literature is limited. Hao et al. (2011) reported a higher volatility and thus lower yields from OH dominated chemistry than for O_3 initiated oxidation. In contrast, there are other experiments which show that OH yields are a little higher than the O_3 yields (N. Donahue, personal communication, 2011; Henry and Donahue, 2011). Finally, we assumed that aerosol formation from isoprene can be neglected due to the low concentrations of this precursor at our study location (e.g. Spirig et al., 2004).

Table 3.1: Chemical reaction scheme used in the numerical experiments of MXLCH-SOA. In reaction rate functions, T is the absolute temperature and χ is the solar zenith angle. First-order reaction rates are in s^{-1} and second-order reactions are in $cm^3\ molec^{-1}\ s^{-1}$. PRODUCTS are reaction products which are not further evaluated in the chemical reaction scheme. In Reaction (R17), $n = 0$ (no OH-recycling). α_1–α_4 are stoichiometric coefficients, see Table 3.2.

Number	Reaction			Reaction rate
R1	$O_3 + h\nu$	$\rightarrow$	$O^{1D} + O_2$	$6.62{\cdot}10^{-5} \cdot e^{-\frac{0.575}{\cos(\chi)}}$
R2	$O^{1D} + H_2O$	$\rightarrow$	$OH + OH$	$1.63{\cdot}10^{-10} \cdot e^{\frac{60}{T}}$
R3	$O^{1D} + N_2$	$\rightarrow$	O_3	$2.15{\cdot}10^{-11} \cdot e^{\frac{110}{T}}$
R4	$O^{1D} + O_2$	$\rightarrow$	O_3	$3.30{\cdot}10^{-11} \cdot e^{\frac{55}{T}}$
R5	$NO_2 + h\nu$	$\rightarrow$	$NO + O_3$	$1.67{\cdot}10^{-2} \cdot e^{-\frac{0.575}{\cos(\chi)}}$
R6	$CH_2O + h\nu$	$\rightarrow$	HO_2	$5.88{\cdot}10^{-5} \cdot e^{-\frac{0.575}{\cos(\chi)}}$
R7	$OH + CO$	$\rightarrow$	$HO_2 + CO_2$	$2.40{\cdot}10^{-13}$
R8	$OH + CH_4$	$\rightarrow$	CH_3O_2	$2.45{\cdot}10^{-12} \cdot e^{-\frac{1775}{T}}$
R9	$OH + ISO$	$\rightarrow$	$ISORO_2$	$1.00{\cdot}10^{-10}$
R10	$OH + MVK$	$\rightarrow$	$HO_2 + CH_2O$	$2.40{\cdot}10^{-11}$
R11	$HO_2 + NO$	$\rightarrow$	$OH + NO_2$	$3.50{\cdot}10^{-12} \cdot e^{\frac{250}{T}}$
R12	$CH_3O_2 + NO$	$\rightarrow$	$HO_2 + NO_2 + CH_2O$	$2.80{\cdot}10^{-12} \cdot e^{\frac{300}{T}}$
R13	$ISORO_2 + NO$	$\rightarrow$	$HO_2 + NO_2 + CH_2O + MVK$	$1.00{\cdot}10^{-11}$
R14	$OH + CH_2O$	$\rightarrow$	HO_2	$5.50{\cdot}10^{-12} \cdot e^{\frac{125}{T}}$
R15	$HO_2 + HO_2$	$\rightarrow$	H_2O_2	*
R16	$CH_3O_2 + HO_2$	$\rightarrow$	PRODUCTS	$4.10{\cdot}10^{-13} \cdot e^{\frac{750}{T}}$
R17	$ISORO_2 + HO_2$	$\rightarrow$	nOH + PRODUCTS	$1.50{\cdot}10^{-11}$
R18	$OH + NO_2$	$\rightarrow$	HNO_3	$3.50{\cdot}10^{-12} \cdot e^{\frac{340}{T}}$
R19	$NO + O_3$	$\rightarrow$	$NO_2 + (O_2)$	$3.00{\cdot}10^{-12} \cdot e^{-\frac{1500}{T}}$
R20	$TERP + O_3$	$\rightarrow$	$\alpha_1C_1 + \alpha_2C_2 + \alpha_3C_3 + \alpha_4C_4$	$5.00{\cdot}10^{-16} \cdot e^{\frac{-530}{T}}$
R21	$TERP + OH$	$\rightarrow$	$\alpha_1C_1 + \alpha_2C_2 + \alpha_3C_3 + \alpha_4C4$	$1.21{\cdot}10^{-11} \cdot e^{\frac{436}{T}}$

* $k = (k_1 + k_2) \cdot k_3$; $k_1 = 2.2{\cdot}10^{-13} \cdot e^{\frac{600}{T}}$; $k_2 = 1.91{\cdot}10^{-33} \cdot e^{\frac{980}{T}} \cdot c_{\mathrm{air}}$; $k_3 = 1 + 1.4{\cdot}10^{-21} \cdot e^{\frac{2200}{T}} \cdot c_{H_2O}$

Table 3.2: Stoichiometric coefficients at $T = 298\,K$ for the different volatility bins of the SOA precursor category TERP, with saturation concentration C_i^* in $\mu g\,m^{-3}$ from Tsimpidi et al. (2010).

i	1	2	3	4
C_i^*	1	10	100	1000
α_i	0.107	0.092	0.359	0.600

Table 3.3: VOC emissions for the case study. Emissions during the day follow a sinusoid with the maximum emission flux ($\mu g\,m^{-2}\,h^{-1}$) as specified.

ISO	α-pinene	TERP
101	111	304

Terpene emissions are prescribed with a sinusoidal profile during the day with a maximum as specified in Table 3.3. The sinusoidal form of the diurnal emission is supported by the terpene flux measurements of Rinne et al. (2007). The prescribed terpene fluxes lie within the range of the measurements by Rinne et al. (2007) for similar temperatures and at the same location, but are higher than the estimates for the same dataset with the mixed layer gradient method by Spirig et al. (2004). One reason for this discrepancy could be the fact that the method used by Spirig et al. (2004) did not account for entrainment and therefore underestimates dilution of the terpenes in the BL.

3.2.3 Organic aerosol formation: gas/particle partitioning

Gas/particle partitioning is dominated by absorption of semi-volatile species into an organic aerosol phase (Pankow, 1994). We assume that the semi-volatile terpene oxidation products are in thermodynamic equilibrium with the aerosol phase, which means that partitioning occurs instantaneously. We account for gas/particle partitioning in MXLCH-SOA by implementing the volatility basis set approach (Donahue et al., 2006). This approach lumps the numerous semi-volatile products that are formed after VOC oxidation into several bins with logarithmically spaced effective saturation concentrations. The mass yields for the different bins are obtained by fitting results from laboratory studies of SOA formation. Here, we use 4 bins with effective saturation concentrations of 1, 10, 100 and $1000\,\mu g\,m^{-3}$ at 298 K, encompassing a relevant range of product vapor pressures (Lane et al., 2008a). The mass stoichiometric coefficients for the different bins of the TERP category of the SOA precursors are taken from Tsimpidi et al. (2010), see Table 3.2. At each time step, the total organic aerosol

concentration C_{OA} is diagnosed from:

$$C_{\mathrm{OA}} = \sum_i (X_{p,i} C_i) + \mathrm{OA_{BG}}\,; \quad X_{p,i} = \left(1 + \frac{C_i^*}{C_{\mathrm{OA}}}\right)^{-1} \tag{3.1}$$

where C_{OA} is the total organic aerosol mass concentration ($\mu g\, m^{-3}$), $\mathrm{OA_{BG}}$ the background organic aerosol concentration ($\mu g\, m^{-3}$), $X_{p,i}$ is the fraction of compound i in the aerosol phase (dimensionless), and C_i^* is the effective saturation concentration of compound i ($\mu g\, m^{-3}$).

Temperature dependence of the saturation concentrations follows Clausius-Clapeyron (Sheehan and Bowman, 2001):

$$C_i^* = C_{i,0}^* \frac{T_0}{T} \exp\left[\frac{\Delta H_{\mathrm{vap}}}{R}\left(\frac{1}{T_0} - \frac{1}{T}\right)\right] \tag{3.2}$$

in which $C_{i,0}^*$ is the effective saturation concentration of compound i at reference temperature T_0 (here 298 K), T is the actual temperature (K), ΔH_{vap} is the enthalpy of vaporization (kJ mol^{-1}), and R is the ideal gas constant (J mol^{-1} K^{-1}). Here, we follow Pathak et al. (2007) and set ΔH_{vap} to 30 kJ mol^{-1} for all condensable products.

A background C_{OA} of 0.8 $\mu g\, m^{-3}$ and of 0.2 $\mu g\, \mathrm{m}^{-3}$ is assumed for the BL and FT, respectively. The BL value is based on the measurements by Raatikainen et al. (2010). These measurements are made in the canopy and therefore serve as an estimate of the order of magnitude for the BL concentration. Since a FT value is not available from measurements, we have performed an analysis to determine the sensitivity to the assumed value, presented in Sect. 3.3.2. The background organic aerosol in BL and FT is assumed to be aged and thus non-volatile, and will therefore not repartition back into the gas phase (Cappa and Jimenez, 2010).

Figure 3.2 shows the sensitivity of the calculated partitioning coefficient for the first bin ($X_{p,1}$) and C_{OA} to variations in T and $\mathrm{OA_{BG}}$ for a range of typical values for this study. While the response of $X_{p,1}$ to variations in T and $\mathrm{OA_{BG}}$ is quite nonlinear, especially at low T and high $\mathrm{OA_{BG}}$, the response of C_{OA} is nearly linear to changes in $\mathrm{OA_{BG}}$. This is due to the fact that the strongest nonlinear behavior of $X_{p,1}$ is found for conditions where $\mathrm{OA_{BG}}$ makes up the largest part of C_{OA}, and therefore the partitioning of semi-volatile species C_1 into the aerosol phase plays only a minor role in determining C_{OA}. The sensitivities of the partitioning coefficients of the other bins show similar patterns.

3.2.4 Observational evaluation: case study

To evaluate our modeling approach, we selected a dataset of surface and boundary layer characteristics (both dynamics and chemistry) that is as complete as possible. Our assumption of

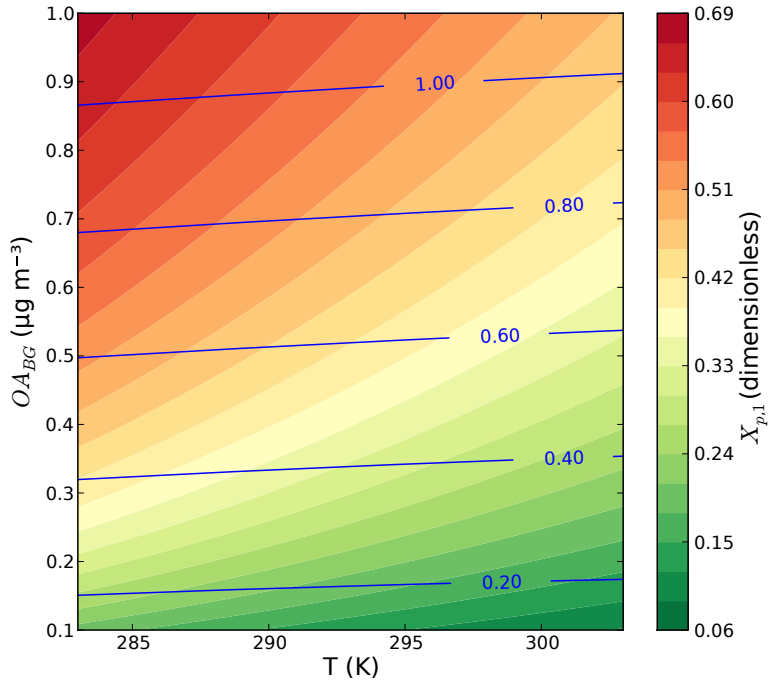

Figure 3.2: Sensitivity of the partitioning coefficient of the first bin ($X_{p,1}$) and organic aerosol concentration (C_{OA}) to temperature (T) and the background organic aerosol concentration (OA_{BG}). Shades indicate $X_{p,1}$ (dimensionless) and the blue contours C_{OA} ($\mu g\, m^{-3}$).

a well-mixed boundary layer is justified for sunny days characterized by convective turbulent conditions. To meet these two requirements, we selected observations from 8 August 2001 at the SMEAR II field station at Hyytiälä (61°51′ N, 24°17′ E) in southern Finland, where ecosystem, meteorological, trace gas and aerosol properties have been measured since 1996 (Hari and Kulmala, 2005).

Surface fluxes of sensible (H) and latent heat (LE) are measured at 23.3 m by means of the eddy covariance technique (Mammarella et al., 2009). These observations are used as forcing for our model and are therefore prescribed as boundary conditions. The model simulation covers 11 h, beginning at 07:50 LT (sunrise is at 07:30 LT). The diurnal evolution of temperature, humidity, O_3 and NO_x, observed at 67.2 m – the highest measurement level available at 52 m above the canopy – and obtained using the SMEAR SmartSearch database (Junninen et al., 2009), is used to determine the ability of the model to reproduce the diurnal variability in the BL. In addition, observations of BL height from temperature and humidity profiles and BL concentrations of terpenes gathered with a tethered balloon (Spirig et al., 2004) enable us to complete the validation.

Table 3.4: The initial and boundary conditions in boundary layer (BL) and free troposphere (FT) as obtained from fitting MXLCH-SOA to the case study observations. All initial conditions are imposed at 07:50 LT. Heat fluxes are applied from 07:50 to 18:50 LT with $\mathrm{H} = \rho c_p \overline{w'\theta'}_s$ *and* $LE = \rho L_v \overline{w'q'}_s$. *t is the time (s) and* t_d *the length of the simulation (s). The subscripts s and e indicate values at the surface and the entrainment zone, respectively.*

Property	Value
Initial BL height h (m)	200
Subsidence rate ω (s^{-1})	0
Surface sensible heat flux $\overline{w'\theta'}_s$ ($K\,m\,s^{-1}$)	$0.11 \sin(\pi t/t_d)$
Entrainment/surface heat flux ratio $\beta = -\overline{w'\theta'}_e/\overline{w'\theta'}_s$ (–)	0.2
Initial BL potential temperature $\langle\theta\rangle$ (K)	288
Initial FT potential temperature θ_{FT} (K)	288.4
Potential temperature lapse rate FT γ_θ ($K\,m^{-1}$)	0.0035
Surface latent heat flux $\overline{w'q'}_s$ ($g\,kg^{-1}\,m\,s^{-1}$)	$0.06 \sin(\pi t/t_d)$
Initial BL specific humidity $\langle q\rangle$ ($g\,kg^{-1}$)	8.0
Initial FT specific humidity q_{FT} ($g\,kg^{-1}$)	6.25
Specific humidity lapse rate FT γ_θ ($g\,kg^{-1}\,m^{-1}$)	−0.0024

3.2.5 Numerical strategy

We designed a series of numerical experiments to investigate the dependence of the SOA evolution on the chemical and dynamical processes and their relationships as depicted in Fig. 3.1. In the first experiment, we study the sensitivity of C_{OA} to the surface conditions. The sensitivity analysis is carried out as a function of the evaporative fraction (EF) and the terpene emission flux (F_{TERP}) (indicated by (1) in Fig. 3.1). EF is defined as LE/(H + LE), i.e. it is the fraction of the surface heat flux that is used for evaporation of water from the surface. In the second experiment, we evaluated the sensitivity of C_{OA} to EF and to large-scale vertical subsidence motions (indicated by (2) in Fig. 3.1). The latter are due to the presence of synoptic high pressure systems that suppress the BL growth. In these analyses,

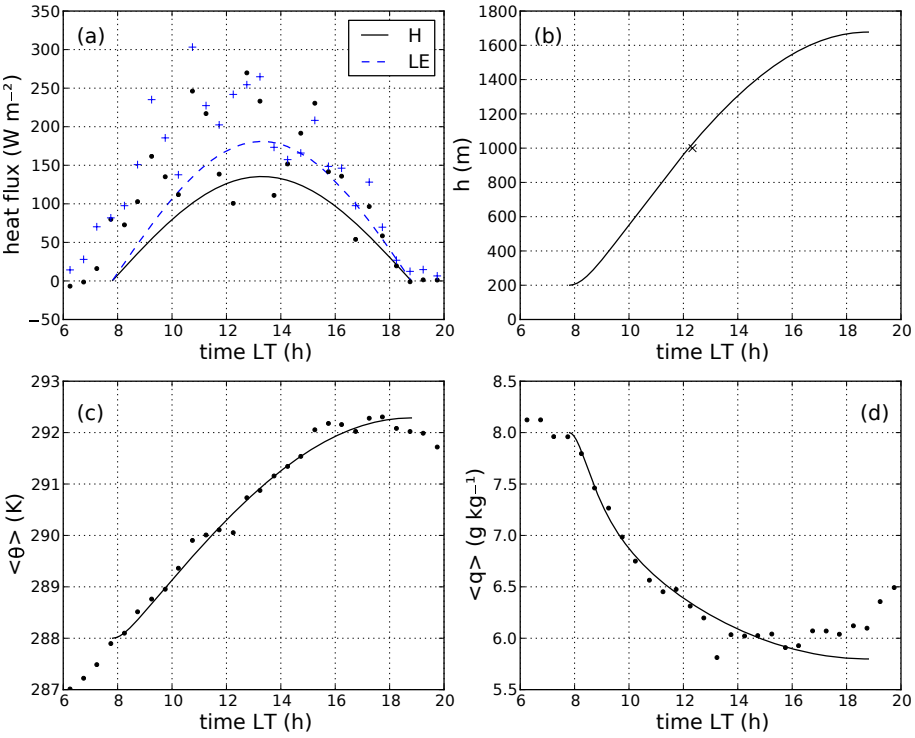

*Figure 3.3: Diurnal evolution of **(a)** surface sensible (H) and latent (LE) heat flux, which are both prescribed, **(b)** boundary layer height (h), **(c)** mixed layer potential temperature ($\langle\theta\rangle$) and **(d)** mixed layer specific moisture ($\langle q\rangle$) for the case study. Dots and crosses indicate tower (at 67.2 m) and balloon measurements, respectively. Model results are indicated by lines.*

we studied C_{OA} at the end of the day (18:50), because then BL growth and entrainment cease and we can evaluate the net effect of the daytime dynamics, emissions and chemistry.

3.3 Results

3.3.1 Model evaluation

Figure 3.3 shows the time evolution of the dynamic variables for the initial and boundary conditions as specified in Table 4.3: the surface heat fluxes (H and LE), boundary layer height (h), mixed layer potential temperature ($\langle\theta\rangle$) and specific moisture ($\langle q\rangle$). The onset of the prescribed surface heat fluxes is delayed by about one hour, as compared to the measurements. By so doing, we ensure that the model calculations begin within the well-mixed assumptions

Table 3.5: Initial mixing ratios in BL and FT and surface emission fluxes of the reactants as obtained from fitting MXLCH-SOA to the case study observations. Species in the reaction mechanism that are not included in this table have zero initial concentrations and zero surface emissions, except TERP and ISO (see Table 3.3). For the molecules O_2 and N_2, we have imposed the values $2{\cdot}10^8$ and $8{\cdot}10^8$ ppb, respectively.

	O_3	NO	NO_2	CH_4	CO
Initial mixing ratio (ppb)					
BL	31.0	0.04	0.1	1800.	100.
FT	39.0	0.0	0.2	1800.	100.
Surface emission flux (ppb m s^{-1})	$-0.20 \sin\left(\frac{\pi t}{t_d}\right)$	$4{\cdot}10^{-3}$	0.0	0.0	0.0

when the ground thermal inversion is already broken. Both H and LE fall within the low end of the observations. This results from fitting the model to observed θ, q and h and could be due to the different footprints of the heat fluxes and θ and q: H and LE are measured at 23.3 m, while θ and q are observed at 67.2 m, and consequently the measurements of H and LE represent a smaller area.

The time evolutions of $\langle\theta\rangle$ and $\langle q\rangle$ are reproduced well. This satisfactory agreement of the $\langle\theta\rangle$ and $\langle q\rangle$ evolutions demonstrates that the model is capable of reproducing the entrainment process well for a given set of surface heat fluxes. Although only one observation is available at 12:20, the calculated BL height is similar to the measured height of 1000 m.

The diurnal trends in the chemical species (Fig. 3.4), with initial concentrations and surface fluxes as specified in Table 4.4, agree well with the observations. This confirms that the processes of entrainment, emission and chemistry (see Fig. 3.1) and their influence on the time evolution of the chemical species are simulated well. The evolution of O_3 is the result of entrainment of O_3 from the FT, especially during the rapid growth of the BL during the morning, a net positive chemical production during the day and its removal by dry deposition. Averaged over the day, the entrainment flux is about 1.4 times as at large as the deposition flux, but in the early morning (08:00) the entrainment flux is 8 times larger than the deposition flux. This is due to the fact that the O_3 deposition flux follows a sinusoidal form during the day (Table 4.4), which has a minimum in the morning. The NO_x measurements must be interpreted carefully since they are probably affected by error in the measurement procedure (P. Keronen, personal communication, 2011). Possible sources of error are the absence of a NO_2 specific converter in the NO_x analyser, which may have biased the observed NO_2 concentration upwards, and the 100 m sampling line, which may have affected the observed NO concentrations. NO_2 measurements are scaled down to match an observed NO_2/NO ratio of 5 as obtained from more reliable measurements in summer 2010 at the same location (P. Keronen, personal communication, 2011). In spite of the large uncertainty regarding the NO_x measurements, we are able to satisfactorily reproduce the order of magnitude of the observed

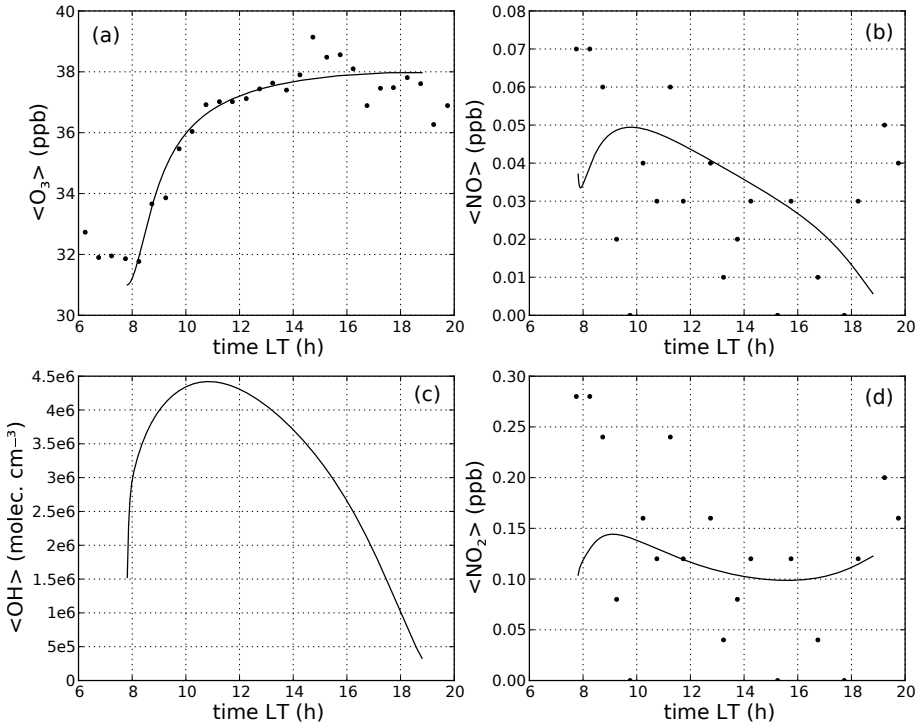

*Figure 3.4: Diurnal evolution of mixed layer concentrations of **(a)** O_3, **(b)** NO, **(c)** OH and **(d)** NO_2 for the case study. NO_2 measurements are scaled down to match the NO_2/NO ratio of 5 obtained during summer 2010 from more reliable measurements than those from August 2001. Dots indicate measurements from the tower at 67.2 m. Model results are indicated by lines.*

NO_x concentrations. Calculated OH concentrations range from $4{\cdot}10^5$ at the end of the day to $4.5{\cdot}10^6$ molec cm^{-3} in the late morning. Unfortunately, no observations of OH in the mixed layer (above the canopy) are available for this environment. Petäjä et al. (2009) report an observed diurnal range in in-canopy OH concentrations in the order of 10^4 to 10^5 molec cm^{-3}. BL concentrations are likely higher, because of the higher O_3 concentration and light intensity and lower concentrations of VOCs, which deplete OH. We find, however, that C_{OA} is not very sensitive to OH levels. For the case study, increasing the OH concentration by a factor 2 resulted in an increase of C_{OA} at the end of the day of only 1 % and reducing it by a factor 2 in a decrease of 3 %. The reason for this weak sensitivity will be further discussed in Sect. 3.3.3.

Figure 3.5 shows the results for terpenes with emission fluxes as specified in Table 3.3. MXLCH-SOA is able to reproduce the order of magnitude of the observed concentrations of both α-pinene and the sum of terpenes ($\langle$TERP$\rangle$). Since there are only four data points

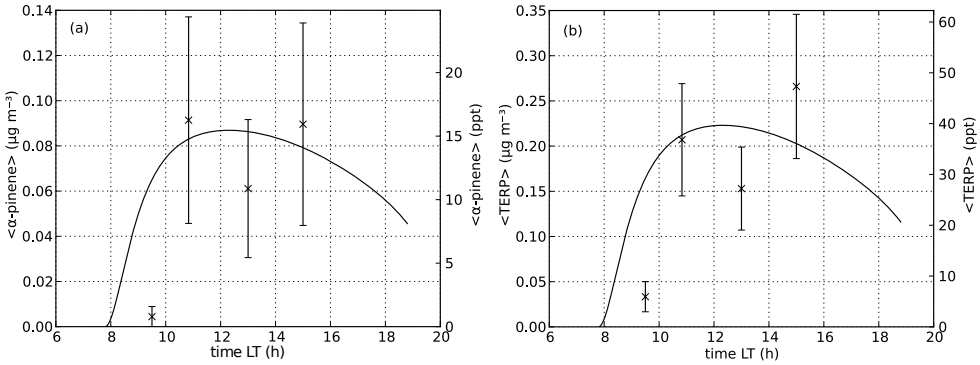

Figure 3.5: ***(a)*** *⟨α-pinene⟩ and* ***(b)*** *sum of terpenes (⟨TERP⟩) for the case study. Crosses indicate balloon measurements and model results are indicated by lines. Errors are 100 % for concentrations lower than 0.03 µg m^{-3}, 50 % for concentrations between 0.03 and 0.15 µg m^{-3} and 30 % for concentrations higher than 0.15 µg m^{-3}. The conversion factor from µg m^{-3} to ppt is 178.*

and the error in the individual measurements is large, we cannot draw conclusions on how well we can reproduce the diurnal evolution of the terpene concentrations from these data. Typically, terpene concentrations will increase during nighttime (e.g. Ruuskanen et al., 2009) due to temperature-driven emissions into a BL that is shallow and stably stratified. Besides, it is characterized by low O_3 concentrations and consequently low chemical destruction. A sensitivity analysis revealed that the diurnal cycle in C_{OA} is not very sensitive to the initial terpene concentration. The reason for this will be discussed further in Sect. 3.3.3.

Overall, comparison of the model results with the observations shows that we can reproduce the time evolution of the dynamics and the order of magnitude of the gas-phase chemistry well, which gives confidence in the validity of MXLCH-SOA for further analyses.

3.3.2 Diurnal evolution of organic aerosol

A key aspect of this study is the ability of MXLCH-SOA to model the organic aerosol concentration C_{OA} as a function of dynamics and chemistry (Fig. 3.1). As expressed in Eq. (4.1), the background organic aerosol concentration OA_{BG} affects C_{OA} both directly and indirectly by influencing the partitioning into the aerosol phase of the semi-volatile reaction products (C_i) that result from TERP oxidation. Therefore, to understand the diurnal evolution of C_{OA} it is crucial to represent the OA_{BG} accurately, both in the BL and the FT, the latter since OA_{BG}

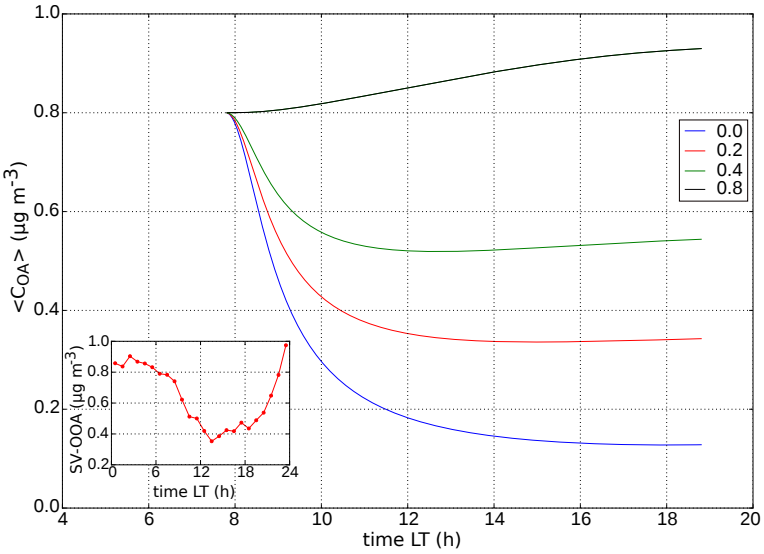

Figure 3.6: Organic aerosol concentration C_{OA} for the case study, including the sensitivity to different FT background OA concentrations (0.0, 0.2, 0.4, 0.8 $\mu g\, m^{-3}$). The inset shows the diurnal cycle of the measured SV-OOA-concentration, averaged over 15 days.

from the FT is entrained into the BL during its growth.

Unfortunately, there are no observed vertical C_{OA} profiles for this environment, which could help constrain our numerical experiments (Heald et al., 2011). In order to determine the sensitivity of the diurnal cycle in C_{OA} to the FT $\mathrm{OA_{BG}}$, we carry out 4 identical numerical experiments, only varying the $\mathrm{OA_{BG}}$ in the FT (Fig. 3.6). By so doing, we are able to study the influence of the $\mathrm{OA_{BG}}$ in the residual layer (the remainder of the BL from the previous day) that was decoupled from the nocturnal boundary layer. We included a case for which BL and FT concentrations are equal. This may not be realistic, because we simulate biogenic OA only, which has a surface source and thus lower concentrations in the FT; however, the high FT biogenic OA is shown for illustrational purposes. Since we expect that C_{OA} is much lower in the FT than in the BL, the other three cases represent FT $\mathrm{OA_{BG}}$ of 0.0, 0.2 and 0.4 $\mu g\, m^{-3}$. For all these cases, we find a net decrease of C_{OA} during the day. Without further observational constraints on the actual FT concentration, we assumed a value of 0.2 $\mu g\, m^{-3}$ for the numerical experiments presented hereafter.

There are only a few measurements of organic aerosol concentrations for the location of our case study, and as a result we are not able to directly compare modeled with measured data. There are, however, observations available at the same site that allow us to qualitatively compare the diurnal behavior of OA. Raatikainen et al. (2010) measured organic aerosol

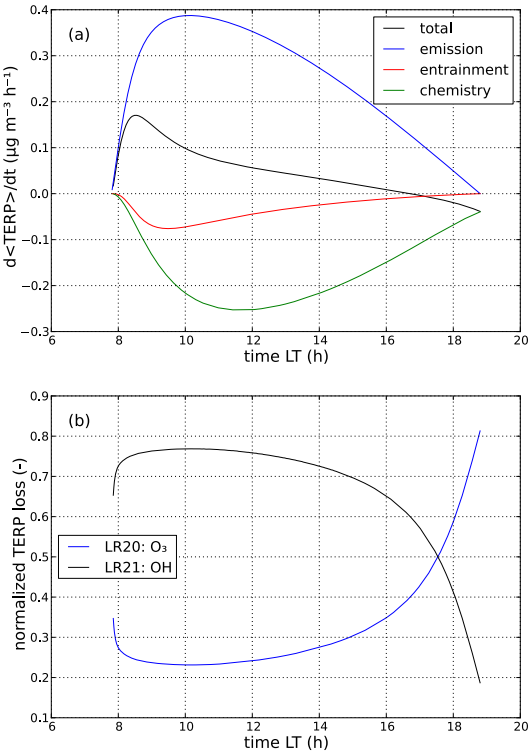

Figure 3.7: Contribution of the individual processes to the terpene tendency (Eq. 3.3) for the case study. ***(a)*** *total tendency and the individual contributions of emission, entrainment and chemistry, and* ***(b)*** *the normalized contributions to the chemical terpene loss for the reactions with O_3 and OH.*

concentrations at Hyytiälä during 15 days in spring 2005. They identified two oxygenated organic aerosol (OOA) groups. One of them, SV-OOA (semi-volatile OOA, formally OOA2), has a clear diurnal cycle, has undergone little oxidation and is qualified as originating from local sources, the most likely being the oxidation of locally emitted VOCs based on the observation that the presence of SV-OOA is independent of air mass history. Therefore, it is interesting to compare the diurnal cycle of SV-OOA with the simulated C_{OA} and we include the SV-OOA data in Fig. 3.6. The measured SV-OOA shows a similar concentration decrease during the day as the modeled C_{OA}. This further indicates the need to have a balanced approach in calculating the C_{OA} taking into account emission, dynamical processes like entrainment and chemical transformations (Fig. 3.1). The absolute concentrations should be compared with care, however, since the measurements were performed inside the canopy while the model results reflect BL averages.

3.3.3 Budgets

To deepen our understanding of the concentration tendencies, we make use of the ability of the mixed layer model to calculate the different contributions of entrainment, emissions and chemistry to the total tendency of chemical species (Tennekes, 1973; Vilà-Guerau de Arellano et al., 2011), in this case C_{OA} and TERP. The TERP budget reads:

$$\frac{\mathrm{d}\langle \mathrm{TERP}\rangle}{\mathrm{d}t} = \overbrace{\frac{F_{\mathrm{TERP}}}{h}\sin\left(\frac{\pi t}{t_d}\right)}^{\text{emission}} + \overbrace{\frac{w_{\mathrm{e}}\Delta TERP}{h}}^{\text{entrainment}} - \overbrace{\sum_j k_j \langle \mathrm{TERP}\rangle\langle OX_j\rangle}^{\text{chemistry}} \tag{3.3}$$

where F_{TERP} is the maximum daily terpene emission flux ($\mu\mathrm{g\,m^{-2}\,h^{-1}}$), as specified in Table 3.3; h is the BL height (m); t is the time since the start of the simulation (s); t_d is the length of the simulation (s); w_{e} is the entrainment velocity ($\mathrm{m\,s^{-1}}$), which in absence of subsidence equals BL growth ($\mathrm{d}h/\mathrm{d}t$); $\Delta TERP$ is the TERP concentration jump between the BL and the FT ($\mu\mathrm{g\,m^{-3}}$) (with the jump of a scalar or reactant C defined as $\Delta C = C_{\mathrm{FT}} - \langle C\rangle$, see also Fig. 3.10); k_j is the reaction rate of TERP with oxidant OX_j (either $\mathrm{O_3}$ or OH); and $\langle OX_j\rangle$ is the mixed layer concentration of oxidant OX_j. Note that h, w_{e}, $\Delta TERP$, $\langle TERP\rangle$ and $\langle OX\rangle$ are calculated simultaneously during the MXLCH-SOA runs and therefore account for the coupling between dynamics and chemistry. This defines the difference between our approach and using box models with a fixed h or a BL growth calculated from measurements: here, the development of the BL and entrainment are governed by the diurnal dynamics of temperature and moisture, through w_{e} in the second term on the right hand side (RHS) of Eq. (3.3), which result from the coupling of the BL with the land surface and the FT.

Figure 3.7 shows the budget of TERP and the relative contributions to the total chemical tendency of the reactions of TERP with $\mathrm{O_3}$ and OH for the case study. Overall, emission and chemistry contribute about equally to the budget (Fig. 3.7a). The prescribed F_{TERP} is low in the early morning, but since the BL is still shallow, the emission term contributes strongly to the TERP budget during the course of the morning and becomes the most important term with a maximum of $0.4\,\mu\mathrm{g\,m^{-3}\,h^{-1}}$ at 10:00. After this time, the BL height increases rapidly, which decreases the importance of this term. The chemistry is dominated by the destruction by OH (Fig. 3.7b), so the late morning peak in the chemistry term is associated with the peak in OH that occurs then. The contribution of $\mathrm{O_3}$ to the chemical destruction of TERP is 25 % during the day, but becomes dominant in the evening as OH is reduced. Entrainment contributes significantly to the total tendency between 9 and 12 when BL growth is strongest with $230\,\mathrm{m\,h^{-1}}$. The maximum contribution of entrainment to the total tendency of TERP is about 20 % of the contribution of the emission. During most of the morning, the TERP tendency is positive, mainly due to the emissions, but at the end of the afternoon the tendency becomes negative due to the fact that chemical destruction continues while the emissions

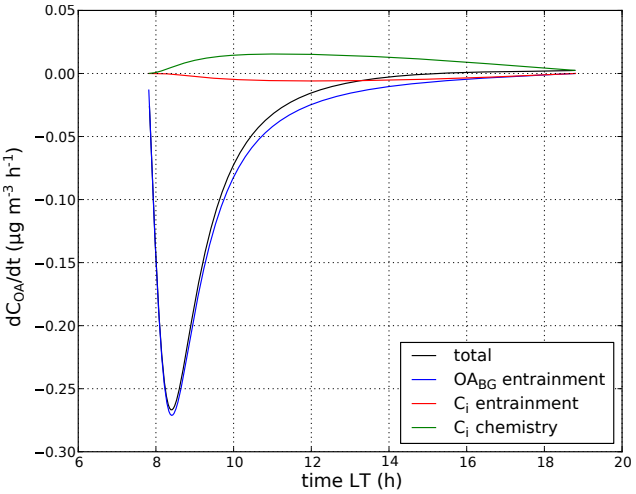

Figure 3.8: Organic aerosol tendency (Eq. 3.4) for the case study. Shown are the total tendency and the contributions of the entrainment of background organic aerosol (OA_{BG}), the entrainment of condensable products from terpene oxidation (C_i), and the chemical production of C_i to the tendency.

decrease.

Damköhler numbers (the ratio of the turbulent time scale to the chemistry time scale) for TERP range from 0.05 to 0.2. Under this regime of relatively slow chemistry, the emission and entrainment (term 1 and 2 on the RHS of Eq. 3.3) play an important role. This further confirms the importance of the atmospheric transport and turbulence for the behavior of TERP.

Similar to Eq. (3.3) for TERP, we can calculate the budget of C_{OA}. The derivation of the C_{OA} budget is more complex than that of TERP, so here we show an approximation which is accurate under the conditions of this study (the full derivation is given in Appendix A):

$$\frac{\mathrm{d}C_{\mathrm{OA}}}{\mathrm{d}t} \simeq \overbrace{\frac{w_{\mathrm{e}}\Delta \mathrm{OA}_{\mathrm{BG}}}{h}}^{\mathrm{OA_{BG}\text{-}entrainment}} + \sum_i X_{p,i}\left[\overbrace{\frac{w_{\mathrm{e}}\Delta C_i}{h}}^{C_i\text{-entrainment}} + \overbrace{\sum_j \alpha_i k_j \langle TERP\rangle\langle \mathrm{OX}_j\rangle}^{C_i\text{-chemistry}}\right]. \tag{3.4}$$

Here, $\Delta \mathrm{OA_{BG}}$ is the jump in the background organic aerosol concentration between the BL and the FT ($\mu \mathrm{g\,m^{-3}}$), $\Delta \mathrm{C_i}$ the concentration jump of the oxidized semivolatile product C_i, and α_i the stoichiometric coefficient for C_i (see Table 3.2).

Note that for the C_{OA} budget, contrary to the TERP budget, there is no emission term since the aerosol is either of secondary origin or present as a background concentration. This

is justified since our budget is focused on the submicron OA concentrations, while primary biological particles (PBAP) are thought to be important only for the supermicron mode (Pöschl et al., 2010).

The evolution of C_{OA} is thus the result of a combination of the influence of the OA_{BG} originating from the FT and the newly formed condensable species from the oxidation of TERP (Fig. 3.5b). Entrainment of background OA dominates the budget of C_{OA} (Fig. 3.8): during the morning, the OA that was concentrated in the shallow BL during the night is diluted when the BL grows and air from the FT with a lower OA_{BG} concentration is entrained. The importance in our simulations of the background OA level in the FT stresses the importance of having upper air measurements (Heald et al., 2011) to understand the evolution of C_{OA} in the BL. The semi-volatile products C_i have net production throughout the day, but their contribution to the C_{OA} budget is relatively small. Only at the end of the day (from 15:30 onwards) is there a net positive tendency of C_{OA}, since the BL growth becomes negligible and the partitioning of terpene C_i to the particle phase outweighs the entrainment term.

These tendencies show that for TERP and C_{OA} emissions, chemistry and entrainment play a different role, which is important in understanding the results of the sensitivity analyses, presented in Sect. 3.3.4. Since TERP is a reactive species with a relatively short lifetime and no background concentration, the relative importance of chemistry in its budget is larger than for OA, which does have a long lived background with a typical lifetime of a week.

To quantify the importance of the newly formed SOA from TERP oxidation (OA_{TERP}) versus the OA_{BG} that is initially present and mixed in from the FT, we define a fresh SOA to background OA ratio:

$$r_{FB} = \frac{OA_{TERP}}{OA_{BG}}. \tag{3.5}$$

This ratio can be interpreted as follows: for $r_{FB} \ll 1$ the OA_{BG} dominates and the C_{OA} will be determined by the dilution of this background organic aerosol. When $r_{FB} \sim 1$, there is an equal contribution of background and newly formed OA. For $r_{FB} \gg 1$, the C_{OA} is determined completely by the formation of SOA during the day. However, values of $r_{FB} \gg 1$ are not expected to be common, since the partitioning of the semi-volatile products into the aerosol phase depends on OA_{BG} (see Eq. 4.1 and Fig. 3.2). For an initial OA_{BG} in the FT of $0.2\,\mu g\,m^{-3}$, the $r_{FB} = 0.22$ at 18:50. This further demonstrates the dominating effect of the background aerosol on the C_{OA} in the BL for the case study.

3.3.4 Sensitivity analysis

Response of C_{OA} to land surface conditions

As shown in the previous budget analyses, it is important to reproduce accurately both the BL dynamics and chemistry tendency, since they together determine the concentration of a given

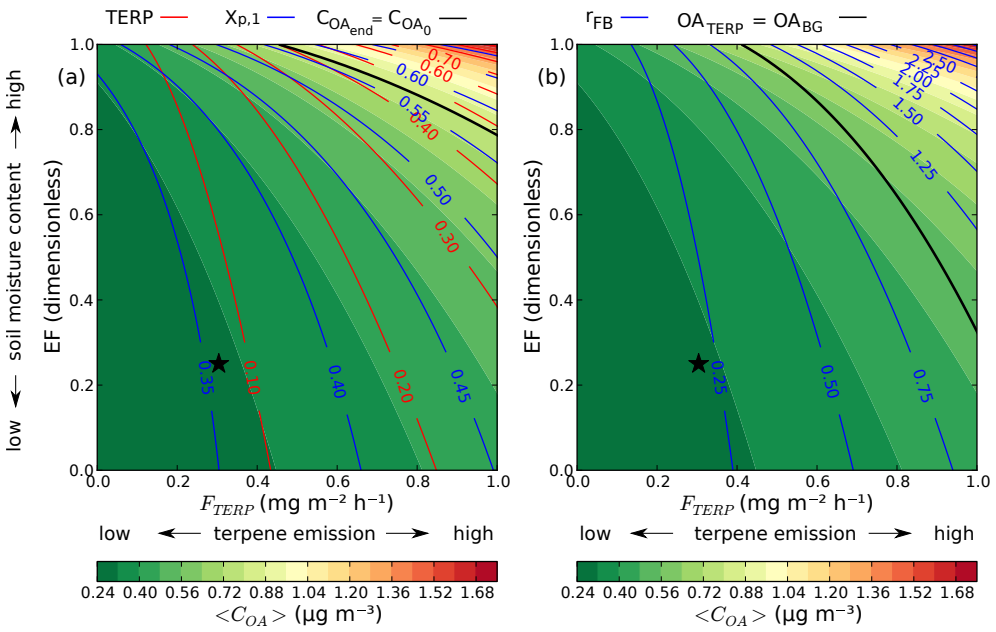

Figure 3.9: ***(a)*** *Sensitivity of organic aerosol concentration C_{OA} and TERP concentration at 18:50 LT to terpene emission (F_{TERP}) and evaporative fraction (EF). Shades indicate organic aerosol concentration C_{OA} ($\mu g\, m^{-3}$), the red contours the TERP concentration ($\mu g\, m^{-3}$), and the blue contours the partitioning coefficient $X_{p,1}$. The black line indicates the conditions for which the C_{OA} at the end of the day equals the initial concentration, and the asterisk indicates the conditions for the case study.* ***(b)*** *Sensitivity of organic aerosol concentration C_{OA} and the OA chemistry background ratio r_{FB} at 18:50 LT to F_{TERP} and EF. Shades indicate C_{OA} ($\mu g\, m^{-3}$) and the blue contours r_{FB}. The black line indicates the conditions for which the C_{OA} consists of equal parts of OA_{TERP} and OA_{BG} ($r_{FB} = 1$), and the asterisk indicates the conditions for the case study.*

species. We therefore extend our analysis to analyze the role of land surface in driving both dynamics and chemistry. The land surface determines how much terpenes are emitted and into what size mixing volume by regulating the partitioning between sensible and latent heat flux (see Fig. 3.7 of the TERP budget). The partitioning of the heat flux governs the growth of the BL, with a much

larger growth when sensible flux dominates over latent heat flux (EF~0), i.e. for dry surface conditions. Under these conditions, the sensible heat flux will strongly heat the BL, which decreases the temperature jump between the BL and FT. This further facilitates the entrainment of warm air from the FT into the BL, which subsequently enhances the BL growth. Conversely, the BL grows less rapidly when the latent heat flux dominates (EF~1) under very

moist surface conditions. This is due to the fact that for a high EF, most available energy is used to evaporate water from the surface and there is little left for BL growth. In Fig. 3.10, typical vertical profiles of θ and q are sketched, to illustrate these effects. Therefore, our first sensitivity analysis addresses the role of different combinations of evaporative fraction (EF) and terpene emission flux (F_{TERP}) on the diurnal evolution of C_{OA}. We explore the complete range of possible conditions of EF: from a BL driven solely by the sensible heat flux (EF = 0) to a BL driven only by the evaporation flux (EF = 1). Similarly, F_{TERP} ranges from 0 to 1 mg m^{-2} h^{-1}, which encompasses the range of terpene fluxes observed at the SMEAR II station (Rinne et al., 2007).

Figure 3.9a shows the calculated C_{OA} and TERP concentration at 18:50. The conditions of EF and F_{TERP} for the case study discussed above are indicated in the figure. As expected, C_{OA} always increases with larger F_{TERP} due to the higher formation rate of biogenic SOA. It also increases with EF, because shallower boundary layers, weaker entrainment and thus less mixing of FT air with low OA concentrations occur when the land surface is dominated by the evaporation flux. The effect on temperature acts in the same direction, i.e. a higher EF leads both to a lower sensible heat flux into the BL and to less entrainment of relatively warm free tropospheric air. Consequently, the temperature in the mixed layer becomes lower. The temperature decreases by 6 K in the experiment going from EF = 0 to EF = 1. Because of the lower temperatures, more semi-volatile material will partition into the aerosol phase, but this has only a minor effect compared to the changes in dilution. This becomes clear from the partitioning coefficient X_{p}, which is shown together with C_{OA} in Fig. 3.9a for the semi-volatile product C_1. X_{p} depends on C_{OA} and T, following Eqs. (4.1) and (3.2). Here, we find that X_{p} closely follows the behavior of C_{OA}, and only a slight deviation from this pattern is caused by the dependence of X_{p} on T. The T dependence is the most pronounced for low EF, when a large sensible heat flux leads to a larger heating of the BL and consequently a large entrainment of relatively warm air from the FT.

Based on the relationship between C_{OA} and TERP concentration, we can distinguish 2 different regimes: one characterized by soils with low moisture content (EF <0.5) and low terpene emissions (F_{TERP} <0.6) and another characterized by high moisture content (i.e. wet soil) and strong terpene emissions. Dry soil causes larger sensible heat fluxes, which lead to rapid BL growth and enhance dilution of C_{OA} due to entrainment of air from the FT. For TERP, on the other hand, the entrainment term has a minor contribution to the total tendency (due to the shorter lifetime of this species), which is dominated by the emissions and the chemical destruction (see Fig. 3.7). Since C_{OA} and TERP are dominated by different processes in this regime, their tendencies are not strongly related. In this regime, the role of entrainment will dominate over that of chemistry.

For a wet soil (EF >0.5) and high emissions (F_{TERP} >0.6), on the other hand, we are in a regime where chemistry plays a larger role in determining the tendency of C_{OA}. Here, the

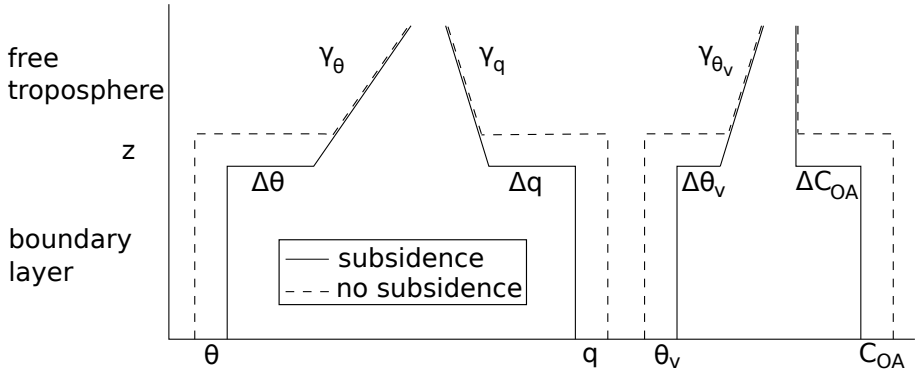

Figure 3.10: Sketches of the vertical profiles of θ, q, θ_v and C_{OA} at the end of the day (18:50), in cases of subsidence and no subsidence. A Δ indicates the jump of a scalar or reactant C defined as $\Delta C = C_{FT} - \langle C \rangle$ and a γ_C the lapse rate of a scalar C in the FT.

larger emission contributes more to the C_{OA} tendency, while the low sensible heat flux results in weak BL growth and entrainment. The combined effect of higher emissions into shallower BL causes a significant contribution of chemistry to the C_{OA} tendency. Only in the upper right corner of Fig. 3.9 do we find conditions for which there is a net increase of C_{OA} during the day, since here condensation outweighs entrainment. These conditions are delimited by the black contour. In this regime, C_{OA} and TERP are strongly related since there the influence of entrainment is relatively small.

The consequences of this sensitivity of C_{OA} for conditions of the case study can be deduced from Fig. 3.9a. C_{OA} at a terpene emission flux of $304\,\mathrm{mg\,m^{-2}\,h^{-1}}$ ranges from 0.30 to $0.62\,\mu\mathrm{g\,m^{-3}}$, a difference of a factor of 2, while the EF increases from 0 to 1. For a constant EF of 0.25 and F_{TERP} ranging from 0 to $1\,\mathrm{mg\,m^{-2}\,h^{-1}}$, C_{OA} could range from 0.26 to $0.49\,\mu\mathrm{g\,m^{-3}}$, a difference of almost a factor of 2. On the other hand, in the dry regime with a low emission there is a large range of conditions of EF and F_{TERP} which can lead to a certain observed C_{OA}. An observed C_{OA} of $0.31\,\mu\mathrm{g\,m^{-3}}$, as in the case study, could result from EF = 0 and $F_{\mathrm{TERP}} = 0.4$, but also from EF = 0.9 and $F_{\mathrm{TERP}} = 0$.

Figure 3.9b shows the behavior of r_{FB} as a function of EF and F_{TERP}. The entrainment and chemistry limited regimes are also well developed here: for low EF and F_{TERP} the background aerosol dominates, while for wet soils (EF > 0.3) and $F_{\mathrm{TERP}} > 0.4$, r_{FB} becomes larger than 1, meaning that there is more $\mathrm{OA_{TERP}}$ present than $\mathrm{OA_{BG}}$. There is a wide range of conditions for which they are equally important: from EF = 1 and $F_{\mathrm{TERP}} \sim 0.4$ to EF $\sim$ 0.3 and $F_{\mathrm{TERP}} = 1$.

Combined response of C_{OA} to subsidence and land surface conditions

As indicated in Fig. 3.1 and in order to complete our analysis, it is interesting to analyze the role of subsidence because on summer days, high pressure systems typically prevent the BL growth by inducing downward air motions. This was, for example, the case over Finland during the HUMPPA-COPEC campaign in summer 2010 (Williams et al., 2011). Further, the soil moisture content determines the partitioning of the surface heat fluxes and thus the energy that is available for BL growth and entrainment.

To understand the influence of subsidence, it is important to note that its effect is twofold: it suppresses BL growth while simultaneously enhancing entrainment. The suppression of BL growth becomes clear when looking at the equation for BL growth, which is the net result of the entrainment velocity w_e on one hand and the subsidence velocity w_s on the other:

$$\frac{dh}{dt} = w_e + w_s. \tag{3.6}$$

In the analysis, we prescribe the large-scale subsidence rate (ω (s^{-1})), defined as the divergence of the horizontal mean wind. It can be thought of as the fraction with which the BL is pushed down each second due to large-scale vertical subsiding motions. The subsidence velocity (w_s ($m\,s^{-1}$)), with a typical order of magnitude of $10^{-2}\,m\,s^{-1}$, is therefore in our modeling approach represented as:

$$w_s = -\omega\, h. \tag{3.7}$$

To understand the effects of subsidence on entrainment, we need to analyze the expression to calculate w_e. It is a function of the buoyancy flux and the virtual potential temperature jump between the BL and the FT ($\Delta\theta_v$) (van Heerwaarden et al., 2009):

$$w_e = \frac{\beta\overline{(w'\theta'_v)}_s}{\Delta\theta_v} \tag{3.8}$$

where β is the (fixed) ratio between the entrainment and surface buoyancy flux (dimensionless), $\overline{(w'\theta'_v)}_s$ is the surface buoyancy flux ($K\,m\,s^{-1}$), and $\Delta\theta_v$ is the jump of the virtual potential temperature between the BL and FT, defined as:

$$\begin{aligned}\Delta\theta_v &= \Delta\theta + 0.61(\langle q\rangle\Delta\theta + \langle\theta\rangle\Delta q + \Delta\theta\Delta q) \\ &\simeq \Delta\theta + 0.61\langle\theta\rangle\Delta q\end{aligned} \tag{3.9}$$

where $\Delta\theta$ and Δq are the differences in θ and q between the BL and the FT, respectively. Figure 3.10 shows sketches of typical vertical profiles of θ, q, θ_v and C_{OA} for conditions with and without subsidence to illustrate these effects.

For a constant EF, the buoyancy flux and therefore the numerator in Eq. (3.8) remain

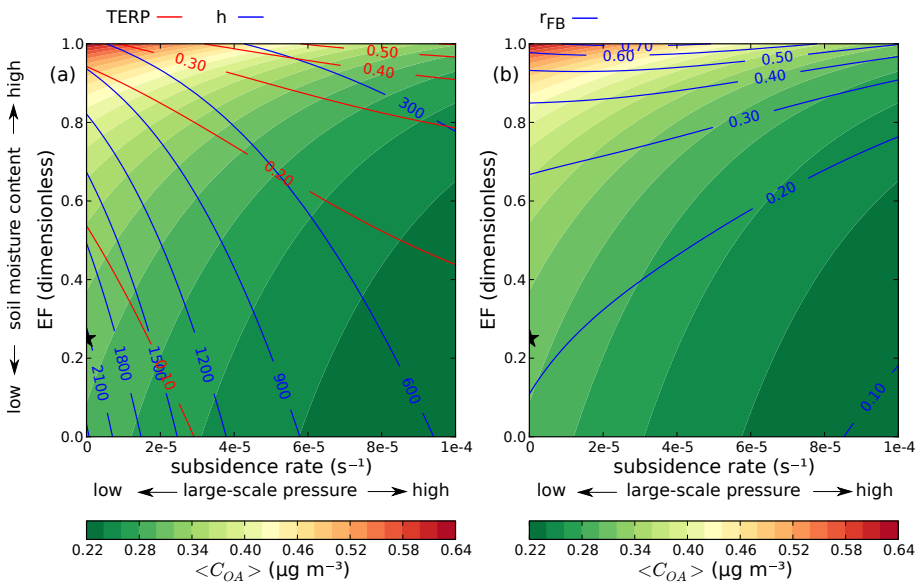

Figure 3.11: ***(a)*** *Sensitivity of organic aerosol concentration (C_{OA}), BL height (h) and TERP concentration at 18:50 LT to subsidence and evaporative fraction (EF). Shades indicate C_{OA} ($\mu g\, m^{-3}$), the blue contours h (m), and the red contours TERP concentration ($\mu g\, m^{-3}$).* ***(b)*** *Sensitivity of C_{OA} and the the OA chemistry background ratio (r_{FB}) at 18:50 LT to subsidence and evaporative fraction (EF). Shades indicate C_{OA} ($\mu g\, m^{-3}$) and the blue contours r_{FB} (–). The asterisk indicates the conditions for the case study.*

constant. Consequently, subsidence only affects w_e through $\Delta\theta_v$. In case of subsidence, the same amount of sensible heat is introduced into a shallower BL, so $\langle\theta\rangle$ increases and $\Delta\theta$ decreases. The specific moisture ($\langle q\rangle$), however, decreases with subsidence, because the increase in moisture due to evaporation into a smaller mixing volume is offset by the enhanced entrainment of dry air. Δq is therefore smaller in the case with subsidence. Taken together, these effects result in a smaller $\Delta\theta_v$ in the case of subsidence: the effect of $\Delta\theta$ on $\Delta\theta_v$ is only partly compensated by the effect of Δq through the second term on the RHS of Eq. (3.9). In all our experiments, we find that w_e is enhanced when subsidence increases. This means that the enhanced entrainment due to a stronger heating of the BL is further enhancing itself by diminishing $\Delta\theta_v$. For EF = 1, the daily average w_e ranges from 1 cm s^{-1} when there is no subsidence to 2 cm s^{-1} for $\omega = 1{\cdot}10^{-4}\ s^{-1}$.

Figure 3.11a shows the sensitivity of C_{OA} to EF, ranging from 0 to 1, and subsidence ranging from no subsidence ($\omega = 0\ s^{-1}$) to strong subsidence ($\omega = 1{\cdot}10^{-4}\ s^{-1}$). By increasing EF, BL height decreases and both C_{OA} and TERP concentration increase. As in the previous sensitivity analysis, the highest sensitivity is found for wet soils. BL height decreases rapidly

when EF > 0.8, which leads to an increase of C_{OA} by ~ 50 % over the whole subsidence range, e.g. from 0.31 to 0.44 $\mu g\,m^{-3}$ at $\omega = 5{\cdot}10^{-5}\ s^{-1}$. TERP concentration doubles for an EF ranging from 0.8 to 1.0, e.g. from 0.24 to 0.48 $\mu g\,m^{-3}$ at $\omega = 5{\cdot}10^{-5}\ s^{-1}$. However, C_{OA} decreases while TERP concentrations increase with stronger subsidence. For C_{OA}, this is because there is a stronger dilution due to entrainment with increasing subsidence. Since OA has a large background fraction compared to the production of SOA from TERP (Fig. 3.8), the enhanced dilution means that C_{OA} decreases despite the lower BL height. TERP concentrations, on the other hand, increase with larger subsidence values, because they are emitted into a shallower BL. Enhanced entrainment partly compensates for this, but has only a small effect on the TERP concentration due to the relatively short lifetime of this species (see also Fig. 3.7). The consequence is that under all conditions considered in our case study, the behavior of C_{OA} is unrelated to that of TERP, due to the different roles that entrainment, emission and chemistry have on their respective budgets.

Figure 3.11b shows the behavior of r_{FB} for varying subsidence and EF. r_{FB} is always below 1, because of the low formation of OA_{TERP} due to a low F_{TERP}. It increases with EF, because both C_{OA}, which enhances the partitioning into the aerosol phase, and TERP increase. For a changing ω and low EF (< 0.8), it decreases with increasing ω, because the enhanced dilution of OA_{BG} affects the partitioning negatively. For EF > 0.8, however, r_{FB} shows some interesting nonlinear behavior: at $\omega = 4{\cdot}10^{-5}$, r_{FB} has a maximum, because there the combination of a high TERP concentration and a high X_p, caused by high C_{OA}, result in the partitioning of a large fraction of C_i into the aerosol phase.

3.4 Conclusions

We have studied the integrated effects of land surface, chemistry, and entrainment on the diurnal evolution of SOA, using MXLCH-SOA, a model that reproduces the dynamics of a diurnal convective atmospheric boundary layer and the chemical transformations of terpenes and their oxidants that lead to SOA formation (Fig. 3.1).

MXLCH-SOA is able to reproduce the diurnal variability of SOA production and relate it with the observed dynamics and gas-phase chemistry for a characteristic case study in the boreal forest. Our findings indicate the importance of including entrainment to explain the observed diurnal cycle in SOA concentration, and suggest that entrainment may contribute ten times more to the total tendency than SOA production during daytime. This contribution is due to a large volume of air that is entrained from the residual layer during the rapid growth of the boundary layer in the morning. A sensitivity analysis further suggests that the boreal forest is in a regime where relatively low terpene emissions are the limiting factor for SOA formation. For environments or situations with wet soils and high VOC emissions, e.g.

the tropics, the effects of entrainment may be weaker, and the SOA concentration and VOC concentration may therefore show a stronger relationship. Furthermore, we also find that under conditions of subsidence there is no straightforward relation between organic aerosol concentrations and terpene concentrations.

Measured SOA and VOC concentrations are the net result of emissions, chemistry and dynamics. To interpret these measurements, it is important to include observations of all of these components in the design of field campaigns. More specifically, the role of the increase of SOA during the night both in the residual layer and in the nocturnal stable boundary layer will be an important factor to understand, since for most studied situations, the SOA evolution during daytime is mainly driven by entrainment. Therefore, it is essential to have early morning profiles of C_{OA} to characterize both the initial concentration in the nocturnal stable BL and the organic aerosol that has built up in the residual layer, because this will be entrained into the convective boundary layer during the morning. Further, to understand ambient SOA concentrations it may be equally important to characterize BL height and entrainment as it is to understand the temperature dependence of the saturation concentration of the semi-volatile species.

Our findings are also important for regional and global modeling studies: the strong sensitivity of C_{OA} to land surface and FT conditions means that uncertainties in the representation of these components may strongly affect the simulated C_{OA}. To model C_{OA} accurately, large-scale models should be able to reproduce the coupling between the land surface, boundary layer dynamics, free troposphere conditions and chemistry and the resulting behavior of organic aerosol and terpene concentrations as presented in the sensitivity analyses. Due to the wide range of conditions under study (Figs. 3.9 and 3.11), our findings can be used to quantify the uncertainty that arises from inaccurately representing these processes in large-scale models. Besides, our results indicate that box models are only applicable for studying ambient SOA formation when they account for boundary layer growth and entrainment and when background organic aerosol levels are well constrained.

Future research on the diurnal evolution of SOA concentrations will include an interactive land surface, since both surface heat fluxes (van Heerwaarden et al., 2009) and terpene emissions (Guenther et al., 1995; Niinemets et al., 2010) are the result of the interaction of the BL with the land surface.

In summary, our findings indicate that in order to understand the diurnal evolution of SOA in the boundary layer the coupled effects of the land surface, dynamics of the atmospheric boundary layer, chemistry, and free troposphere conditions should be studied simultaneously. A balanced representation of all these processes should be considered when preparing and conducting both field campaigns and modeling.

Appendix: Derivation of the C_{OA} budget

We derive the budget equation of C_{OA} by taking the time derivative of Eq. (4.1):

$$\frac{dC_{\mathrm{OA}}}{dt} = \frac{d\mathrm{OA}_{\mathrm{BG}}}{dt} + \sum_i \left[X_{p,i} \frac{dC_i}{dt} + C_i \frac{dX_{p,i}}{dt} \right]. \tag{3.10}$$

If $C_i \frac{dX_{p,i}}{dt} \ll X_{p,i} \frac{dC_i}{dt}$, which is the case for our case study, the former term can be ignored and then Eq. (3.10) reduces to:

$$\frac{dC_{\mathrm{OA}}}{dt} \simeq \frac{d\mathrm{OA}_{\mathrm{BG}}}{dt} + \sum_i X_{p,i} \frac{dC_i}{dt}. \tag{3.11}$$

The individual terms can be further written out as:

$$\frac{d\mathrm{OA}_{\mathrm{BG}}}{dt} = \overbrace{\frac{w_e \Delta \mathrm{OA}_{\mathrm{BG}}}{h}}^{\text{entrainment}} \tag{3.12}$$

$$\frac{dC_i}{dt} = \overbrace{\frac{w_e \Delta C_i}{h}}^{\text{entrainment}} + \overbrace{\sum_j \alpha_i k_j \langle \mathrm{TERP} \rangle \langle \mathrm{OX}_j \rangle}^{\text{chemistry}}. \tag{3.13}$$

4

Influence of meteorological forcings and isoprene chemistry on the organic aerosol budget in a tropical forest

We study the organic aerosol (OA) budget in a tropical forest by analyzing a case that is representative for the OP3 campaign at Borneo. A model is designed that aims for a balanced representation of the chemical and meteorological processes that drive the diurnal evolution of reactants in the atmospheric boundary layer (BL). The model is able to reproduce the observed diurnal dynamics of the BL, including the evolution of most chemical species involved in secondary organic aerosol (SOA) formation. A budget analysis reveals a clear signal of the entrainment process in the diurnal evolution of SOA. Further, we perform a series of sensitivity analyses to determine the effect of meteorological forcings and isoprene chemical pathways on the OA budget. Subsidence and advection of cool air have opposing effects on the OA concentration, although both suppress BL growth. Recycling of the OH radical in the oxidation of isoprene may affect the amount of SOA that is formed, but must be understood better before its impact can be definitely

This chapter is based on: R. H. H. Janssen, J. Vilà-Guerau de Arellano, J. L. Jimenez, L. N. Ganzeveld, N. H. Robinson, J. D. Allan, H. Coe and T. A. M. Pugh, Influence of meteorological forcings and isoprene chemistry on the organic aerosol budget in a tropical forest, submitted to J. Geophys. Res.

determined. SOA formation from isoprene is calculated for both the low- and high-NO_x pathway, with the latter dominating the isoprene peroxy radical chemistry. Further, we implement a parametrization that accounts for the effect of the NO_2/NO ratio on isoprene SOA formation. In a final analysis, we study the significance of SOA formation through the reactive uptake of isoprene epoxydiols (IEPOX) on acidic sulfate aerosol. Despite the incorporation of these new pathways, the OA concentration is systematically underestimated by about a factor of 2.

4.1 Introduction

Tropical forests are potentially an important source of biogenic secondary organic aerosol (SOA), due to high emissions of isoprene and terpenes (Langford et al., 2010; Karl et al., 2007) and potentially high concentrations of their most important oxidant, the hydroxyl radical (OH) (Lelieveld et al., 2008). Recently, a number of measurement campaigns have been conducted to gain insight in the sources and formation mechanisms of SOA in forests in Amazonia (AMAZE, Chen et al., 2009), West-Africa (AMMA, Capes et al., 2009) and South-East Asia (OP3, Robinson et al., 2011a,b, 2012). When interpreting observations made in the atmospheric boundary layer (BL) during these campaigns, it is important to realize that the evolution of chemical species in the BL is a function of chemical conversion, emission/deposition, advection and the vertical exchange of compounds between the free troposphere (FT) and the BL driven by entrainment (Vilà-Guerau de Arellano et al., 2009; Ouwersloot et al., 2012) and gas/particle partitioning in case of SOA. In addition, subsidence and advection of heat and moisture influence the growth of the BL and therefore modify its dilution capacity and the exchange of species between the BL and FT, as controlled by entrainment (Ouwersloot et al., 2012). Here, we investigate the diurnal budget of OA by combining a model with observations from the OP3 campaign.

There is still a considerable gap between the understanding of ambient biogenic SOA and the ability of models to reproduce its observed concentration. Both Capes et al. (2009) and Chen et al. (2009) underestimated SOA concentrations in isoprene-dominated tropical environments but could not rule out the possibility of canceling errors, due to the limited observational constraints on these estimates. These sources of uncertainty were the identification and emission rates of biogenic SOA precursors, SOA formation mechanisms, oxidant concentrations, the SOA particle mass yields, the influence of vertical mixing and advection, and the unknown contribution of the background OA concentration (OA_{BG}). On the other hand, Slowik et al. (2010) were able to reproduce observed OA concentrations in a rural environment dominated by terpene emissions. Sjostedt et al. (2011), however, underestimated OA compared to the measurements in an environment where isoprene was more abundant,

both using the same model as Slowik et al. (2010) and an approach based on VOC destruction rates.

The underestimation of modeled OA in environments with high isoprene emissions may be due to a lack of understanding of the chemical pathways that lead to the formation of SOA from isoprene (ISOA). Current parameterizations of ISOA formation are therefore subject to large uncertainties (Carlton et al., 2009). More specifically, Surratt et al. (2010) suggested that peroxy methacryloyl nitrate (MPAN) and isoprene epoxydiols (IEPOX) are important intermediate gas-phase species under high- and low-NO_x conditions, respectively. The mechanisms of SOA formation through these reaction pathways have only recently started to be explored (Paulot et al., 2009; Surratt et al., 2010; Chan et al., 2010; Lin et al., 2012b).

Another issue related to isoprene chemistry in tropical forests, is the mismatch between measurements and theoretical calculations of OH concentrations, which has been attributed to regeneration of OH in the oxidation of isoprene (Lelieveld et al., 2008). Several mechanistic pathways leading to OH recycling have been proposed, but none of them has been able to explain the gap between measurements and models (Stone et al., 2011). Taraborrelli et al. (2012) recently formulated a detailed mechanism for isoprene oxidation by assembling and completing several previously proposed mechanisms, with which they were able to reproduce OH concentrations under pristine tropical conditions to within the bounds of the measurement uncertainty. Another point of view was presented by Mao et al. (2012), who suggested that the high observed OH concentrations may be the result of a measurement artifact. Their findings, however, are very much dependent on instrument design and environmental conditions. The effect of OH recycling on SOA formation has so far been subject of only one study (Lin et al., 2012a) and it is still unclear how the formation of ISOA forming products depends on OH concentrations (Carlton et al., 2009).

The OP3 campaign provides a challenging case since the aerosol at Borneo is influenced by complex terrain and multiple sources. The measurement tower is located on top of a 200 m hill, which means that it could be influenced by anabatic flows, which are upslope flows driven by heating of the slope by insolation (e.g. Thunis and Bornstein, 1996). The proximity of the coast means that the site may be influenced by sea breeze circulations (Robinson et al., 2012) and heterogeneities at smaller spatial scales can induce advection of heat, moisture and chemical species (Ouwersloot et al., 2011). Moreover, the aerosol has multiple sources: Robinson et al. (2012) investigated the effect of the island on the vertical distribution of aerosol through the troposphere, based on aircraft observations and showed that air is enriched in OA as it passes over the island, which indicates a large on-island source of biogenic SOA. An analysis of air mass back trajectories for the site based on ECMWF wind fields, however, revealed that during the campaign there was no period during which the rain forest was the only source of aerosol and that significant levels of (off-island) sulfate aerosol

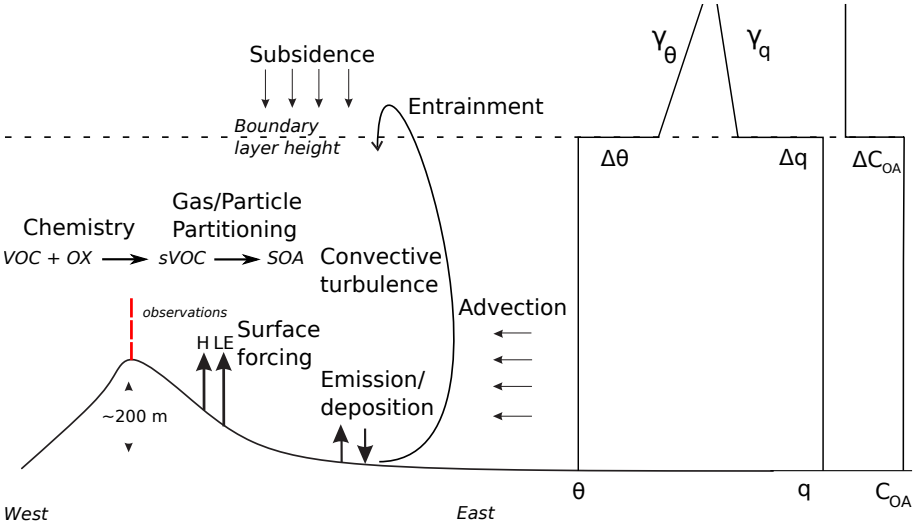

Figure 4.1: Conceptual representation of the main dynamic and chemical contributions to the organic aerosol budget during the OP3-campaign and sketches of typical vertical profiles of potential temperature (θ), specific humidity (q) and organic aerosol concentration (C_{OA}).

were transported to the site (Robinson et al., 2011b). This is in contrast with the Amazon, which experiences periods with predominant in-basin influences during which biogenic SOA dominates the aerosol mass (Chen et al., 2009).

Extending on the work of Robinson et al. (2011b, 2012), we focus on the interpretation of ground-based OA measurements made during OP3 and how various dynamic and chemical terms contribute to the aerosol budget. A schematic overview of these factors is presented in Fig. 4.1. We aim for an integrated and balanced approach, by accounting for atmospheric processes acting on different spatial scales and for chemical processes, related to both gas-phase and secondary aerosol chemistry and partitioning. In our study we overcome some of the previously mentioned issues by prescribing VOC emissions as constrained by above-canopy flux measurements, by accounting for entrainment and by performing an experiment in which OH concentrations are matched with observations by including OH regeneration in isoprene oxidation in the model. Since this case is well-constrained with data it gives the opportunity to assess which processes contribute most to these large uncertainties and we shed some light on some other factors that are not that well-constrained and are yet uncertain or difficult to estimate, for example subsidence.

To this end, we use MXLCH-SOA, a 0-D model for the dynamics of the convective boundary layer which includes gas-phase chemistry and gas/particle partitioning (Janssen

et al., 2012). The model is updated to include SOA from isoprene using the volatility basis set (VBS) approach. After examining the complete data set, we select a representative case study, discuss the performance of the model when compared to the case study observations and show the contributions of several factors to the budget of OA and its precursors. Then, we analyze the impact of large-scale meteorological forcings on the OA concentration, discuss the potential role of OH recycling in SOA formation, discuss the influence of NO_2/NO ratio on the formation of MPAN SOA, and analyze the formation of SOA from IEPOX. The latter has been suggested to yield a specific tracer (hereinafter called 82Fac) (Lin et al., 2012b) that is present in the OA observed by an aerosol mass spectrometer (AMS) at Borneo (Robinson et al., 2011a).

4.2 Methods

4.2.1 Observations of the diurnal variability during OP3

Data gathered during the OP3 campaign enable us to study the diurnal variation of atmospheric compounds modulated by surface and BL processes. OP3 was conducted in Malaysia in 2008 (Hewitt et al., 2010) and here we use data from OP3 III (23 June to 20 July) at the Bukit Atur Global Atmospheric Watch station, located in the Danum Valley rain forest conservation area in Sabah, Borneo (4°58′ N, 117°50′ E, 426 m a.s.l.). The site was located in a clearing at the top of a 200 m hill, above most of the surrounding forest. The observations were made from a measurement tower of 100 m on top of this hill and measurement heights in this paper are indicated as height relative to the base of the tower. Figure 4.1 shows a schematic overview of the measurement setting and processes that potentially influence the formation and evolution of local OA.

Figure 4.2 shows mean diurnal cycles during OP3 III, based on half-hourly averages over a period of 4 weeks. It includes the most representative dynamic, surface and chemistry variables, as represented by potential temperature (θ), isoprene flux (F_{ISO}), isoprene concentration (ISO) and concentration of OOA2, an oxidized organic aerosol (OOA) factor, respectively. θ rises during the day due to the sensible heat flux and entrainment of warm air, F_{ISO} follows a diurnal cycle driven by temperature and light intensity (Langford et al., 2010), ISO follows F_{ISO}, but is also modified by chemical transformations and BL dynamics, and the full complexity of the behavior of OOA2 is under study here.

We selected one representative day for which we initialize and evaluate the diurnal evolution of chemistry and dynamics of our model with observations: 7 July 2008. To determine the representativeness of this specific day for a typical day at the measurement site during OP3 III, we compared observations from this day to the campaign mean (Fig. 4.2). Similar diurnal trends are present in the data of the case study and in the campaign averages. Ad-

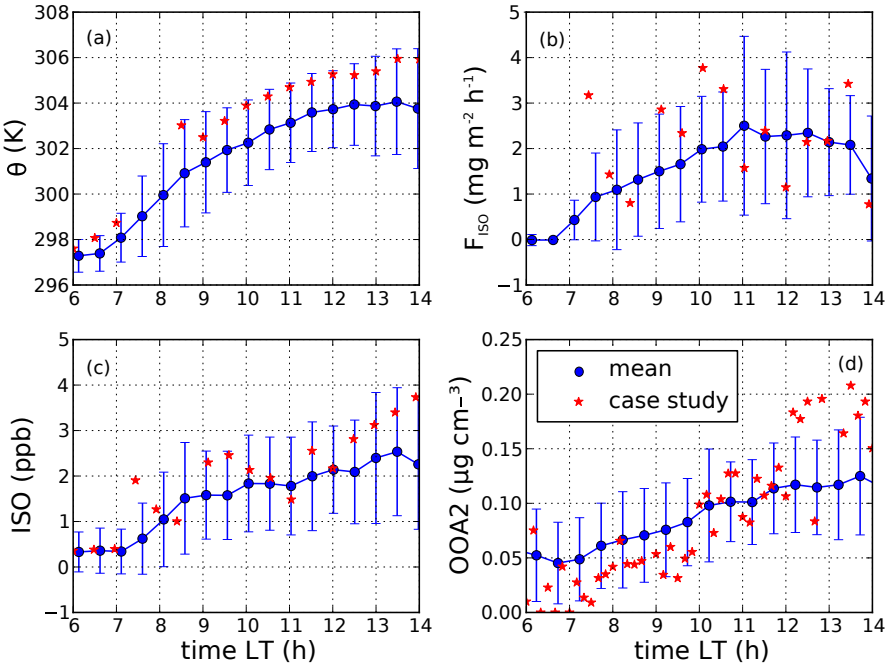

Figure 4.2: Campaign mean and case study diurnal evolution of measured a) potential temperature (θ), b) isoprene emission flux (F_{ISO}), c) isoprene concentration (ISO) and d) concentration of the SV-OOA factor (OOA2). The error bars indicate the standard deviation.

ditionally, the observations from the case study fall within the standard deviation of these averages, except for OOA2 in the afternoon.

Furthermore, the selection of this day is based on the relatively smooth evolution of the surface heat fluxes during this day, which ensures convection and turbulent mixing occurring throughout the BL. Additionally, the observed diurnal cycle of the ozone photolysis rate jO^1D followed the theoretical clear sky diurnal evolution relatively smoothly compared to other days during the campaign, although there were some fluctuations, probably caused by clouds (not shown). These conditions were valid until ~14:00 LT. After 14:00, temperature dropped drastically and also moisture and concentrations of chemical species suddenly changed. Possible explanations for such behavior are the formation of clouds or the arrival of the sea breeze at the site. To avoid the complex transport and chemistry associated with the presence of clouds on top of the BL, we finalize our analysis at 14:00 and focus on the period with strong boundary layer growth and OA formation. The validity of the assumption of a well-mixed layer during this day is further supported by vertical profiles of O_3 and NO_x, which were obtained by measuring these species at several heights between 5 and 75 m (not

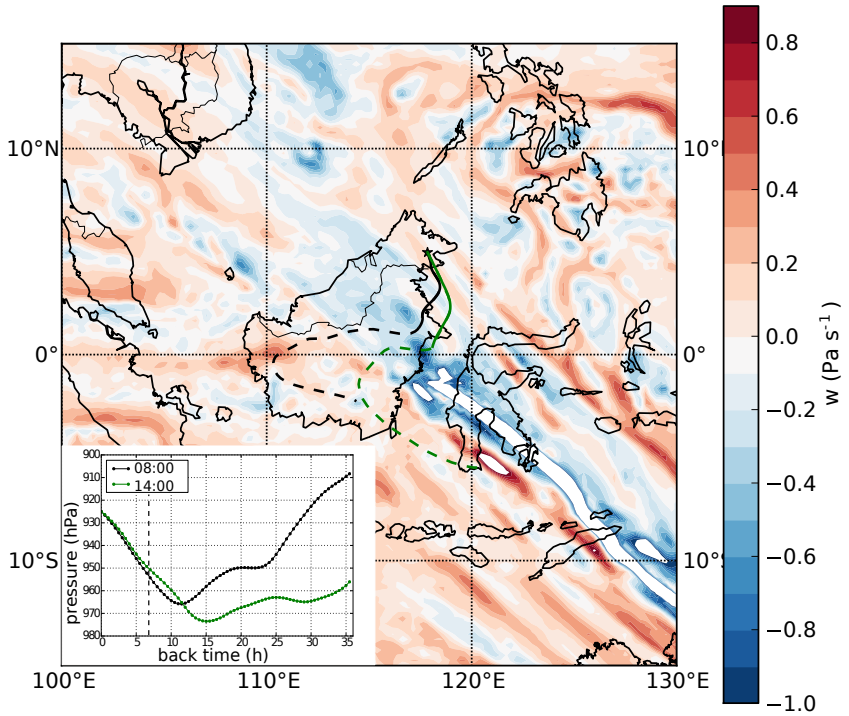

Figure 4.3: Vertical wind speed w at 850 hPa at 14:00 LT on 7 July 2008 and 120 (dashed lines) and 36 h (solid lines) air mass back-trajectories arriving at Bukit Atur at 08:00 (black) and 14:00 (green), respectively, at a pressure altitude of 925 hPa. Note that positive values of vertical wind speed reflect subsidence, since it is expressed in units of pressure. Both are based on ECMWF wind fields with a resolution of 1.125°×1.125°. The inset shows the pressure level of the back-trajectories with the dotted line indicating their arrival time over land.

shown). Especially from 45 m upwards, O_3 and NO_2 measurements are very similar at different heights, indicating that above this height we are probing mixing ratios within the BL. On the other hand, this means that observations below 45 m could be in the surface layer and may therefore deviate from mixed-layer values.

Finally, an important reason for the selection of this day is the availability of the most complete data set of dynamics, gas-phase chemistry (most importantly VOCs and oxidants) and OA. Upper air observations of OA concentrations are potentially very useful for understanding the evolution of OA in the BL (Janssen et al., 2012). While several vertical profiles of OA over the measurement site have been obtained, unfortunately no flight was carried out on this particular day (Robinson et al., 2012). Therefore, we use observations from other days to get an estimate of FT OA concentrations.

On 7 July 2008, the measurement site was influenced by air masses arriving from the South-East (Fig. 4.3), which means that the air masses were affected by substantial amounts of both off-island and on-island emissions. Consequently they contained sulfate aerosol from off-island sources and were affected by isoprene emissions from oil palm plantations located to the South East of the observational site (see Hewitt et al. (2010) for a detailed land-use map). The air masses traveled about 7 h over land before arriving at the measurement site. The pressure altitude during the period over land indicates that the air masses were close to the surface and within the BL. An additional meteorological factor important for our research is the presence of subsiding air motions. The site and its surroundings were influenced by subsidence, as can be inferred from ECMWF reanalysis fields of vertical velocity at the 850 hPa level (Fig. 4.3). The downward movement of air with 0.2 Pa s^{-1} over Bukit Atur corresponds with a vertical velocity of -2 cm s^{-1}.

4.2.2 Description of MXLCH-SOA

A full description of MXLCH-SOA is given in Janssen et al. (2012) and references therein. In short, it describes the dynamics of a convective BL, which is considered to be well-mixed (Tennekes, 1973), coupled to a reduced chemistry scheme which contains the essentials of the O_3-NO_x-VOC-HO_x system (Vilà-Guerau de Arellano et al., 2011) and gas/particle-partitioning using the VBS approach (Donahue et al., 2006). At each time step, the total organic aerosol concentration C_{OA} is calculated from:

$$C_{\mathrm{OA}} = \sum_i (X_{p,i} C_i) + \mathrm{OA_{BG}}\,; \quad X_{p,i} = \left(1 + \frac{C_i^*}{C_{\mathrm{OA}}}\right)^{-1}, \tag{4.1}$$

where C_{OA} is the organic aerosol mass concentration (μg m^{-3}), $X_{p,i}$ is the fraction of semi-volatile compound i in the aerosol phase (dimensionless), C_i is the concentration of the semi-volatile organic compound (SVOC), originating from isoprene (IC_i) or terpene (TC_i) (μg m^{-3}), $\mathrm{OA_{BG}}$ the background organic aerosol concentration (μg m^{-3}), which is assumed to be non-volatile, and C_i^* is the effective saturation concentration of compound i (μg m^{-3}).

SOA formation from isoprene is implemented in two ways. In the default mechanism, as used in the base case, SVOCs originate directly from first-step oxidation of isoprene by OH (Table 4.1) using yields derived from lab studies (Kroll et al., 2006), which is common practice in air quality models (e.g. Slowik et al., 2010; Tsimpidi et al., 2010). Oxidation of isoprene by OH produces both the SVOC species IC_i and IRO_2, an isoprene peroxy radical, which further influences the gas-phase chemistry and therewith OH regeneration. IC_i partition into the aerosol phase, together with the SVOCs formed from terpene oxidation (TC_i). The only difference between the isoprene and terpene oxidation products is their molecular weight (136 and 180 g mol^{-1}, respectively). The SVOC yields strongly depend on NO_x con-

Table 4.1: Chemical reaction scheme used in the reduced scheme with T the absolute temperature in Kelvin and χ the solar zenith angle. First-order reaction rates are in s^{-1}, second-order reaction rates in $cm^3\ molecule^{-1}s^{-1}$. Aerosol-forming reactions and products are printed in bold font. $\alpha_1^I - \alpha_3^I$ and $\alpha_1^T - \alpha_4^T$ are stoichiometric coefficients for ISO and TERP, respectively, see Table 4.2. In R20 n is the rate of OH-recycling, PRODUCTS are species which are not further evaluated in this chemical reaction scheme. Reaction of ISO with O_3 is not considered.

Number			Reaction	Reaction Rate
R1	$O_3 + h\nu$	$\rightarrow$	$O^1D + O_2$	$3.00 \cdot 10^{-5} \cdot e^{\frac{-0.575}{cos(\chi)}}$
R2	$O^1D + H_2O$	$\rightarrow$	2OH	$1.63 \cdot 10^{-10} \cdot e^{\frac{60}{T}}$
R3	$O^1D + N_2$	$\rightarrow$	O_3	$2.15 \cdot 10^{-11} \cdot e^{\frac{110}{T}}$
R4	$O^1D + O_2$	$\rightarrow$	O_3	$3.30 \cdot 10^{-11} \cdot e^{\frac{55}{T}}$
R5	$NO_2 + h\nu$	$\rightarrow$	$NO + O_3$	$1.67 \cdot 10^{-2} \cdot e^{\frac{-0.575}{cos(\chi)}}$
R6	$CH_2O + h\nu$	$\rightarrow$	HO_2	$1.47 \cdot 10^{-4} \cdot e^{\frac{-0.575}{cos(\chi)}}$
R7	OH + CO	$\rightarrow$	$HO_2 + CO_2$	$2.40 \cdot 10^{-13}$
R8	$OH + CH_4$	$\rightarrow$	CH_3O_2	$2.45 \cdot 10^{-12} \cdot e^{\frac{-1775}{T}}$
R9	**OH + ISO**	$\rightarrow$	$IRO_2 + \alpha_1^I\mathbf{IC_1} + \alpha_2^I\mathbf{IC_2} + \alpha_3^I\mathbf{IC_3}$	$2.70 \cdot 10^{-11} \cdot e^{\frac{390}{T}}$
R10	OH + [MVK+MACR]	$\rightarrow$	$HO_2 + CH_2O$	$2.40 \cdot 10^{-11}$
R11	$OH + HO_2$	$\rightarrow$	$H_2O + O_2$	$4.80 \cdot 10^{-11} \cdot e^{\frac{250}{T}}$
R12	$OH + H_2O_2$	$\rightarrow$	$H_2O + HO_2$	$2.90 \cdot 10^{-12} \cdot e^{\frac{-160}{T}}$
R13	$HO_2 + O_3$	$\rightarrow$	$OH + 2O_2$	*
R14	$HO_2 + NO$	$\rightarrow$	$OH + NO_2$	$3.50 \cdot 10^{-12} \cdot e^{\frac{250}{T}}$
R15	$CH_3O_2 + NO$	$\rightarrow$	$HO_2 + NO_2 + CH_2O$	$2.80 \cdot 10^{-12} \cdot e^{\frac{300}{T}}$
R16	$IRO_2 + NO$	$\rightarrow$	$HO_2 + NO_2 + CH_2O + 0.6$[MVK+MACR]	$1.00 \cdot 10^{-11}$
R17	$OH + CH_2O$	$\rightarrow$	HO_2	$5.50 \cdot 10^{-12} \cdot e^{\frac{125}{T}}$
R18	$2HO_2$	$\rightarrow$	$H_2O_2 + O_2$	**
R19	$CH_3O_2 + HO_2$	$\rightarrow$	PRODUCTS	$4.10 \cdot 10^{-13} \cdot e^{\frac{750}{T}}$
R20	$IRO_2 + HO_2$	$\rightarrow$	nOH + PRODUCTS	$1.50 \cdot 10^{-11}$
R21	$OH + NO_2$	$\rightarrow$	HNO_3	$3.50 \cdot 10^{-12} \cdot e^{\frac{340}{T}}$
R22	$NO + O_3$	$\rightarrow$	$NO_2 + O_2$	$3.00 \cdot 10^{-12} \cdot e^{\frac{-1500}{T}}$
R23	$NO + NO_3$	$\rightarrow$	$2NO_2$	$1.80 \cdot 10^{-11} \cdot e^{\frac{110}{T}}$
R24	$NO_2 + O_3$	$\rightarrow$	$NO_3 + O_2$	$1.40 \cdot 10^{-13} \cdot e^{\frac{-2470}{T}}$
R25	$NO_2 + NO_3$	$\rightarrow$	N_2O_5	***
R26	N_2O_5	$\rightarrow$	$NO_3 + NO_2$	****
R27	$N_2O_5 + H_2O$	$\rightarrow$	$2HNO_3$	$2.50 \cdot 10^{-22}$
R28	$N_2O_5 + 2H_2O$	$\rightarrow$	$2HNO_3 + H_2O$	$1.80 \cdot 10^{-39}$
R29	**TERP + O_3**	$\rightarrow$	$\alpha_1^T\mathbf{TC_1} + \alpha_2^T\mathbf{TC_2} + \alpha_3^T\mathbf{TC_3} + \alpha_4^T\mathbf{TC_4}$	$5.00 \cdot 10^{-16} \cdot e^{\frac{-530}{T}}$
R30	**TERP + OH**	$\rightarrow$	$\alpha_1^T\mathbf{TC_1} + \alpha_2^T\mathbf{TC_2} + \alpha_3^T\mathbf{TC_3} + \alpha_4^T\mathbf{TC_4}$	$1.21 \cdot 10^{-11} \cdot e^{\frac{436}{T}}$

* $k = 2.03 \cdot 10^{-16} \cdot (\frac{T}{300})^{4.57} e^{\frac{693}{T}}$

** $k = (k1+k2)/k3$; $k1 = 2.21 \cdot 10^{-13} \cdot e^{\frac{600}{T}}$; $k2 = 1.91 \cdot 10^{-33} \cdot e^{\frac{980}{T}} \cdot c_{air}$; $k3 = 1 + 1.4 \cdot 10^{-21} \cdot e^{\frac{2200}{T}} \cdot c_{H_2O}$

*** $k = 0.35 \cdot (k_0 k_\infty)/(k_0 + k_\infty)$; $k_0 = 3.61 \cdot 10^{-30} \left(\frac{T}{300}\right)^{-4.1} \cdot c_{N_2}$; $k_\infty = 1.91 \cdot 10^{-12} \left(\frac{T}{300}\right)^{0.2}$

**** $k = 0.35 \cdot (k_0 k_\infty)/(k_0 + k_\infty)$; $k_0 = 1.31 \cdot 10^{-3} \left(\frac{T}{300}\right)^{-3.5} \cdot e^{\frac{-11000}{T}} \cdot c_{N_2}$; $k_\infty = 9.71 \cdot 10^{14} \left(\frac{T}{300}\right)^{0.1} \cdot e^{\frac{-11080}{T}}$

Table 4.2: Stoichiometric coefficients at $T = 298\,K$ for the different volatility bins of the SOA precursor categories TERP and ISO, with saturation concentration C_i^* in $\mu g\,m^{-3}$ from Tsimpidi et al. (2010).

i	1	2	3	4
C_i^*	1	10	100	1000
TERP, low-NO_x	0.107	0.092	0.359	0.600
TERP, high-NO_x	0.012	0.122	0.201	0.500
ISO, low-NO_x	0.009	0.030	0.015	–
ISO, high-NO_x	0.001	0.023	0.015	–

centrations and we account for this by linearly interpolating the high- and low-NO_x yields (Table 4.2) as a function of the branching of the reaction of RO_2 from isoprene and terpenes through the NO and the HO_2 channel, respectively (Lane et al., 2008b).

In the default mechanism, we omit the formation of IEPOX of which markers are present in the OA at the site (Robinson et al., 2011a; Lin et al., 2012b). In a sensitivity analysis we include a first-order estimate of ISOA from this new pathway. In future studies, MXLCH-SOA could be used to evaluate the performance of more detailed ISOA forming mechanisms.

In our reduced chemical mechanism (Table 4.1), the gas-phase oxidation of isoprene is highly simplified and all first generation products of isoprene oxidation are lumped into a single species, which combines methyl vinyl ketone and methacrolein (MVK+MACR). Together, they have a yield of 60% (e.g. Karl et al., 2009). In the comparison with observations, it is important to note that in the PTR-MS measurements that we use here, MVK and MACR are also observed as one lumped species, since they have the same molecular weight.

4.2.3 Initialization of MXLCH-SOA

Initial and boundary conditions are obtained by fitting MXLCH-SOA to the case study observations of dynamics and chemistry, thereby constituting the base case upon which further experiments are based. The initial OA_{BG} in the BL is taken as the total OA concentration, as derived from AMS measurements (Robinson et al., 2011a). An initial BL concentration of 0.60 μg m^{-3} is obtained, consisting of 0.04 μg m^{-3} OOA2, 0.06 μg m^{-3} 82Fac, a factor attributed to IEPOX SOA, 0.30 μg m^{-3} OOA1, a low-volatile OOA factor, and 0.20 μg m^{-3} 91Fac, an OA factor associated with biomass burning (Robinson et al., 2011a,b). The OA_{BG} in the FT is also set to 0.60 μg m^{-3}, i.e. BL OA_{BG} = FT OA_{BG}. Vertical profiles of OA obtained from aircraft observations support the assumption that OA concentrations in the FT over East Borneo can be at most equal to the OA concentrations in the BL, but not higher (Robinson et al., 2012). Since entrainment does not dilute the modeled OA_{BG} when concentrations in BL and FT are equal (see Eq. 4.7), this is the most favorable assumption for

Table 4.3: The initial and boundary conditions in boundary layer (BL) and free troposphere (FT) as obtained from fitting MXLCH-SOA to the case study observations. All initial conditions are imposed at 06:30 LT. Heat fluxes are applied from 06:30 to 14:00 with $\mathrm{H} = \rho c_p \overline{w'\theta'}_s$ *and* $LE = \rho L_v \overline{w'q'}_s$*. t is the time (s) and* t_d *the length of the day (s). The subscripts s and e indicate values at the surface and the entrainment zone, respectively.*

Property	Value
Initial BL height h (m)	300
Subsidence rate ω (s^{-1})	$3{\cdot}10^{-5}$
Surface sensible heat flux $\overline{w'\theta'}_s$ (K m s^{-1})	$0.30 \sin(\pi t/t_d)$
Entrainment/surface heat-flux ratio $\beta = -\overline{w'\theta'}_e/\overline{w'\theta'}_s$ (dimensionless)	0.2
Initial BL potential temperature $\langle\theta\rangle$ (K)	298
Initial FT potential temperature θ_{FT} (K)	303.5
Potential temperature lapse rate FT γ_θ (K m^{-1})	$0.0030_{h<800m}$ $0.0095_{h\geq800m}$
Advection of potential temperature A_θ (K m^{-1}))	$-3{\cdot}10^{-4}$
Surface latent heat flux $\overline{w'q'}_s$ (g kg^{-1} m s^{-1})	$0.16 \sin(\pi t/t_d)$
Initial BL specific humidity $\langle q\rangle$ (g kg^{-1})	11.5
Initial FT specific humidity q_{FT} (g kg^{-1})	11.4
Specific humidity lapse rate FT γ_q (g kg^{-1} m^{-1})	−0.0026

Table 4.4: Initial mixing ratio in BL and FT and surface emission fluxes of the reactants as obtained from fitting MXLCH-SOA to the case study observations. Species in the reaction mechanism that are not included in this table have zero initial concentrations and zero surface emissions.

Species	Initial mixing ratio (ppb)		Surface emission/deposition flux
	BL	FT	(ppb m s^{-1})
O_3	17.5	19.0	$-0.45 \sin\left(\frac{\pi t}{t_d}\right)$
NO	0.05	0.0	$9 \cdot 10^{-3}$
NO_2	0.15	0.10	1.5**
ISO	0.40	0.0	$0.35 \sin\left(\frac{\pi t}{t_d}\right)$
TERP	0.08	0.0	$0.04 \sin\left(\frac{\pi t}{t_d}\right)$
OA_{BG}	0.60*	0.60*	0.0
MVK+MACR	0.0	0.0	2.4**
TC_i	0.0	0.0	2.4**
IC_i	0.0	0.0	2.4**
CH_4	1800.	1800.	0.0
CO	100.	100.	0.0
O_2	$2{\cdot}10^8$	$2{\cdot}10^8$	0.0
N_2	$8{\cdot}10^8$	$8{\cdot}10^8$	0.0

*μg m^{-3}, **V_d (cm s^{-1})

calculated OA concentrations in the BL.

Dry deposition has been suggested to be an important sink for oxidized VOCs (Karl et al., 2010) and consequently to decrease SOA production significantly (Bessagnet et al., 2010). Therefore, we included it by applying a deposition velocity of 2.4 cm s^{-1} for MVK+MACR and for all SVOCs, which is the above-canopy deposition velocity for MVK+MACR as found in flux measurements in the Amazon (Karl et al., 2010). Pugh et al. (2010) found that such a large deposition velocity is needed to reconcile modeled MVK+MACR concentrations with measurements. For SVOCs, the V_d of 2.4 cm s^{-1} is taken as an upper limit as not every SVOC will be taken up and metabolized by vegetation as effectively as MVK+MACR (Karl et al., 2010). Since the actual deposition velocity for SVOCs is uncertain, we included a simulation in which their deposition is switched off ($V_d = 0$). In this way, we obtain an upper and a lower limit for the effect of dry deposition of SVOCs.

4.2.4 Numerical experiments

A set of numerical experiments is designed to gain insight in the dynamical and chemical factors that drive the diurnal variability of the organic aerosol concentration as observed on 7 July 2008 during the OP3 campaign. We draw specific attention to physical and chemical

processes that are not routinely taken into account by large scale models or that are often omitted in the interpretation of measurements. Figure 4.1 shows the factors that we account for in the interpretation of observed OA and in this section, we introduce experiments that aim to show the sensitivity of OA formation and concentration to large scale forcings and several issues related to SOA formation from isoprene.

Large-scale meteorological forcings

With large-scale forcings, we refer to all the meteorological phenomena not directly driven by boundary layer processes. It can encompass mesoscale flows induced by different degrees of surface spatial heterogeneities (from small spatial scale to sea breeze) (Ouwersloot et al., 2011) to phenomena like subsiding air motions driven by synoptic scale circulations. We designed two experiments to investigate the influence of large-scale meteorological forcings on the BL dynamics and their subsequent impact on OA. In the first experiment we analyze the sensitivity of observed OA to subsiding air motions due to divergence of the horizontal wind. In a previous study, Janssen et al. (2012) showed that OA concentrations in the BL are sensitive to subsidence, because it suppresses BL growth and enhances entrainment. The subsidence velocity w_s (m s^{-1}) is in our modeling approach represented as:

$$w_s = -\omega \cdot h, \tag{4.2}$$

where ω is the subsidence rate (s^{-1}) and h the BL height (m). In the sensitivity analysis we switch subsidence off by setting ω to 0 and compare it to the base case, as defined in Table 4.3.

Second, we analyze the sensitivity to advection of heat by the mesoscale flow. The different contributions to heat advection are combined and prescribed to the model as a single advection term (A_θ). The best match with the observations is obtained when this term is negative throughout the day, meaning that relatively cool air is advected (Table 4.3). In our model setup, we assume that the advection of heat is uniformly distributed within the BL. In the sensitivity analysis we switch advection of heat off by setting A_θ to 0 and compare it to the base case.

OH recycling

In a second sensitivity analysis concerning the sensitivity of OA to chemistry, we evaluate the sensitivity of simulated OA to OH recycling, since this most important oxidant may be underestimated with respect to measurements in high isoprene environments (Lelieveld et al., 2008). The influence of OH recycling on SOA formation has been accounted for by applying a more detailed chemical mechanism in a global modeling study by Lin et al. (2012a). In that

study it led to decreased SOA yields, because of modifications in the gas-phase oxidation of isoprene. We do not explicitly account for these reaction pathways, but we consider that it can still be useful to include OH recycling to determine how OH concentrations matching the observations affect the formation of terpene SOA (TSOA) for a case study that is well-constrained by observational data. In our model, OH recycling is parameterized by applying a variable stoichiometric coefficient n in the reaction of IRO_2 with HO_2 (R20) (Lelieveld et al., 2008; Vilà-Guerau de Arellano et al., 2011). We compare the base case (no recycling, n=0) with experiments in which n is set to 1 and 2, respectively.

SOA formation from MPAN: effect of NO_2/NO ratio

Methacryloylperoxynitrate (MPAN) has been found to be an important second-generation reactive intermediate in the formation of isoprene SOA under high-NO_x conditions (Surratt et al., 2010; Chan et al., 2010). Increasing NO_x concentrations were thought to lead to decreasing formation of low-volatile products from isoprene oxidation that can partition into the aerosol phase (Kroll et al., 2006), until Chan et al. (2010) found SOA formation from MACR increased with NO_2 concentration. They showed the importance of the RO_2+NO_2 pathway of unsaturated aldehydes (e.g. MACR) photo oxidation as a route leading to SOA formation and found isoprene SOA yields through this pathway up to 3 times higher than previously found under high-NO_x conditions. Here, we implement this effect to our knowledge for the first time in a model of SOA formation. We do not account explicitly for the formation of MPAN, but we approximate the trends found by Chan et al. (2010) by scaling isoprene SOA yields to the NO_2/NO ratio. This is done by linearly interpolating between the high- and low-NO_x yields of isoprene SOA, so that they are the default NO channel yields when NO_2/NO = 0 and increase to 1.5 times the HO_2 channel yields when NO_2/NO = 10:

$$\gamma = 0.1 \cdot \frac{NO_2}{NO} \tag{4.3}$$

$$\alpha_i = (1-\gamma)\alpha_i^{high-NO_x} + 1.5 \cdot \gamma \cdot \alpha_i^{low-NO_x} \tag{4.4}$$

where γ is the ratio of NO_2 and NO multiplied by a factor 0.1 to normalize the range to a scale from 0 to 1, when going from a NO_2/NO ratio of 0 to 10. In the sensitivity analysis we compare the SOA formation in the base case with a case in which we account for the observed NO_2/NO ratio and with simulations in which we explore the full bandwidth of this effect by setting γ to 0 and 1, respectively. In this analysis, we only account for changing SVOC yields with changing NO_2/NO ratio, but it should be noted that a change in this ratio can also affect ⟨OH⟩ and in that way SOA formation.

Table 4.5: Paulot et al. (2009) mechanism for oxidation of isoprene under low-NO_x conditions, which replaces R9 and R20 in Table 4.1 in the sensitivity analysis for the chemical mechanism of SOA formation from isoprene (Sect. 4.5.4).

R29	ISO + OH	→	IRO_2	$2.70 \cdot 10^{-11} \cdot e^{\frac{390}{T}}$
R30	IRO_2 + HO_2	⟶	0.880 ISOPOOH + 0.120 OH + 0.047 MACR + 0.073 MVK + 0.120 HO_2 + 0.120 CH_2O	$7.40 \cdot 10^{-13} \cdot e^{\frac{700}{T}}$
R31	ISOPOOH + OH	→	IEPOX + OH	$1.90 \cdot 10^{-11} \cdot e^{\frac{390}{T}}$
R32	ISOPOOH + OH	→	0.70 ISOPOO + 0.300 HC_5 + 0.300 OH	$3.80 \cdot 10^{-12} \cdot e^{\frac{200}{T}}$
R33	IEPOX + OH	→	IEPOXOO	$5.78 \cdot 10^{-11} \cdot e^{\frac{-400}{T}}$
R34	IEPOXOO + HO_2	→	0.725 HAC + 0.275 GLYC + 0.275 GLYX + 0.275 MGLY + 1.125 OH + 0.825 HO_2 + 0.200 CO_2 + 0.375 CH_2O + 0.074 HCOOH + 0.251 CO	$7.40 \cdot 10^{-13} \cdot e^{\frac{700}{T}}$

SOA formation from IEPOX

Under low-NO_x conditions, isoprene epoxydiols (IEPOX) have been found to be important reactive intermediates in the formation of isoprene SOA (Paulot et al., 2009; Surratt et al., 2010; Lin et al., 2012b). The chemical pathways for SOA formation from IEPOX are not incorporated explicitly in MXLCH-SOA. However, we mimic the catalyzing role of acidic sulfate aerosol on the formation of SOA from IEPOX by incorporating the chemical mechanism suggested by Paulot et al. (2009) (see Table 4.5) and using a fixed aerosol yield of 6.4%, which is the highest yield from experiments by Lin et al. (2012b). In this way, we neglect the complex underlying chemistry, but we obtain a first-order estimation of the magnitude of its effect. In the experiment, the Paulot et al. (2009) mechanism replaces the reactions R9 and R20 as used in the default mechanism. In this mechanism there is some regeneration of OH, but we only evaluate its impact on SOA through IEPOX formation here.

4.3 Interpretation of observations by modeling

We are able to satisfactorily reproduce the dynamics as observed on 7 July 2008 at Bukit Atur, see Fig. 4.4 with initial and boundary conditions as specified in Table 4.3. The BL height reaching between 800 to 1000 m, as observed by over Borneo from LIDAR (Pearson et al., 2010) and aircraft measurements (Robinson et al., 2012), appears to be the result of the local surface forcing of the sensible (H) and latent heat flux (LE) with superimposed subsidence and advection. Due to the high H (with a maximum of ~400 W m^{-2}), this low BL height can only be explained when subsidence and advection are accounted for: 1) subsidence directly suppresses the convective motions that are induced by the surface heat flux and 2) advection

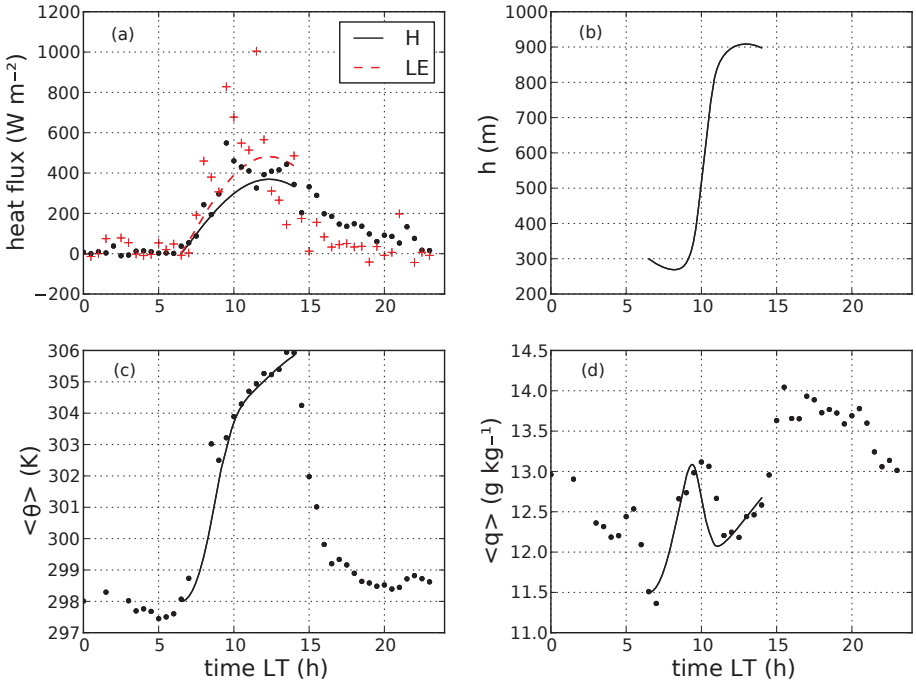

Figure 4.4: Diurnal evolution of ***(a)*** *surface sensible (H) and latent (LE) heat flux, which are both prescribed,* ***(b)*** *boundary layer height (h),* ***(c)*** *mixed layer potential temperature ($\langle\theta\rangle$) and* ***(d)*** *mixed layer specific moisture ($\langle q\rangle$) for the case study. Dots indicate tower measurements at 45 m and model results are indicated by lines.*

of relatively cold air cools the BL and consequently increases its potential temperature difference with the FT ($\Delta\theta$), which hinders thermal plumes in breaking through this potential temperature inversion to entrain warm air from the FT. In Fig. 4.1, a typical vertical profile of potential temperature (θ) is sketched to illustrate these effects. These large-scale meteorological forcings may explain the low BL height over Borneo compared to the Amazon, where mixed-layer heights typically exceed 1000 m (Martin et al., 1988). Later, we explicitly investigate the effect of these meteorological forcings on C_{OA}.

The mixed-layer potential temperature ($\langle\theta\rangle$) shows a steep increase of 3 K h^{-1} after the heat fluxes become positive, at 06:30. This is caused by direct heating of the BL by the sensible heat flux and by entrainment of warm air during the rapid growth of the BL between 09:00 and 11:30, which are both further enhanced by subsidence. Unfortunately, two observations are missing at 07:30 and 08:00, but the fact that we are able to reproduce the strong gradient in $\langle\theta\rangle$ gives us confidence in the correct representation of its evolution. Specific moisture ($\langle q\rangle$),

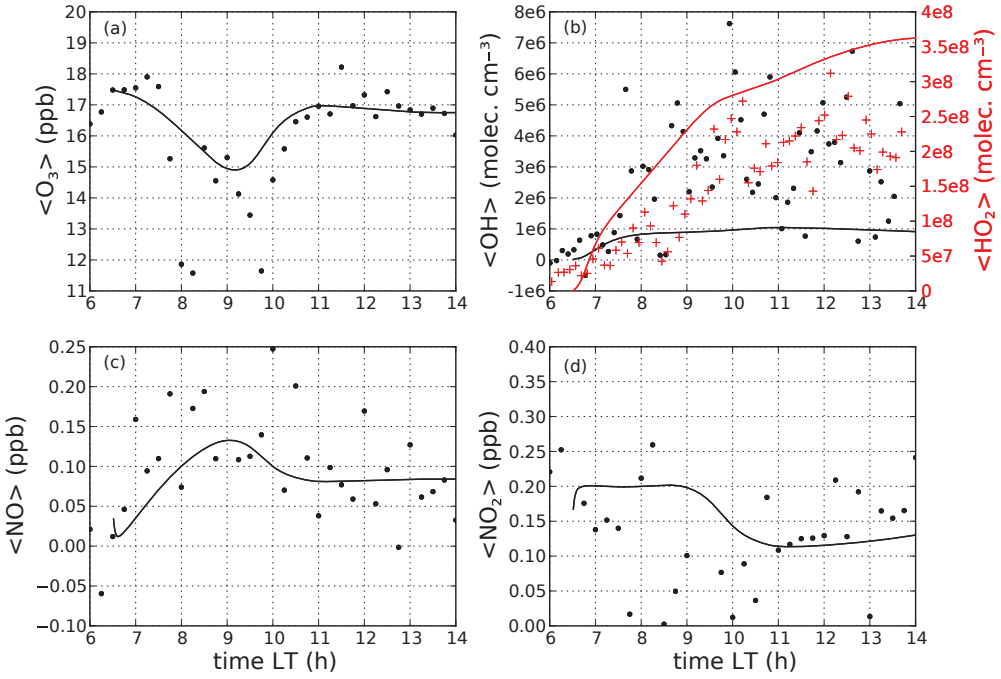

*Figure 4.5: Diurnal evolution of mixed layer concentrations of **(a)** O_3, **(b)** OH, and HO_2 **(c)** NO and **(d)** NO_2 for the case study. Markers indicate measurements from the tower at 75 m (O_3, NO and NO_2) or 5 m (OH and HO_2).*

which initially increases due to the evaporation flux, decreases after 09:30 because drier air is entrained during the BL growth and increases again when BL growth ceases around 11:00.

The evolution of the gas-phase species O_3, NO_x and HO_x is shown in Fig. 4.5 with initial conditions as specified in Table 4.4. O_3 and NO_x mixing ratios and evolution are reproduced satisfactorily within the bounds set by the scatter in the observations, only $\langle NO_2 \rangle$ is overestimated between 09:00 and 11:00. The exact reason for this is unknown, but it may be due to missing chemistry. The crucial point here is that NO concentrations are simulated well, which is needed to calculate the branching of the low- and high-NO_x SOA yields. Our model calculations show that at $\langle NO \rangle$ ~0.1 ppb, >80% of the terpene and isoprene RO_2 reacts with NO, meaning that we are mostly under high-NO_x conditions. Note that since HO_2 is overestimated by roughly a factor 1.5, this is a lower limit for the branching fraction of the high-NO_x channel. OH is underestimated by a factor of 2-6, depending on considering the lower or the upper bound set by the scatter in the observations. We will discuss possible influences on SOA formation in Sect. 4.5.2.

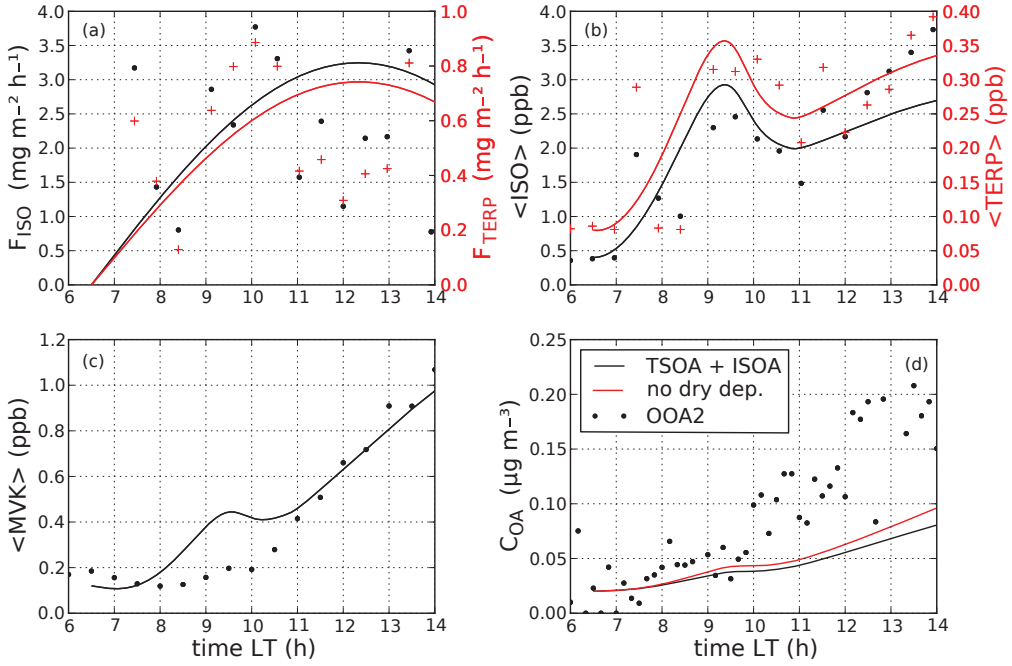

*Figure 4.6: Diurnal evolution of **(a)** ISO- and TERP-flux, which are both prescribed, and mixed layer concentrations of **(b)** ISO and TERP, **(c)** MVK+MACR and **(d)** OA for the case study. Markers indicate measurements from the tower at 75 (F_{ISO} and F_{TERP}, ISO, TERP, MVK+MACR) or 33 m (OA).*

Figure 4.6 shows the diurnal evolution of VOCs and OA. Note that the F_{ISO} and F_{TERP} are prescribed and scaled to match the fluxes observed by Langford et al. (2010). Temperature driven terpene emissions may continue during night time and in the early morning, but are much lower than those during day time (Langford et al., 2010) and therefore omitted here. Reasonable agreement is found for mixing ratios of ISO and TERP, which show a similar pattern as specific moisture. An initial increase in their concentrations between 06:30 and 09:30 is followed by a decrease, which is related to the rapid BL growth. In the afternoon, both ⟨ISO⟩ and ⟨TERP⟩ increase again due to continuing emissions and weaker entrainment. The contribution of chemical destruction is rather constant from 09:00 onwards, due to a rather constant simulated ⟨OH⟩ (Fig. 4.5). A more thorough budget analysis is given in Sect. 4.4.

⟨MVK+MACR⟩ is overestimated between 09:00 and 11:00 by around 0.2 ppb. An overestimation of MVK+MACR was found previously in studies of tropical regions (Ganzeveld

et al., 2008; Pugh et al., 2010) and several possible explanations have been proposed, including an underestimation of dry deposition and entrainment of MVK+MACR from the residual layer. The applied deposition velocity (V_d) for MVK+MACR of 2.4 cm s^{-1} as suggested by Karl et al. (2010) partly resolves this issue by lowering their concentrations by 15% compared to the case without deposition. Since we set the FT concentration of MVK+MACR to zero, entrainment in this case only dilutes BL concentrations and can not explain the overestimation. The simplicity of the isoprene oxidation scheme applied here may explain this overestimation. It is relevant to mention that the modeled C_{OA} does not directly depend on ⟨MVK+MACR⟩, since we do not explicitly account for SOA formation from MACR.

Both observed and modeled OA concentrations increase during the day, due to SOA formation (Fig. 4.6d). However, the modeled C_{OA} is lower than the observed OOA2 and as the day progresses this underestimation increases to 60% at the end of the simulation. Possible contributors to this underestimation are a misrepresentation of the pathways leading to ISOA formation or too low OH concentration. These will be subject of the sensitivity analyses in Sect. 4.5. Also the high deposition velocity of the SVOCs could cause an underestimation C_{OA}, due to low SOA formation. The simulation with dry deposition of the SVOCs turned off shows the maximum effect of dry deposition of SVOCs, resulting in a 22% higher C_{OA} at the end of the simulation compared to the case with deposition.

4.4 Budget analysis of VOCs, SVOCs and OA

To understand how dynamics and chemistry interact and how the diurnal evolution of OA results from this interaction, it is useful to analyze the cascade of processes that lead to SOA formation from gas-phase precursors. Here, we show the budgets of key species in the formation of OA: VOCs from biogenic emissions, an intermediate semi-volatile species SVOC, and OA as their end product, and how these budgets are coupled to the diurnal variability of the boundary layer dynamics. For completeness, we also added an advection term to the budget equations (Eqs. 4.5-4.7).

The budget of a VOC reads as follows (Janssen et al., 2012):

$$\frac{\mathrm{d}\langle \mathrm{VOC}\rangle}{\mathrm{d}t} = \overbrace{\frac{F_{\mathrm{VOC}}}{h}\sin\left(\frac{\pi t}{t_d}\right)}^{\text{emission}} + \overbrace{\frac{w_{\mathrm{e}}\Delta VOC}{h}}^{\text{entrainment}} - \overbrace{\sum_j k_j\langle \mathrm{VOC}\rangle\langle OX_j\rangle}^{\text{chemistry}} + \overbrace{U_k\frac{\partial\langle VOC\rangle}{\partial x_k}}^{\text{advection}} \tag{4.5}$$

where F_{VOC} is the maximum daily VOC emission flux, assuming a sinusoidal diurnal emission profile (ppb m s^{-1}, see Table 4.4); h is the BL height (m); t is the time since the start of the simulation (s); t_d is the length of the period during which the heat fluxes are positive (s); w_{e} is the entrainment velocity (m s^{-1}); ΔVOC is the VOC mixing ratio difference

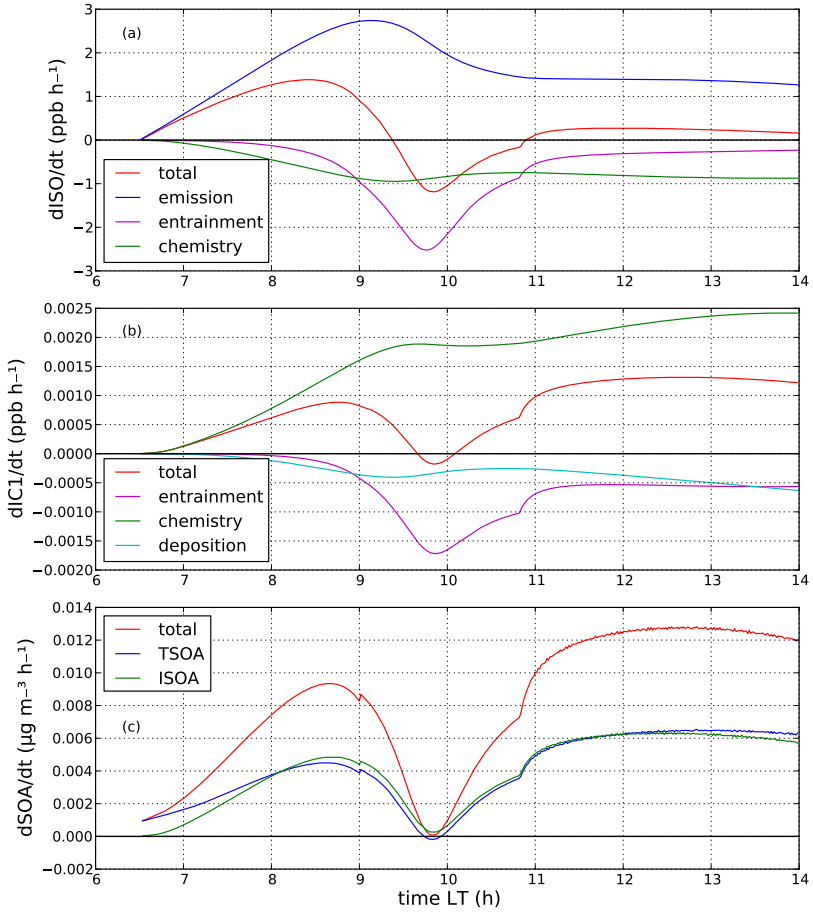

Figure 4.7: Contribution of the individual processes to the budgets of ***(a)*** *ISO (Eq. 4.5),* ***(b)*** *the SVOC IC_1, which results from oxidation of ISO (Eq. 4.6) and* ***(c)*** *SOA (Eq. 4.7), split up in the terpene SOA (TSOA) and the isoprene SOA (ISOA) fraction. Note that the contribution of entrainment to the $\langle OA \rangle$-tendency is zero since the concentrations of OA_{BG} in BL and FT are equal. Therefore, the partitioning of SVOCs from terpenes and isoprene into the aerosol phase forms the only contribution.*

(jump) between the BL and the FT (ppb) (with the jump of a scalar or reactant C defined as $\Delta C = C_{\mathrm{FT}} - \langle C \rangle$); k_j is the reaction rate of VOC with oxidant OX_j (either $\mathrm{O_3}$ or OH); $\langle OX_j \rangle$ is the mixed layer mixing ratio of oxidant OX_j (ppb); U_k is horizontal wind speed ($\mathrm{m\,s^{-1}}$); and $\partial\langle VOC \rangle$ the concentration difference (ppb) over the distance in the horizontal ∂x_k (m).

A similar equation holds for SVOCs, but they do not have an emission term and are removed from the atmosphere by dry deposition, so their budget equation is:

$$\frac{\mathrm{d}\langle C_\mathrm{i} \rangle}{\mathrm{d}t} = \overbrace{\frac{w_\mathrm{e}\Delta C_i}{h}}^{entrainment} + \overbrace{\sum_j \alpha_i k_j \langle \mathrm{VOC} \rangle \langle \mathrm{OX}_j \rangle}^{chemistry} + \overbrace{U_k \frac{\partial \langle C_i \rangle}{\partial x_k}}^{\text{advection}} - \overbrace{\frac{V_{dCi}\langle C_i \rangle}{h}}^{\text{deposition}} \tag{4.6}$$

where $\Delta \mathrm{C_i}$ is the concentration jump of the SVOC C_i (ppb); α_i the stoichiometric coefficient for C_i; ∂C_i its horizontal concentrations difference (ppb); and Vd_{Ci} its deposition velocity ($\mathrm{m\,s^{-1}}$).

And finally the budget of OA reads:

$$\frac{\mathrm{d}\langle OA \rangle}{\mathrm{d}t} = \overbrace{\frac{w_\mathrm{e}\Delta \mathrm{OA_{BG}}}{h}}^{\mathrm{OA_{BG}}\text{-entrainment}} + \overbrace{\sum_i \left[X_{p,i}\frac{dC_i}{dt} + C_i \frac{dX_{p,i}}{dt} \right]}^{\text{G/P-partitioning}} + \overbrace{U_k \frac{\partial \langle OA \rangle}{\partial x_k}}^{\text{advection}} - \overbrace{\frac{V_{dOA}\langle OA \rangle}{h}}^{\text{deposition}} \tag{4.7}$$

where $\Delta \mathrm{OA_{BG}}$ is the jump in the background organic aerosol concentration between the BL and the FT ($\mu\mathrm{g\,m^{-3}}$); $\partial\langle OA \rangle$ the horizontal concentration difference ($\mu\mathrm{g\,m^{-3}}$) and V_{dOA} the deposition velocity of OA ($\mathrm{m\,s^{-1}}$).

In Eqs. 4.5-4.7, the BL height h modulates the contributions of the emission, entrainment and deposition terms and the entrainment velocity w_e appears in the entrainment term. Through the dependence on h and w_e, the evolution of the chemical species is coupled to the dynamics of the boundary layer, which in turn are affected by large-scale meteorological forcings, as will be shown in Sect. 4.5.1.

Figure 4.7 shows how the evolution of C_{OA} depends on the behavior of its precursors. The isoprene (ISO) tendency (Fig. 4.7a), which is shown as an example VOC here, has a positive contribution from the emission term, especially between 08:00 and 10:00 when the emission increases (Fig. 4.6a) and the BL is still shallow as the morning ground inversion is not yet broken. This results in the peak in the ISO mixing ratio seen in both the observations and model results just around 09:30 (Fig. 4.6b). Entrainment is important during the period of fast BL growth, between 09:00 and 11:00. As shown by the negative value, entrainment contributes to the decrease of ISO by introducing residual layer/free tropospheric air characterized by lower ISO mixing ratio. Our findings are corroborated by the observed ISO concentration, which decreases between 09:30 and 11:00 (Fig. 4.6b). The chemical destruction term, only by OH in this case, is rather constant from 09:00 onwards, but becomes

the most important loss term after 11:00.

The chemical destruction of ISO is mirrored in the chemical production of IC_1 (Fig. 4.7b). Due to the low yield of IC_1 (see Table 4.1), the production of IC_1 is a factor $\sim 10^3$ smaller than the destruction of ISO. This low yields results in small concentrations changes of IC_1 compared to those of ISO. Since the FT concentration is set to zero, the concentration jump is equal to the BL concentration. Therefore, the ratio between entrainment and deposition terms depends solely on the ratio of the entrainment and deposition velocities. w_e peaks at 10:00 at 13 cm s^{-1} and in our case, the entrainment contribution is larger that of the dry deposition process with V_d = 2.4 cm s^{-1}.

The contribution of the entrainment term to the SOA precursors is clearly visible in the evolution of OA (Fig. 4.7c). The budget of OA includes the entrainment of OA_{BG}, but here the concentrations are equal in BL and FT and therefore the OA_{BG} entrainment term is zero (first term on the right hand side (RHS) of Eq. 4.7). This is because the OA consists of OA_{BG} and fresh SOA. The former has no concentration gradient between BL and FT and the latter is calculated at each time step as the fraction of the SVOCs that enter the aerosol phase, in which the effect of entrainment is already accounted for. In case of a large concentration jump of OA_{BG} between BL and FT, the entrainment term is important for the evolution of OA (Janssen et al., 2012). The minimum in the gas/particle-partitioning (second term on the RHS of Eq. 4.7) is therefore caused by the dilution of the SVOCs due to entrainment. The OA tendency has its peak in the afternoon at 12:30, similarly as the SVOC tendency. This is caused not only by the fact that more SVOC is present, but also by the presence of a larger available organic mass for SVOCs to partition in. Consequently, partitioning of the SVOCs into the aerosol phase will be efficient, i.e. in Eq. 4.1, $X_{p,i}$ increases with increasing C_{OA}. TSOA and ISOA contribute in similar quantities to the calculated SOA formation. ISOA has lower yields than TSOA, but the emission of ISO is a factor 5 larger than that of TERP, which compensates for this. However, the ISOA shown here should be regarded as a lower limit and the formation of ISOA through specific reactive intermediates will be discussed in Sect. 4.5.3 and 4.5.4.

We omit advection of any of these species and therefore implicitly assume the footprint area of the site to be horizontally homogeneous for the emission of VOCs, the formation of SVOCs and the OA concentration. Especially for long-lived species as OA, this assumption may not hold and we can not rule out a possible contribution of advection to the OA budget. On the other hand, the satisfactory agreement of the measurements on this particular day and the campaign averages (Fig. 4.2), makes it unlikely that the source of the air masses arriving at the site is of major importance for the diurnal variability.

Another process that has not been taken into account is the dry deposition of OA, since dry deposition of sub-micron aerosols over forests is not well constrained by observations. Recently, Farmer et al. (2012) observed a V_d for the sub-micron mode aerosol mass of 0.02

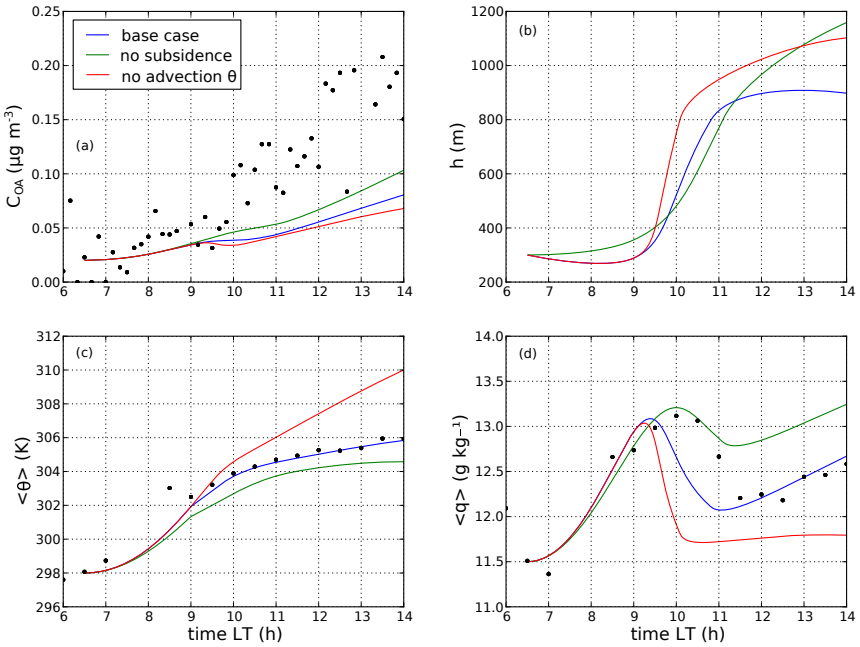

Figure 4.8: Sensitivity of modeled ***(a)*** *organic aerosol concentration C_{OA},* ***(b)*** *BL height h,* ***(c)*** *mixed layer potential temperature $\langle\theta\rangle$ and* ***(d)*** *mixed layer specific humidity $\langle q\rangle$ to subsidence and advection of heat. Shown are the base case (see Table 4.3), an experiment without subsidence and an experiment with no advection of θ.*

cm s^{-1} over temperate and tropical forests, which indicates that the contribution of dry deposition would be small. If it would be included it would act to further increase the discrepancy between measured and modeled OA.

4.5 Sensitivity analyses

4.5.1 Large scale meteorological forcings

Large-scale meteorological forcings influence the coupled system of BL height (h), mixed layer potential temperature ($\langle\theta\rangle$) and specific moisture ($\langle q\rangle$). Consequently, they affect the OA concentration through their influence on h and w_e, as shown in the previous section. In case of subsidence, the BL is suppressed by large-scale downward vertical motions, that lead to a stronger heating of the BL because the same amount of heat is distributed over a

shallower layer. As a consequence, the potential temperature jump at the BL-FT interface decreases, which enhances the entrainment velocity (Janssen et al., 2012). In our case study, not taking subsidence into account would have led to an overestimation of h of 250 m at the end of the numerical experiment (Fig. 4.8), an underestimation of $\langle\theta\rangle$ by 1.5 K and a BL, which is too moist. Because of the increased entrainment velocity, OA is diluted more under the presence of subsidence, resulting in 27% lower OA at the end of the simulation.

Advection of θ in this case acts to cool the BL. Therefore the potential temperature jump across the BL-FT interface increases, which weakens entrainment (so opposite to the effect of subsidence) and BL growth. Not taking advection of cool air into account results in a BL which is 200 m higher at the end of the run than in the case with advection (similar as for subsidence), an overestimation of $\langle\theta\rangle$ by 4 K and an underestimation of $\langle$q$\rangle$ by 0.9 g kg^{-1}. Due to the weaker entrainment when advection of cool air is considered, the OA precursors are diluted less, leading to more SOA formation and a 16% higher C_{OA} in the case with advection (Fig. 4.8).

Subsidence and advection of cold air, while both decreasing BL height, therefore have opposing effects on C_{OA}.

4.5.2 OH recycling

The evolution of OA has so far been simulated in this paper without considering OH recycling from isoprene (n = 0 in R20). In this section we explore n=1 and n=2 in R20. This corresponds to daily average recycling rates of OH with respect to the OH consumed by the first-step oxidation of isoprene of 19 and 54%, respectively, which is below the range of 75 to 120%, as estimated recently by Taraborrelli et al. (2012). Nevertheless, including OH recycling leads to a better agreement with the observations of $\langle$OH$\rangle$, especially for n=2 (Fig. 4.9).

This enhancement of $\langle$OH$\rangle$ leads to an increase of the calculated C_{OA} at the end of the simulation by 25% and 75% for n=1 and n=2, respectively. This enhancement of the calculated C_{OA}, however, is not enough to explain the observed OOA2. On the other hand and as expected from reactions R9 and R30, ISO and TERP are depleted at a faster rate when OH is recycled, which leads to an underestimation of their concentrations as n is increased, especially in the afternoon when isoprene oxidation and OH recycling have a maximum. This is similar to the findings of Pugh et al. (2010) for observations made during OP3 I. They questioned the validity of the assumption of a well-mixed layer and suggested that the segregation of isoprene into distinct plumes could deplete OH in those plumes, which may have affected the measurements. However, the high degree of segregation assumed in their simulations of this effect (50%), was later dispelled by Pugh et al. (2011) and Ouwersloot et al. (2011), who found a reduction of the rate constant of the isoprene and OH reaction due to incomplete

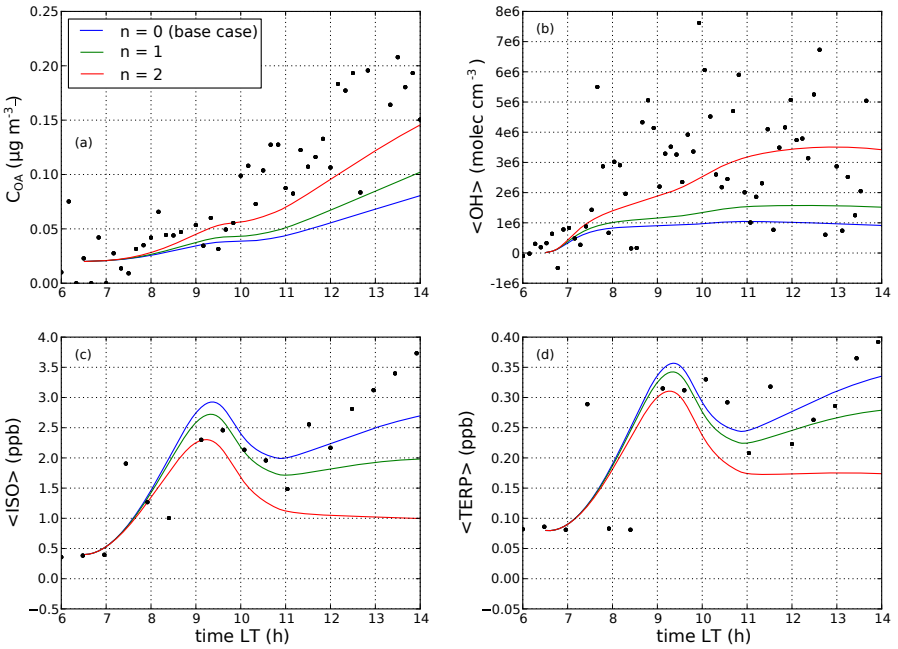

Figure 4.9: Sensitivity of ***(a)*** *organic aerosol C_{OA},* ***(b)*** *OH,* ***(c)*** *ISO and* ***(d)*** *TERP to OH recycling. Shown are experiments for n = 0, 1 and 2 in R20, respectively.*

mixing of less than 15%.

The main point here is that we are able to reproduce the evolution of ISO and TERP satisfactorily for n=0 as a function of emission, entrainment and chemistry. Hereby, the emissions are constrained by the flux measurements and the correct representation of BL dynamics gives us confidence in the representation of entrainment. Seen in this way, the first-step oxidation by OH (and O_3 in case of TERP), is apparently represented reasonably well in the base case. So while increasing n leads to an improved representation of ⟨OH⟩ and C_{OA}, it serves to worsen the match with the observed ⟨TERP⟩ and ⟨ISO⟩. OH recycling thus has the potential to influence modeled SOA formation in high isoprene environments, but current knowledge is not sufficient to constrain its effects.

4.5.3 SOA formation from MPAN: effect of NO_2/NO ratio

We study the sensitivity of the formation of isoprene SOA with MACR and MPAN as intermediate species on the NO_2/NO ratio, as proposed by Eqs. 4.3 and 4.4. We find that at the

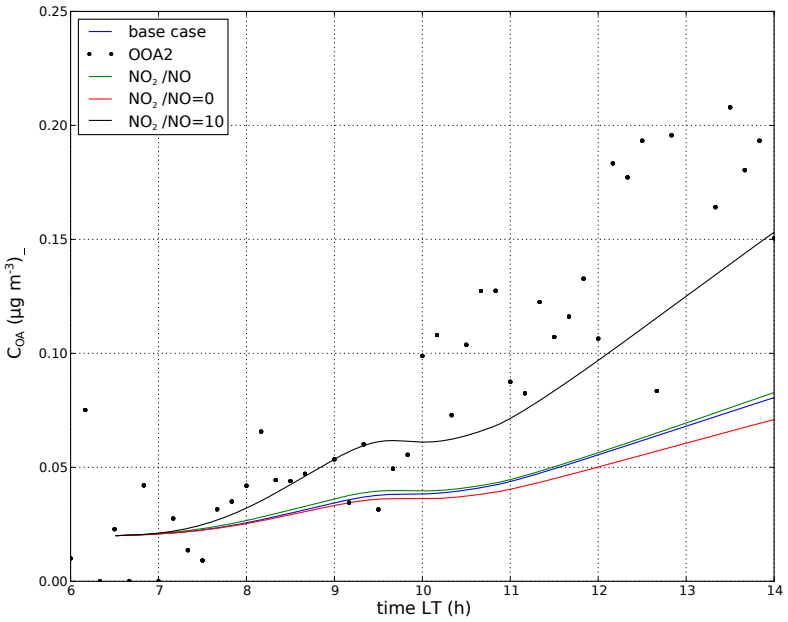

Figure 4.10: Sensitivity of organic aerosol C_{OA} to NO_2/NO ratio. Besides the base case, simulations are shown for actual NO_2/NO, NO_2/NO=0 and NO_2/NO=10, respectively.

actual NO_2/NO ratio of about 1.5, the simulated SOA formation is very similar to that in the base case (Fig. 4.10), since the high NO_x yields dominate. The whole range is explored, and this reveals that the ratio may affect simulated ambient OA concentrations significantly. Calculated C_{OA} decreases by 12% and increases by 94% at the end of the simulation for NO_2/NO=0 and 10, respectively. In the upper limit, C_{OA} compares well with the observed OOA2 until 09:30, but is still underestimated afterwards.

The influence of the RO_2+NO_2 channel for SOA formation may be more evident in regions where NO_2/NO ratios are higher due to anthropogenic emissions or slower photochemistry. The parametrization proposed here can be included in models aiming to study this effect.

4.5.4 SOA formation from IEPOX

Our last sensitivity study focuses on the formation of IEPOX SOA, catalyzed by acidic sulfate aerosol (Table 4.5). We find concentrations of IEPOX in the order of $\sim 10^{-1}$ ppb after mid-

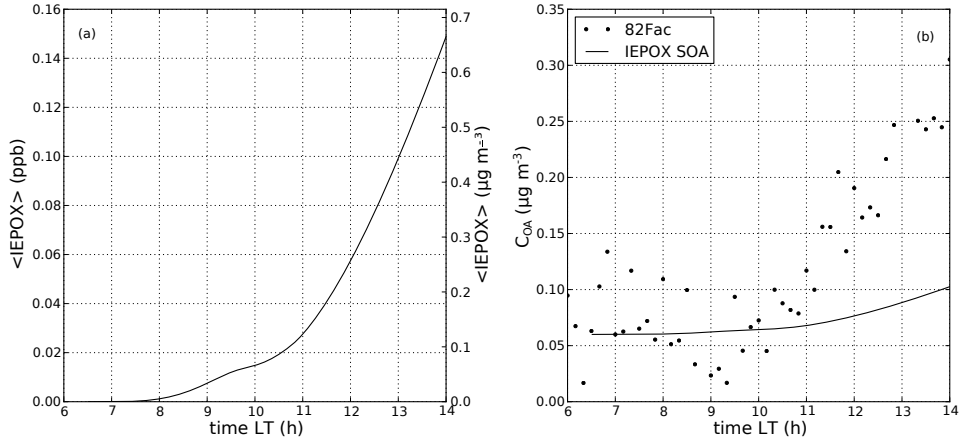

*Figure 4.11: Concentration of **(a)** IEPOX and **(b)** IEPOX SOA, assuming a fixed yield for the latter of 6.4%, which is the upper limit under acidic conditions found by Lin et al. (2012b).*

day (Fig. 4.11a), which is of the same order-of-magnitude as calculated by a global model for Borneo (Paulot et al., 2009). The branching between the IRO_2 + HO_2 and the IRO_2 + NO reactions determines the efficiency with which IEPOX is formed. As in the previous experiments, the NO channel dominates, with the HO_2 channel contributing only ~13% to the destruction of IRO_2.

IEPOX SOA is modeled here with a fixed yield of 6.4%, which is the largest yield found in the experiments of Lin et al. (2012b). 82Fac shows a decrease, possibly due to entrainment, from 08:00 to 09:00 and after that time increases rapidly to reach a concentration which is one order-of-magnitude greater at 14:00 than its minimum at 09:00 (Fig. 4.11b). We are not able to match the strong increase of 82Fac as observed between 09:00 and 14:00. An IEPOX SOA yield of 35% would be required to explain this rapid increase.

There are several possible causes for the underestimation of the concentration of 82Fac by the model. First, using a fixed yield of IEPOX SOA implies that effects of the OA_{BG} on gas/particle-partitioning are not accounted for, which may affect the aerosol yield of semi-volatile species (see Eq. 4.1). Then, the yield of IEPOX SOA found in chamber studies (Lin et al., 2012b) may be a too low, possibly due to yet unknown chemical pathways. Finally, we consider a meteorological factor, long range horizontal transport by advection. Advection may be important because OA has, in contrast to VOCs, a long atmospheric lifetime of days to a week. This means that observed OA could reflect integrated VOC oxidation over a larger area and period rather than in situ production of OA from VOCs. As a consequence, it is plausible that IEPOX SOA is advected to the measurement site that is formed from isoprene

emitted at the oil palm plantations located 50 km and further to the South-East, which emit 4-7 times more isoprene than the forest (Hewitt et al., 2010). However, it is not known what the 82Fac looks like after aging and it could be transformed into OOA2 or OOA1 by the time it reaches the site. Although we can not rule out the contribution of advection, there are two reasons to expect that the fast increase of 82Fac is likely not due to advection. First, the fact that 82Fac was not observed in morning air plane profiles, but that it was observed in the afternoon flights, may indicate that the 82Fac is formed rapidly and mainly from local sources. Second, the time at which the fast increase of 82Fac begins (after 10:00, see Fig. 4.11b) corresponds well with the modeled increase of IEPOX and IEPOX SOA.

4.6 Conclusions

We studied the diurnal evolution of organic aerosol, its gas-phase precursors and their oxidants, coupled to the dynamics of a convective boundary layer for a characteristic situation observed above the tropical forest at Borneo during the OP3 field campaign. Observations of BL dynamics and chemical species combined with a boundary layer model of physics and chemistry are used to determine the dominant processes in the SOA formation driven by terpene and isoprene emissions. We are able to satisfactorily reproduce the diurnal variability of the BL in terms of its height, potential temperature and specific humidity as driven by land surface and large-scale meteorological forcings. Advection of cooler air and subsidence are important contributions to the characterization of the BL as observed over Borneo and complicate the characterization of a tropical BL climatology. Because of their influence on BL height and entrainment, subsidence and advection of heat affect the diurnal evolution of chemical species in the BL and should be taken into account when interpreting observations of OA. Subsidence and advection of cool air, while both decreasing BL height, have opposing effects on the diurnal trend of C_{OA}.

An analysis of the budgets of VOCs, SVOCs and OA shows the importance of studying dynamical and chemical processes simultaneously in order to understand the diurnal variability of reactants. Specifically, it shows how the OA budget is strongly modified by the various processes that shape the diurnal cycle of its gas-phase precursors, in which the signal of entrainment is clearly visible.

By confronting our model with a rather complete set of data of gas-phase chemistry and organic aerosol, we are able to exclude the influence of some factors that in other studies have been suggested to explain underestimation by models of biogenic OA concentrations. Nevertheless, as in previous studies we underestimate OA concentrations by about a factor of 2, even though we are able to reproduce the diurnal evolution of isoprene and terpene concentrations with observed and prescribed fluxes and we explicitly take the impact of entrainment

on VOCs and their oxidants into account.

In our investigation of the role of isoprene chemistry in SOA formation, we find that OH recycling decreases the model-measurement discrepancy of OA concentrations, but at the cost of a worse comparison with VOC concentrations. Before isoprene SOA formation can be quantified, the OH puzzle must be solved. Furthermore, accounting for the dependence of isoprene SOA formation on the NO_2/NO ratio has no significant effect here, but could be important in regions with a higher NO_2/NO ratio. In a final sensitivity analysis, we underestimate the concentration of 82Fac, an OA component specifically related to SOA from isoprene epoxides (IEPOX), although we incorporate the state-of-the-art knowledge on the formation of IEPOX SOA in our model. There are several factors which may explain this underestimation, and further insights in the formation and evolution in the atmosphere of IEPOX SOA are needed to get a definitive answer. We find that the low-NO_x pathway leading to IEPOX formation is only a minor one under observed NO concentrations. Nevertheless, the concentration of 82Fac is of comparable magnitude as that of OOA2, suggesting that a minor pathway in the gas-phase chemistry of isoprene can still lead to substantial SOA formation. This strong dependence of isoprene SOA formation on NO_x chemistry implies that if NO concentrations increase in Borneo by increased anthropogenic activities, the type and amount of isoprene SOA has the potential to change significantly.

Although incorporating these new pathways does not yet explain the discrepancies between modeled and observed biogenic OA, we propose that models need to account for the different pathways by which isoprene chemistry drives SOA formation, both through formation of its second-generation products following the low- and high-NO_x pathways and through its effect on gas-phase chemistry by OH recycling.

Finally, we advocate the use of conceptual but realistic models similar to the one presented here to bridge the gap between observations made during chamber studies and field campaigns, on one hand, and the gap between local observations and large-scale forcings, on the other hand, to gain further understanding of the organic aerosol budget in tropical forests.

5

Estimating seasonal variations in cloud droplet number concentration over the boreal forest from satellite observations

Seasonal variations in cloud droplet number concentration (N_{CD}) in low-level stratiform clouds over the boreal forest are estimated from MODIS observations of cloud optical and microphysical properties, using a sub-adiabatic cloud model to interpret vertical profiles of cloud properties. An uncertainty analysis of the cloud model is included to reveal the main sensitivities of the cloud model. We compared the seasonal cycle in N_{CD}, obtained using 9 yr of satellite data, to surface concentrations of potential cloud activating aerosols, measured at the SMEAR II station at Hyytiälä in Finland. The results show that N_{CD} and cloud condensation nuclei (CCN) concentrations have no clear correlation at seasonal time scale. The fraction of aerosols that actually activate as cloud droplet decreases sharply with increasing aerosol concentrations. Furthermore, information on the stability of the atmosphere shows that low N_{CD} is linked to stable atmospheric conditions. Combining these findings leads to the conclusion that cloud droplet activation for the studied clouds over the boreal forest is limited by convection. Our results suggest that it is important to take the strength of convection into account when studying the influence

This chapter is published as Janssen et al. (2011).

of aerosols from the boreal forest on cloud formation, although they do not rule out the possibility that aerosols from the boreal forest affect other types of clouds with a closer coupling to the surface.

5.1 Introduction

The biosphere makes a very large contribution to the levels of atmospheric aerosols and cloud condensation nuclei (Andreae and Rosenfeld, 2008). However, the feedbacks that are possibly associated with the emissions of natural aerosols have only recently started to receive substantial attention and therefore the scientific understanding of their drivers, climate impacts and interactions is low (Carslaw et al., 2010). One proposed feedback mechanism which involves aerosols of natural origin concerns the boreal forests of the Northern high latitudes. Kulmala et al. (2004a) proposed that aerosols produced by forests modify the radiation balance via their influence on cloud properties such as albedo, thereby posing a negative feedback on the surface temperature and on the productivity of the forest itself. They based their hypothesis on the observation that in the boreal forest, there is a strong coupling between the seasonal cycle in temperature, vegetation productivity, biogenic emissions of Volatile Organic Compounds (VOC) and the growth rate of freshly formed aerosol particles. Ongoing research has further confirmed the role of boreal forests as a contributor to both aerosol number by facilitating new particle formation from gaseous precursors (Kavouras et al., 1998; O'Dowd et al., 2002, 2009; Laaksonen et al., 2008) and their subsequent growth by providing condensable species in the form of VOC oxidation products (Allan et al., 2006; Tunved et al., 2006, 2008; Dal Maso et al., 2008).

Some studies have been undertaken to estimate the effect that the vegetation-aerosol-cloud feedback may have on the surface radiation balance in the boreal forest. Spracklen et al. (2008) estimated the radiative forcing of the 1st indirect aerosol effect from biogenic aerosols over the boreal forest to be between -1.8 and $-6.7\,\mathrm{W\,m^{-2}}$ using a chemical transport model that includes parameterizations of nucleation and condensational growth coupled to a simple radiation model. Another study that used a more conceptual approach to estimate the radiative forcing of particle formation over the boreal forest yielded numbers up to $-14\,\mathrm{W\,m^{-2}}$ (Kurtén et al., 2003). This would imply that the aerosol effect may be able to compensate for a hypothesized present-day net warming of the boreal forests through the combined effect of a decrease in surface albedo and enhanced CO_2-uptake (Betts, 2000; Bala et al., 2007).

New particle formation events are important contributors to the aerosol particle number over the boreal forest (Kulmala et al., 2001; Dal Maso et al., 2007). The occurrence of particle formation events has a typical annual variation over the Scandinavian boreal forest, with peaks in springtime and autumn and minima in winter and summer (Dal Maso et al., 2007). It has been shown that the aerosols that are produced during these nucleation events grow

rapidly to sizes at which they can serve as cloud condensation nuclei (CCN) (Lihavainen et al., 2003) and consequently are able to participate in cloud droplet formation (Kerminen et al., 2005). The growth rates of these newly formed particles are strongly correlated to concentrations of monoterpene oxidation products (Laaksonen et al., 2008; Allan et al., 2006). Monoterpenes are emitted in large quantities by boreal forests, following a strong seasonal pattern, determined by a pronounced seasonal cycle in temperature, light intensity and vegetation productivity (Hakola et al., 2003; Lappalainen et al., 2009). Once oxidized, these organics condense onto freshly nucleated clusters to grow them to sizes larger than 3 nm, which allows them to survive as individual aerosols (O'Dowd et al., 2002; Cavalli et al., 2006), and contribute to their further growth to a diameter of 50 to 100 nm, which allows them to act as CCN (Tunved et al., 2008). The findings of these studies were confirmed by Sihto et al. (2011) who derived, from information on the hygroscopicity of the aerosol at Hyytiälä, that aerosols that have grown to the size of CCN consist for a large part (~80 %) of organic material.

The number of aerosols that eventually activate into cloud droplets depends on the aerosol concentration, size distribution and chemical properties and on the updraft velocity, which determines the maximum supersaturation in a cloud parcel (McFiggans et al., 2006; Reutter et al., 2009). Once activated into cloud droplets, aerosols affect the cloud optical and microphysical properties through various Aerosol Indirect Effects (AIE). Twomey (1977) suggested that adding aerosols increases the droplet concentration and decrease the droplet size of clouds with a given liquid water path (LWP), which in turn leads to an increase of the cloud albedo (1st indirect effect). Albrecht (1989) proposed that the changes in cloud microphysics lead to a less efficient formation of precipitation and an increase in cloud lifetime (2nd indirect effect), while Lohmann and Feichter (2005) discussed several semi-direct effects such as cloud warming due to increased absorption of solar radiation by black carbon aerosols.

Satellite remote sensing is a widely used tool for determining the AIE. Retrievals of cloud optical thickness and effective radius are required to determine the sensitivity of cloud radiative properties to changes in aerosol concentration (Nakajima et al., 2001; Platnick and Twomey, 1994). Using either of these variables as indicator of the AIE requires the assumption of a constant LWP, which is generally not the case. A way to circumvent this problem is to estimate the cloud droplet number concentration (N_{CD}), since it directly links cloud optical and microphysical properties to the aerosol concentration at cloud base. Several methods have been developed for this purpose, each one requiring different assumptions about the sub-adiabatic character of and the mixing that occurs inside clouds (Bennartz, 2007; Boers et al., 2006; Szczodrak et al., 2001).

The method developed by Boers et al. (2006) (hereinafter referred to as B06), was validated by Roebeling et al. (2008), combining ground-based observations of cloud depth (h) and LWP with calculations of the cloud model using data from the SEVIRI-instrument on-

board METEOSAT as input. This showed very good agreement for strictly selected cases over the Netherlands.

Until now, however, there is little observational evidence for the influence of aerosols, which are formed in the boreal forest, on cloud optical and microphysical properties. Most of these measurements are performed at a clean background site in northern Finland, Pallas (Komppula et al., 2005; Kerminen et al., 2005; Lihavainen et al., 2008), which is at the northern border of the boreal forest. Recently, Lihavainen et al. (2010) estimated aerosol-cloud interactions over Pallas, using a combination of ground-based and MODIS data of cloud and aerosol properties. Their focus was how quantification of the aerosol burden affects the measured strength of aerosol-cloud interactions comparing ground-based and satellite measurements.

In our study we combine satellite observations of cloud properties over the SMEAR II measurement station at Hyytiälä in Finland with ground-based observations of aerosol concentrations and meteorological fields from ECMWF-reanalysis (1) to assess the seasonal variability in N_{CD} of low level liquid water clouds over the boreal forest and (2) to determine the role of surface aerosol concentration and meteorology in explaining this variability.

In Section 2 we first present the applied methodology including a description of the selection of the satellite and surface data, an introduction of the cloud model and a detailed uncertainty analysis. Section 3 shows the results of our analysis, including the observed cloud properties and their relation to aerosol concentrations and meteorology. The paper is concluded by a discussion and conclusions Sect. 4.

5.2 Data and methods

We present an analysis of cloud properties as observed by the MODIS-instrument onboard the Terra satellite in combination with ground based measurements of aerosol concentration and meteorological fields obtained from the ECMWF-server. As it is not possible to derive N_{CD} directly from the reflection spectra of solar radiation by clouds, we apply a model which generalizes the properties of stratiform liquid water clouds to estimate N_{CD}. The advantage of using satellite based measurements is that it allows to monitor the seasonal cycle in cloud optical and microphysical properties over several years, and thus get a statistically robust signal. We calculated median values of the satellite, aerosol and meteorological data, divided over 24 bins. For a period of 182 days, this resulted in a bin size of 7.6 days.

5.2.1 Satellite data selection

We used 9 yr (2000–2008) of MODIS-Terra Level2 (collection 005)-data (Platnick et al., 2003), which comprise pixel level retrievals (1 km resolution) of cloud optical and microphys-

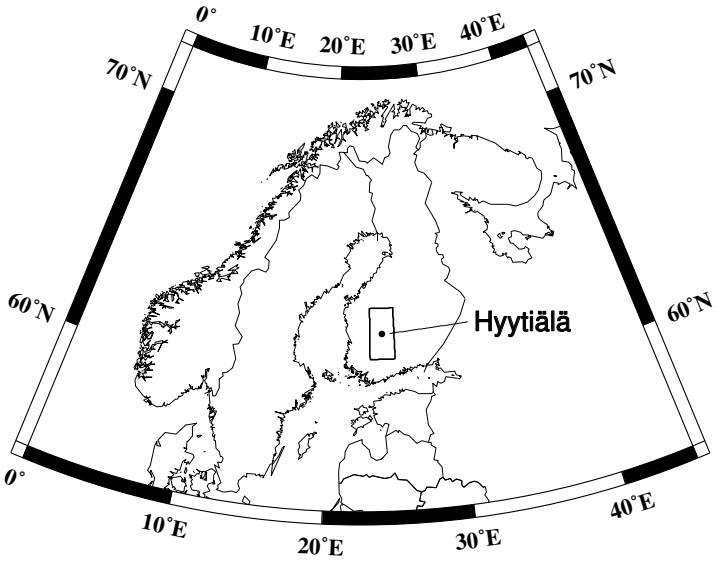

Figure 5.1: Map indicating the location of the SMEAR II field station at Hyytiälä, Finland and the $2 \times 2°$ latitude-longitude box over which the MODIS and ECMWF data are averaged.

ical properties. We averaged cloud properties over a $2 \times 2°$ latitude-longitude box centered over the SMEAR II measurement station, Hyytiälä, Finland (Fig. 5.1).

Since the cloud model is only valid for single-layered water clouds we selected clouds according to their cloud optical thickness τ ($3.7 < \tau < 20$) and cloud top pressure $p_{\rm ct}$ ($p_{\rm ct} >$ 780 hPa, corresponding to a cloud top height lower than about 2.5 km) based on the ISCCP (International Satellite Cloud Climatology Project) definition of stratocumulus. We realize that these criteria represent only an approximate climatological relationship between satellite derived cloud properties and the classical morphological cloud types and therefore do not rule out the inclusion of other types of clouds. Therefore, we tested the sensitivity of our results for the τ-criterion by including also clouds that are optically thicker. We constrained the retrievals to days for which the solar zenith angle did not exceed 60°, which roughly limited our retrievals to the months of April to September, coinciding with the boreal forest growing

season. Furthermore, we selected only data with a satellite sensor zenith angle smaller than 60°, to avoid the data to be affected by 3-D-radiative effects in the cloud (Várnai and Marshak, 2007). We only included pixels for which MODIS cloud phase qualified as "opaque water clouds" to exclude the possible influence of ice clouds on the retrieval.

The occurrence of drizzle could affect the MODIS retrievals of cloud droplet effective radius (r_{eff}), since it causes a bi-modal cloud droplet distribution, consisting of cloud droplets and drizzle. Since the MODIS retrievals assume a single-modal distribution of cloud droplets the retrieved r_{eff} may be underestimated in such cases (Bennartz et al., 2010). Therefore, we excluded all satellite observations for which a simultaneous observation of precipitation was done at the SMEAR II station. We acknowledge, however, that this does not rule out the possible occurrence of non-ground reaching precipitation.

5.2.2 Ground-based measurements

The observations are performed at the SMEAR II field station at Hyytiälä (61°51′ N, 24°17′ E) in southern Finland, where ecosystem, meteorological and aerosol properties are measured since 1996 (Hari and Kulmala, 2005). During the growing season (April–September), the air masses that arrive at the site are mostly of marine origin, except for the months of April when advection of continental air dominates and July when advection of marine and continental air masses have equal shares (Sogacheva et al., 2008). Levels of anthropogenic pollution are low, especially during periods when air masses arrive from the sparsely populated northern sector. For a more detailed site description, see Kulmala et al. (2001).

Aerosol size distribution data are obtained from a differential mobility particle sizer (DMPS) (Aalto et al., 2001) that measured aerosols in the range from 3 to 500 nm until December 2004 and aerosols between 3 and 1000 nm in diameter after that date. The number concentrations of aerosols above a certain activation diameter was obtained by summing the aerosols from that diameter up to the upper limit of the measured size distribution, thus assuming a fixed chemical composition of the aerosol over the size distribution.

Cloud condensation nuclei at various supersaturations have been measured with a CCN counter from July 2008 to June 2009. A more detailed description of these measurements is given by Sihto et al. (2011).

5.2.3 Cloud model

We used the cloud model of B06 to calculate N_{CD} and h from satellite observations of cloud droplet effective radius (r_{eff}) and cloud optical thickness (τ).

The model represents the microphysics and thermodynamics of a single-layered water

cloud based on functions of the following form:

$$N_{\mathrm{CD}} = A_1 \tau^{1/2} r_{\mathrm{eff}}^{-5/2} \tag{5.1}$$

and

$$h = A_2 \tau^{1/2} r_{\mathrm{eff}}^{1/2}, \tag{5.2}$$

where:

N_{CD}: cloud droplet number concentration (cm^{-3})

h: cloud physical thickness (m)

r_{eff}: effective radius of cloud droplets (μm)

τ: cloud optical thickness (–)

$A1$, $A2$: factors that contain the model's uncertainties with respect to cloud thermodynamics and microphysics.

The factors $A1$ and $A2$ are not constant, but depend on assumptions about the following four cloud thermodynamic and microphysical factors: (1) the subadiabatic behavior of the cloud, represented by the subadiabatic fraction F_{r} of the liquid water path, (2) the shape of the liquid water profile (linear or C-shaped), (3) the ratio between the volume radius and effective radius of the cloud droplets k_1 and (4) if the variation in the vertical profile of the liquid water content (LWC) is associated with variation in the droplet concentration or droplet volume radius or both.

The reason that the model is only valid for stratiform clouds is that these clouds are relatively homogeneous, so that the vertical profiles of LWC, N_{CD} and other physical cloud properties can be generalized rather easily. The model thus infers low-level, stratiform clouds in or just above the boreal forest boundary layer, the clouds most likely to be affected by the aerosols from the forest.

For the derivation of the model we refer to the papers of B06 and Boers and Rotstayn (2001). Here we limit ourselves to an introduction of the governing equations of the cloud model and focus in particular on the associated uncertainties. The equations to calculate N_{CD} and h from the input of satellite-based cloud optical properties respectively with the factors $A1$ and $A2$ fully written out are:

$$N_{\mathrm{CD}} = 2^{-2/3} 3^{1/2} \pi^{-1} \left(\frac{\rho_{\mathrm{a}}}{\rho_{\mathrm{w}}} \right)^{1/2} A_{\mathrm{ad}}^{1/2} k_1^{-3} F_i^{-1/2} (F_{\mathrm{r}}, \alpha)\, G_i^{5/2} (F_{\mathrm{r}}, \alpha)\, \tau^{1/2} r_{\mathrm{eff}}^{-5/2}, \tag{5.3}$$

and

$$h = \left[\frac{2}{3} \left(\frac{\rho_{\mathrm{w}}}{\rho_{\mathrm{a}}} \right) A_{\mathrm{ad}}^{-1} F_i^{-1} (F_{\mathrm{r}}, \alpha)\, G_i^{-1} (F_{\mathrm{r}}, \alpha) \cdot \tau \cdot r_{\mathrm{eff}} \right]^{1/2} \tag{5.4}$$

where:

ρ_a: density of air (kg m^{-3})

ρ_w: density of water (kg m^{-3})

A_{ad}: adiabatic lapse rate of liquid water mixing ratio (g g^{-1} m^{-1})

k_1: ratio between the second moment of the droplet size (volume radius r_v) distribution and its 3rd moment (effective radius r_{eff}) (–)

α: factor that determines shape of liquid water vertical profile (–)

F_r: subadiabatic fraction (–)

F_i and G_i are functions related to the mixing model that is used.

It is obvious from these relationships that N_{CD} and h depend on a large number of parameters which are often poorly constrained. Therefore, a thorough uncertainty analysis is required.

5.2.4 Uncertainty analysis

Calculation of N_{CD} and h is subject to uncertainties in the retrievals of r_{eff} and τ by MODIS and uncertainties that arise from using the cloud model. In this section we discuss possible error sources in both retrieval and the cloud model, whether they are random or systematic and how they propagate through the analysis. We are aware of the fact that the uncertainty estimates are themselves often uncertain, but the following analysis will give some insight in the contributions of the individual input parameters to the total uncertainty estimate.

Since the relation between the input variables and output variables of Eqs. 5.3 and 5.4 follows a power law (i.e. $X = Y^{\beta}$), the sensitivity of any output variable to any input parameter or variable can be written as:

$$\frac{\partial X}{\partial Y} = \beta \frac{X}{Y} \tag{5.5}$$

where:

β: exponent of the power law relation between X and Y.

If we assume that the errors are normally distributed we can use Gaussian error propagation and write the relative errors of N_{CD} and h, respectively, as follows:

$$\left[\frac{\partial N_{CD}}{N_{CD}}\right]^2 = \left[3\frac{\partial k_1}{k_1}\right]^2 + \left[\frac{1}{Z_1}\frac{\partial Z_1}{\partial Fr}\right]^2 + \left[\frac{1}{2}\frac{\partial A_{ad}}{A_{ad}}\right]^2 + \left[\frac{5}{2}\frac{\partial r_{eff}}{r_{eff}}\right]^2 + \left[\frac{1}{2}\frac{\partial \tau}{\tau}\right]^2 \tag{5.6}$$

$$\left[\frac{\partial h}{h}\right]^2 = \left[\frac{1}{Z_2}\frac{\partial Z_2}{\partial Fr}\right]^2 + \left[\frac{1}{2}\frac{\partial A_{ad}}{A_{ad}}\right]^2 + \left[\frac{1}{2}\frac{\partial r_{eff}}{r_{eff}}\right]^2 + \left[\frac{1}{2}\frac{\partial \tau}{\tau}\right]^2 \tag{5.7}$$

where:

$$Z_1(F_r) = F^{-\frac{1}{2}}(F_r, \alpha) G^{\frac{5}{2}}(F_r, \alpha) \tag{5.8}$$

$$Z_2(F_r) = F^{-\frac{1}{2}}(F_r, \alpha)\, G^{-\frac{1}{2}}(F_r, \alpha) \tag{5.9}$$

In the assessment of the uncertainties in the input parameters and other model parameters we have made a distinction between the random and the systematic part of those errors.

Uncertainty in effective radius ($r_{\mathbf{eff}}$) and cloud optical thickness (τ)

The retrievals of MODIS Level 2 (the already processed raw spectral data) cloud optical and microphysical properties are described by Platnick et al. (2003). We used data from Collection 005, which are the first MODIS Cloud Optical Properties retrievals to include pixel-level uncertainty estimates (King et al., 2006). The mean error for both r_{eff} and τ is about 13 %. Based on these references, we estimate a random component of 25 %, which, after spatially averaging the pixel values in the latitude-longitude box and temporally averaging these in bins, results in an error of 10 %. This error estimate acknowledges the systematic error in MODIS, but the temporal and spatial averaging levels out the random part of the error.

Uncertainty in ratio between volume and effective radius (k_1)

The parameter k_1 relates the volume radius to the r_{eff} of a droplet size distribution and therefore contains information on the skewness and dispersion of the droplet size distribution. For the typical values of N_{CD} that we find in our study (<100 cm^{-3}), the range of possible values of k_1 is relatively small. Following B06, we take $k_1 = 0.87 \pm 0.03$, so that $dk_1/k_1 = 0.03/0.87 = 3$ %.

Uncertainty in subadiabatic fraction (F_r)

The cloud model considers the fact that mixing in of air into the cloud is a non-adiabatic process by means of applying a subadiabatic fraction F_r to the cloud liquid water profile. For single-layered water clouds F_r will roughly vary between 0.3 and 0.9, depending on the intensity of turbulent entrainment and vertical mixing of the clouds and surrounding air. A smaller F_r, for fixed values of the other parameters, means that the liquid water is distributed over a larger vertical portion of the cloud, causing larger values of h and smaller values of N_{CD}. Since we have no further information on the actual F_r, we applied a value of 0.6 for F_r, comparable to the values used in previous studies (B06, Roebeling et al., 2008). For the uncertainty in F_r, we follow B06 and set F_r to 0.6 ± 0.3. We numerically evaluated the cloud model for these variations in F_r, which yielded an error of 26 % for typical values of r_{eff}, τ and A_{ad} found in our study.

Uncertainty in adiabatic lapse rate of liquid water content mixing ratio (A_{ad})

The adiabatic lapse rate of liquid water mixing ratio A_{ad} ($g\,g^{-1}\,m^{-1}$) depends on temperature and pressure (Betts and Harshvardhan, 1987). Since it is equal to the amount of water that condenses when a parcel of air rises along the moist adiabat, it is coupled to the moist adiabatic lapse rate Γ_m. To obtain the range in A_{ad} during the season, we need information on the cloud base temperature and pressure. For Hyytiälä, the seasonal surface temperature range defined as the mean temperature in the warmest minus the mean temperature in the coldest month in the period of our retrievals is about 13 °C (e.g. Kulmala et al., 2004a). By assuming a mean cloud base at 1000 m and a well-mixed boundary layer, the cloud base temperature (T_{cb}) can be estimated using:

$$T_{cb} = T_s - h_{cb}\Gamma_d \tag{5.10}$$

where:

T_s: surface temperature (K)

h_{cb}: cloud base height (m)

Γ_d: dry adiabatic lapse rate ($K\,m^{-1}$)

Under these assumptions, we arrive at an estimated minimum and maximum cloud base temperature over Hyytiälä of −7 °C and 6 °C, respectively. For an estimated mean cloud base pressure of 900 hPa, the corresponding minimum and maximum values of A_{ad} is 1.09×10^{-8} and 1.78×10^{-8}, respectively. This yields a mean A_{ad} of $1.44 \times 10^{-8} \pm 0.35 \times 10^{-8}$ implying an error of 24 %.

Variations in A_{ad} are likely to be systematic on seasonal time scales, because of its coupling to temperature. Since a higher (lower) A_{ad} leads to a higher (lower) N_{CD}, this will lead to an overestimation of the N_{CD} in spring and autumn and an underestimation in summer.

Uncertainty in other parameters

Finally there are two parameters that control the vertical profiles of cloud optical properties in the cloud model, but which do not contribute significantly to the uncertainty in the calculations of N_{CD} and h, but which are discussed here for completeness.

The parameter α determines the curvature of the liquid water profile in the cloud model. Following B06, the value is fixed at 0.3. They found that vertically averaged values of N_{CD} and h are insensitive to the choice of α.

Mixing with dry air from outside the cloud causes the liquid water path to deviate from the adiabatic water path. There are basically two contrasting possible assumptions on the effects of non-adiabaticity on the vertical profile of the liquid water path (1) either the departure from the adiabatic liquid water path is caused by a change in droplet volume, while cloud droplet number N_{CD} is constant, or (2) the N_{CD} is changed, while the droplet volume remains con-

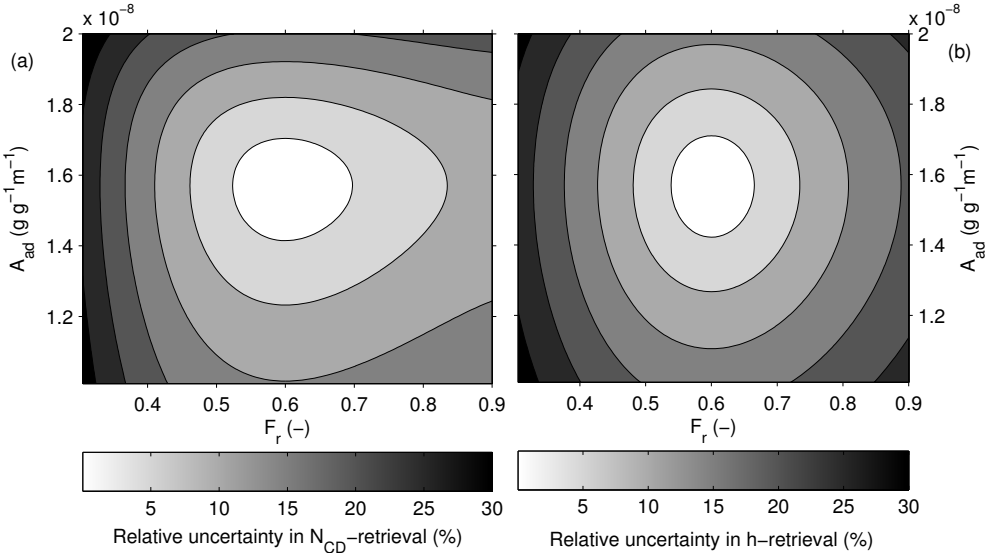

Figure 5.2: Sensitivity analysis of the cloud model to subadiabatic fraction F_r and the adiabatic lapse ratio of liquid water content mixing ratio A_{ad}, which are the two major contributors to the total uncertainty in the retrievals of N_{CD} and h. The uncertainty is given in percent relative to the retrievals for the best guess of the respective parameters for **(a)** *N_{CD} and* **(b)** *h. The calculations are performed with $r_{eff} = 12$ and $\tau = 9$.*

stant. The former is referred to as homogeneous mixing, since the mixing evaporates water from all cloud droplets at an equal rate. The second situation is referred to as inhomogeneous mixing, because the cloud droplets are evaporated due to dilution of the cloud parcel with environmental air, while the volume of the remaining droplets is conserved. Interestingly, both assumptions result in about the same vertically averaged N_{CD} (B06), so our results are insensitive to the assumption on homogenous or inhomogeneous mixing conditions. We have chosen to use the inhomogeneous mixing assumption in our analysis.

Combining all the discussed uncertainties in the individual input parameters, using Eqs. 5.6 and 5.7, we obtain a relative error in the calculation of N_{CD} and h of respectively 38 % and 21 %. The most important parameters contributing to these errors are F_r and A_{ad}. To illustrate the sensitivity of the cloud model to these two major sources of uncertainty on the error estimate, their combined effect is shown in Fig. 5.2.

These large errors mean that the CCN that reach cloud base only partly explain N_{CD} and h as calculated by the model, due to variations in cloud microphysics and thermodynamics that are not constrained by the satellite data.

5.3 Results

We present an analysis of the seasonal cycle in N_{CD} and the relationship between N_{CD} and surface aerosol concentration and meteorology.

5.3.1 Seasonal cycle in N_{CD}

The seasonal cycles of satellite retrieved cloud properties from MODIS are shown in Fig. 5.3. The seasonal cycles in r_{eff} and τ show both largest values at the beginning of April and a rapid decrease to a minimum in late April. After that both variables increase again. A large interannual variability results in large uncertainties in the retrievals of r_{eff} in April. The cause of this large interannual variability for this period is not clear. The number of data points per bin and thus the occurrence of stratiform cloud cases does not show a clear seasonal variability (Fig. 5.3c), except for the last bin which has a significantly lower number of data points than the others.

We conducted a sensitivity analysis to assess the changes in retrieved variable values as a function of the spatial domain over which the cloud properties are averaged. Changing the size of the box to $1 \times 1°$ and $3 \times 3°$ did not significantly impact these outcomes. To test the sensitivity of the retrievals to the definition of the cloud type, we relaxed the τ-constraint to include clouds with an optical thickness up to 100. This also did not change the seasonal cycle in observed cloud properties qualitatively.

The calculated seasonal cycle in N_{CD} mainly follows the variations in r_{eff} (Fig. 5.4a). Seasonal variations in τ only slightly dampen the seasonal cycle in N_{CD}. The real seasonal cycle in N_{CD} is expected to be less pronounced than depicted in Fig. 5.4, because of the dampening effect of the seasonal variation in A_{ad} on the N_{CD}, due to its coupling to temperature as previously discussed in the section on error propagation. The range of absolute numbers of N_{CD} (between 40 and 100 per cm^3) is rather low for continental areas and resemble the numbers found by B06 for a remote marine location. N_{CD} peaks in late April and early May. After experiencing a minimum in mid-summer, N_{CD} seems to increase again in September, although this increase is not significant.

The calculations of cloud thickness h follow the pattern of r_{eff} and τ, although the uncertainty of this result is large (Fig. 5.4d). This large uncertainty is a result of the uncertainty in several input parameters of the cloud model, that vary on seasonal time scales, a point which was also reported by B06. Roebeling et al. (2008), however, found good agreement between retrieved h from the cloud model and h as observed by ground based observations. A changing h due to aerosol effects could in principle affect the cloud albedo, but this effect is not well understood and therefore we will not further discuss it.

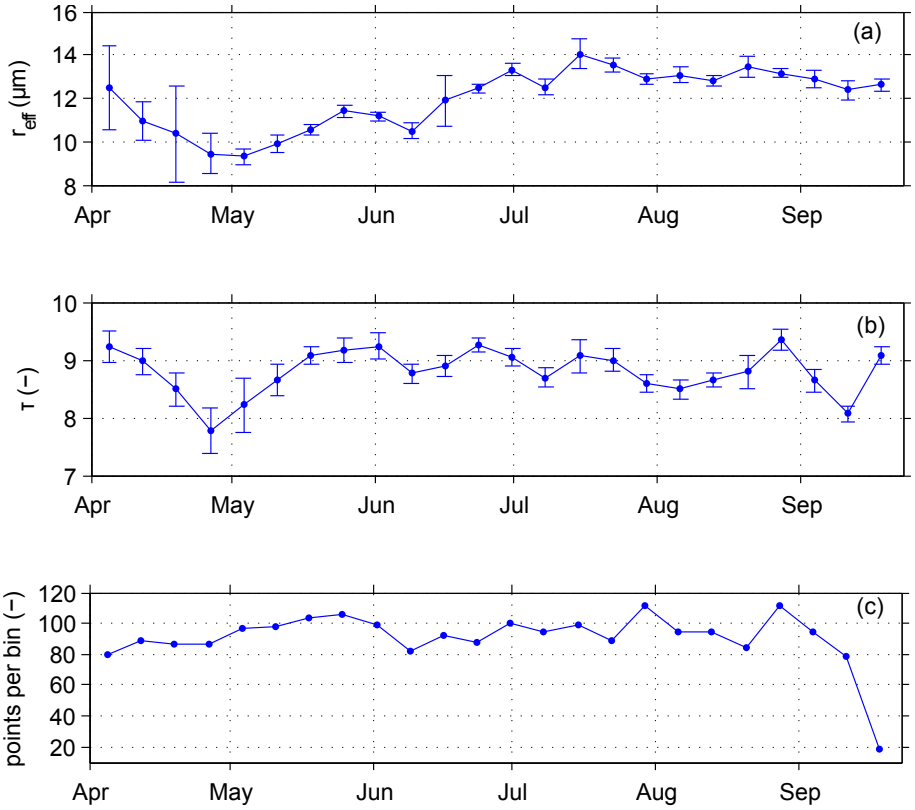

Figure 5.3: Seasonal cycle in **(a)** *MODIS effective radius* r_{eff} *and* **(b)** *cloud optical thickness* τ *over Hyytiälä for the years 2000 to 2008* **(c)** *number of datapoints per bin. Each datapoint corresponds to one of 24 bins, each representing the median value of the variable over all years.*

5.3.2 Relation to surface aerosol concentrations and meteorology

To find out if the seasonal cycle in N_{CD} is driven by the number of activated aerosols we compared it to surface concentrations of potential cloud nucleating aerosols. Since CCN-measurements are not available for the whole period of available satellite observations, we applied observations of aerosols with a diameter above a certain cut-off diameter as a proxy for CCN-concentrations (N_{CCN}) since size is in general a good indicator of ability of aerosols to act as CCN (Dusek et al., 2006). We find that the number concentration of aerosols with a diameter larger than 100 nm ($N_{>100}$ from here onwards) is the best proxy for N_{CCN} at 0.2 % supersaturation (Fig. 5.5) with a correlation of $r = 0.78$ for the period July–September 2008 and April–June 2009. The chosen supersaturation is similar to the supersaturation of 0.25 %

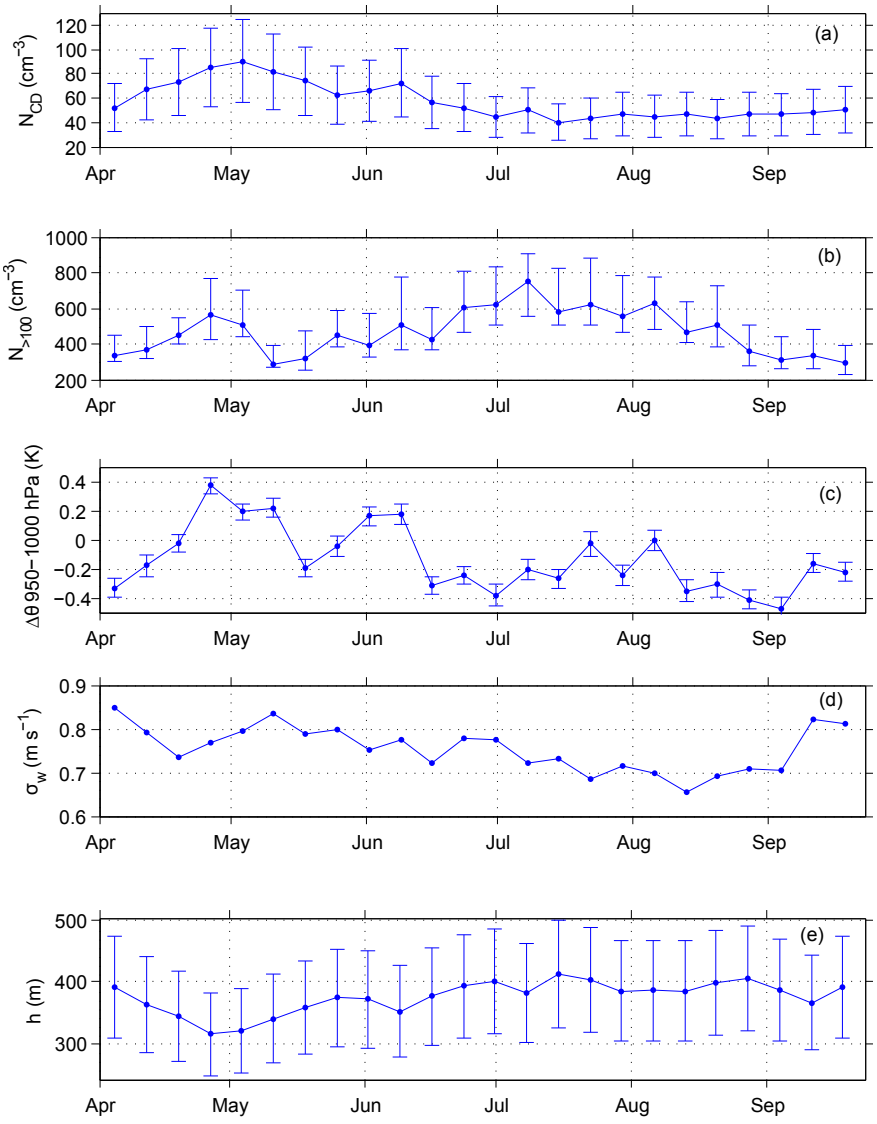

Figure 5.4: Median seasonal cycle over 2000–2008 in **(a)** *cloud droplet number concentration N_{CD},* **(b)** *surface observations of CCN-proxy concentrations $N_{>100}$,* **(c)** *potential temperature difference between the 1000 and 950 hPa-level $\Delta\theta_{1000-950}$,* **(d)** *standard deviation of the vertical wind speed σ_w and* **(e)** *cloud depth h. The errorbars in N_{CD} and h indicate the uncertainty as calculated in Sect. 2.4. The errorbars in $N_{>100}$ indicate the concentrations of aerosols larger than 80nm ($N_{>80}$, upper limit) and larger than 120nm ($N_{>120}$, lower limit), respectively, to account for the seasonal variation in critical diameter for CCN-activity of aerosols at Hyytiälä (Sihto et al., 2011). Errorbars in $\Delta\theta_{1000-950}$ designate the standard error. Meaning of datapoints as in Fig. 5.3.*

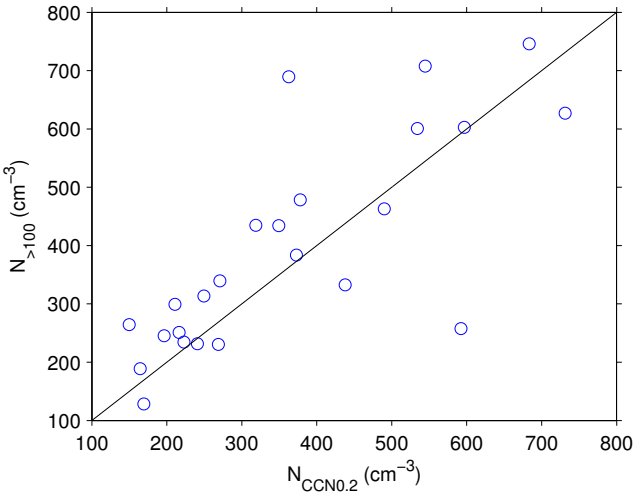

Figure 5.5: Comparison of cloud condensation nuclei concentration at 0.2 % supersaturation $N_{CCN0.2}$ and number concentration of aerosols with a diameter larger than 100 nm $N_{>100}$ for the period July–September 2008 and April–June 2009. The line with a slope of 1 is included for visual guidance. Correlation coefficient $r = 0.78$.

as used by B06 under weak convective conditions.

The seasonal cycle in N_{CD}, however, does not resemble the seasonal cycle in $N_{>100}$ (Fig. 5.4). The latter does have a similar peak in spring as the former, but the maximum in summer in $N_{>100}$ cannot be seen in the N_{CD}. Actually, comparing individual years, it turned out that the collective peak in spring is mainly reflecting a bias due to one year in which $N_{>100}$ had a very strong maximum in spring, which did not coincide with a maximum in N_{CD} for that year. The lack of correlation of N_{CD} and $N_{>100}$ can be seen from Fig. 5.6a. The correlation coefficient of the median seasonal cycles over all years in N_{CD} and $N_{>100}$ is $r = -0.24$, while for individual years it varies between $r = -0.36$ and $r = 0.28$. In addition, the absolute numbers of N_{CD} and $N_{>100}$ differ approximately by one order of magnitude which further supports the lack of a strong coupling between surface aerosol concentration and low-altitude clouds.

Sihto et al. (2011), however, found that at Hyytiälä the critical aerosol diameter for cloud droplet activation (d_{crit}) for a given supersaturation can vary considerably throughout the season, especially for low supersaturations. This may be caused by the seasonal variation in chemical composition of the aerosol at Hyytiälä: the aerosol contains a large fraction of organics in summer and has a relatively large contribution from anthropogenic sources in winter. It means that the seasonal dynamics of N_{CCN} may be different from those of $N_{>100}$.

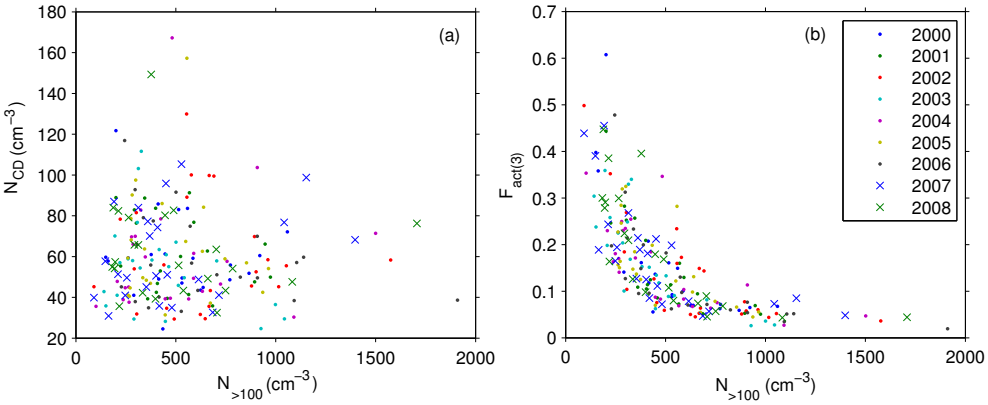

Figure 5.6: **(a)** *Comparison of CCN-proxy $N_{>100}$ and cloud droplet number concentration N_{CD} and* **(b)** *the activated fraction $F_{act(3)}$, defined as the ratio of N_{CD} and $N_{>100}$. Each data point represents the median of one bin, each bin representing a period of about one week over the years 2000 to 2008. The different marker colors and styles indicate the different years, as shown in the legend.*

For CCN at 0.2 % supersaturation d_{crit} varies roughly between 80 and 120 nm during the growing season (Fig. 4 in Sihto et al., 2011). To test whether the lack of correlation with N_{CD} was a result of specifically using $N_{>100}$ as a proxy for low supersaturation CCN, we also tested the seasonal cycle in aerosol concentrations for values of d_{crit} of 80 and 120 nm ($N_{>80}$ and $N_{>120}$, respectively). $N_{>80}$ and $N_{>120}$ are added to Fig. 5.4 as respectively the upper and lower bound of the errorbars around $N_{>100}$. The seasonal cycle of all these variables show the same two peaks in spring and summer, respectively, and therefore we conclude that the lack of correlation between N_{CD} and N_{CCN} does not strongly depend on the selection of the particular threshold diameter of the aerosol.

We discuss the activation of aerosols into cloud droplets in terms of the activated fraction (F_{act}), here defined as:

$$F_{act} = \frac{N_{CD}}{N_{CCN}} \approx \frac{N_{CD}}{N_{>100}}(-) \tag{5.11}$$

where:

N_{CD}: cloud droplet number concentration (cm^{-3})

N_{CCN}: surface CCN-concentration (cm^{-3})

$N_{>100}$: proxy for surface N_{CCN} at 0.2 % supersaturation (cm^{-3})

F_{act} thus gives information on the sensitivity of the cloud droplet activation to N_{CCN}. This means that we do not distinguish between whether activation of cloud droplets is limited by the transport of CCN from the surface to cloud base or whether the actual activation of the

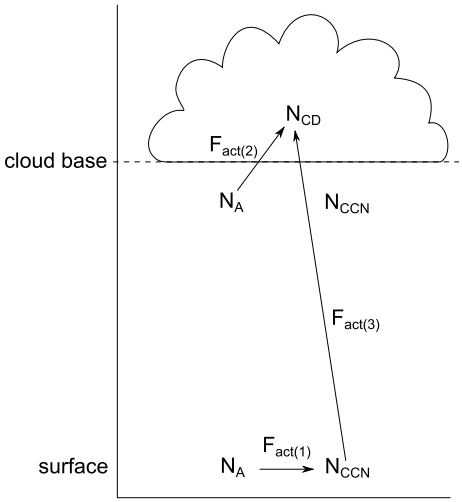

Figure 5.7: Schematic illustration of the different definitions of activated fraction (F_{act}) as found in literature: F_{act} may refer to (1) the ratio of the ratio of the total aerosol concentration (N_A) and CCN-concentration (N_{CCN}) at the surface (e.g. Jurányi et al., 2010; Sihto et al., 2011) to (2) the ratio of N_A at cloud base and N_{CD} (e.g. Kulmala et al., 1993; Reutter et al., 2009). In the present study, F_{act} refers to (3) the ratio between N_{CCN} at the surface and N_{CD}.

CCN as cloud droplets is limiting. It is important to note that this definition of F_{act} differs from others that are found in literature. In studies on cloud droplet activation, the activated fraction is defined as the ratio between the total aerosol concentration (N_A) at cloud base and N_{CD} (Kulmala et al., 1993; Reutter et al., 2009). Another definition is used in studies of CCN-activation (Jurányi et al., 2010; Sihto et al., 2011), where F_{act} is defined as the ratio between N_A and N_{CCN} at the surface. These different definitions are illustrated in Fig. 5.7.

To illustrate the different activated fractions, we have calculated $F_{act(1)}$ and $F_{act(3)}$ for the period that we have data for N_A, N_{CCN} and N_{CD}, i.e. July to September 2008. Figure 5.8 shows that N_{CCN} increases with increasing N_A. $F_{act(1)}$, which is the ratio of these, does not have a clear pattern over this period, but when looking at a longer period, Sihto et al. (2011) found a seasonal cycle in $F_{act(1)}$ at this site. The behaviour of $F_{act(3)}$ for this period is similar to that of the whole measurement period, showing little sensitivity of N_{CD} to $N_{CCN0.2}$. How $F_{act(2)}$ would behave, can be illustrated by the following limiting cases: (1) if CCN-activation is transport limited, meaning that few CCN are transported from the surface to cloud base, we would expect a high $F_{act(2)}$, since few CCN reach cloud base, but those that do are activated. (2) If CCN-activation is limited by the activation itself, many CCN reach cloud base, but few are activated, resulting in a low $F_{act(2)}$. In reality, these 2 effects will be combined, but based on our results we cannot distinguish between them.

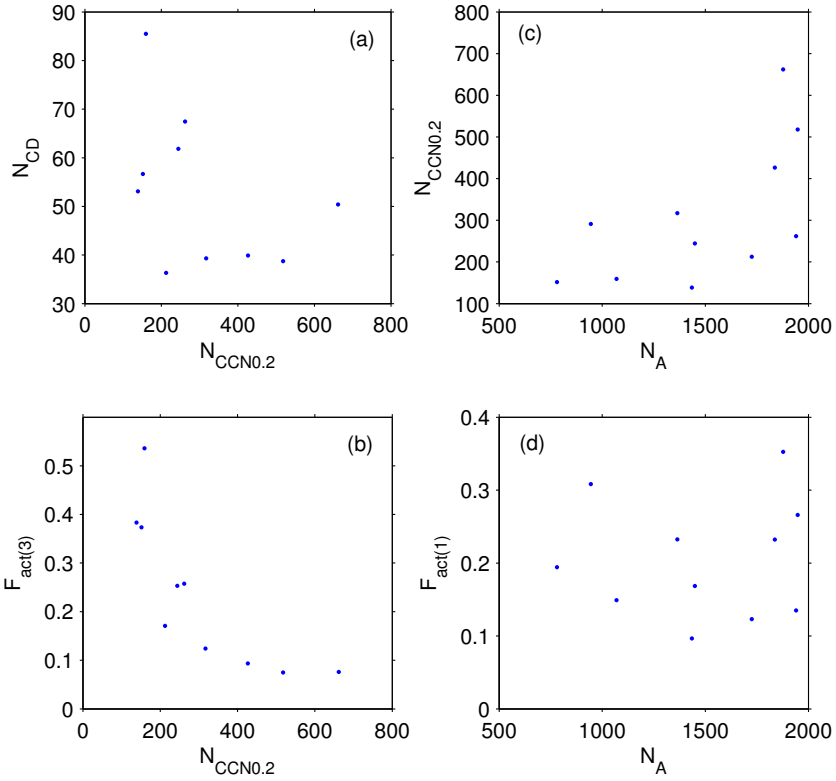

Figure 5.8: The activated fraction Fact for the period July–September 2008, for which there are data available of aerosol concentration N_A, CCN-concentration at 0.2% supersaturation $N_{CCN0.2}$ and cloud droplet concentration N_{CD}. **(a)** *Comparison of $N_{CCN0.2}$ and N_{CD},* **(b)** *$F_{act(3)}$, defined as the ratio of N_{CD} and $N_{CCN0.2}$,* **(c)** *comparison of N_A and $N_{CCN0.2}$ and* **(d)** *$F_{act(1)}$, defined as the ratio of $N_{CCN0.2}$ and N_A.*

In Fig. 5.6b we show that $F_{act(3)}$ is large for low $N_{>100}$ and small for high $N_{>100}$. This suggests that cloud droplet activation is not limited by the availability of cloud-nucleating aerosols; when $N_{>100}$ increases, droplet activation reaches saturation as can be seen from the decreasing $F_{act(3)}$. This situation is described as a regime where cloud droplet activation is updraft limited in a theoretical study of the influence of aerosol number, size and hygroscopicity on the cloud droplet activation of aerosols by Reutter et al. (2009) (see also Kulmala et al., 1993). When the updraft velocity is small, only a small fraction of the aerosols that reach cloud base activate as cloud droplets. Because these aerosols attract water, the supersaturation in the cloud is quenched, which inhibits further cloud droplet activation. Adding more aerosols will consequently not lead to more cloud droplets. The behavior of $F_{act(3)}$, as

presented in Fig. 5.6b, is similar to their results for conditions of low updraft velocities and hence low supersaturations (Fig. 4 in Reutter et al., 2009).

Information on the strength of convection could give more insight in the processes behind this behavior. As an indicator for convection, we use the potential temperature difference close to the surface, which represents thermal (in)stability in the sub-cloud layer. We obtained these data from the ECMWF ERA-Interim dataset on the ECMWF Data Server for the same spatial domain as we have obtained cloud properties for. Figure 5.4 shows a strong correlation between N_{CD} and the potential temperature difference between 1000–950 hPa ($\Delta\theta_{1000-950}$) with a correlation coefficient $r = 0.76$. The median seasonal cycle over all years in N_{CD} and $\Delta\theta_{1000-950}$ both show two peaks in spring and early summer, while the minimum in N_{CD} during summer is less pronounced in $\Delta\theta_{1000-950}$.

For the individual years, the correlations between N_{CD} and $\Delta\theta_{1000-950}$ are weaker and vary between 0.25 and 0.46, but the sign is consistently positive. A similar, but somewhat weaker, relation was found between N_{CD} and the potential temperature difference between 1000–900 hPa.

We also looked at the relationship between updraft velocities and N_{CD}. We use the standard deviation of the updraft velocity (σ_w) as measured at the SMEAR II station, since σ_w is a more reliable measure of vertical motions than the absolute values of the updrafts (Leaitch et al., 1996; Rosenfeld and Feingold, 2003). We found that the correlation between σ_w and N_{CD} is weak, but positive with $r = 0.46$. This weak correlation could be caused by the fact that we compare point measurements with spatial averages and that we use measurements in the surface layer to discuss activation at cloud base.

5.4 Discussion and conclusions

Our results show that there is a clear seasonal cycle in N_{CD} in low level liquid water clouds over Hyytiälä. This seasonal cycle can, however, not be explained by seasonal variations in concentrations of cloud active aerosols. Rather, the sharp decrease of activated fraction with increasing N_{CCN} suggests that droplet activation in the clouds that are included in our analysis is updraft-limited (cf. Reutter et al., 2009). The good correlation between N_{CD} and the stability of the boundary layer, as diagnosed from the potential temperature difference, further indicates that the transport and mixing of the aerosols from the surface to cloud base is an important factor for determining which part of the aerosols actually activate into cloud droplets. Both findings could be explained by the fact that the studied clouds, low-level stratiform clouds over the boreal forest, represent a cloud type and environment, respectively, which are not associated with the occurrence of strong convection. However, based on this analysis, we cannot say whether the transport of aerosols from the surface to cloud base or

the actual activation of those aerosols in the cloud is the limiting factor for cloud droplet activation (Fig. 5.7). Therefore, we use the term convective limitation to acknowledge that both the effects of transport and activation and possibly a combination of them could be limiting factors for cloud droplet activation.

We acknowledge, however, that the effects of the chemical composition of the aerosols that serve as CCN should be studied further to clarify its role in the seasonal cycle in CCN-activation over the boreal forest. Especially under conditions of weak convection which results in low supersaturations the effect of the hygroscopicity could become important (e.g. Dusek et al., 2006). This effect is already clear from the uncertainty due to a seasonal variation in activation diameter as found by Sihto et al. (2011). This uncertainty is included as the error bars of Fig. 5.4b.

Formation of convective cumulus clouds, on the other hand, is closely coupled to surface conditions (e.g. Brown et al., 2002) and to conditions of stronger convection and therefore higher updraft velocities. Consequently, for these clouds the signal of the N_{CD} is more likely to follow the N_{CCN} at the surface. So our results, with a focus on stratiform clouds, do not rule out the possibility that aerosols from the boreal forest influence the other types of clouds over the forest. However, our results suggest that it is important to take the strength of convective transport into account when studying the AIE over boreal forests.

This convection-limitation may therefore be one of the factors to explain the weaker aerosol-cloud interaction as derived from satellite measurements of cloud properties combined with ground-based measurements of aerosol concentration, compared to ground-based measurements of both aerosols and cloud properties only as found by Lihavainen et al. (2010) for the northern high-latitude site Pallas. For the boundary layer clouds which are included in their satellite observations, the transport of aerosols to- and their activation in the cloud may be a limiting factor for their influence on cloud properties. This may be less important for the very low altitude clouds, which are that close to the surface that they surround the measurement station during some of the time.

Opposite to our results, Boers et al. (2006) found a clear relation between N_{CD} and N_{CCN}. They, however, studied clouds over the ocean, which do not experience the strong diurnal cycle in atmospheric boundary layer as over land. Therefore a well-mixed boundary layer is almost constantly present, which facilitates the transport of aerosol particles from the ocean surface to cloud base. The low values of N_{CD} that they find may indicate an aerosol-limited regime of cloud droplet activation.

The method to retrieve N_{CD} that we applied in our study represents the state-of-the-art of current remote sensing techniques at high latitudes. Still, the error in the calculation of N_{CD} is large due to uncertainties in the representation of cloud microphysics and thermodynamics. This large error may cause N_{CD} to vary independently from the number of CCN that actually reach cloud base. In this case, we find that there is a seasonal cycle in N_{CD} that has a distinct

shape that cannot be explained by a systematic seasonal variance in one of the input factors or cloud model parameters. Roebeling et al. (2008) showed that the method of B06 works well for carefully selected conditions (no drizzle, single layer, homogeneous in space and time, water phase), preferably supported with ground-based observations (lidar, radar, information about cloud base height and temperature). However, in their study over the Netherlands the number of cases that met the boundary conditions was limited. The same may be the case over Finland. Thus proving the first AIE from satellite retrievals requires very careful selection of representative cases. Therefore, we recommend that these satellite derived observations of N_{CD} should be validated with in-situ measurements of cloud properties over the boreal forest, for example by radiosonde or airplane measurements or by ground based remote sensing.

The data presented in this study are among the first observations of cloud properties over the boreal forest, related to the production of cloud active aerosols by the forest. We find that the N_{CD} in the studied clouds is insensitive to aerosol concentrations at the surface. Furthermore, information on the vertical structure of the atmosphere indicates that low N_{CD} is related to stable atmospheric conditions. From the combination of these two findings we conclude that convection may be a limiting factor for the activation of aerosols from the boreal forest as cloud droplets. Our analysis suggests that studies that do not take the role of convection into account when assessing the impact of aerosols from the boreal forest on cloud properties may overestimate their indirect radiative forcing. It stresses the need for a stronger involvement of the boundary layer and cloud research communities in such analysis of land-atmosphere interactions focusing on aerosols-cloud feedback mechanisms.

6 Conclusions

This chapter summarizes the main findings of the two parts of thesis. Since the answers to the research questions are already discussed in detail in the individual chapters, only the most important conclusions will be explained here.

6.1 Diurnal evolution of organic aerosol over boreal and tropical forests

The first research question of this thesis is: how do local surface forcings and large-scale meteorological forcings shape the evolution of organic aerosol over the boreal and tropical forest? This question is dealt with in Chapters 3 and 4 in case studies for the boreal and tropical forest, respectively. To answer this question a modeling tool (MXLCH-SOA) is developed, which represents land surface conditions and dynamical and chemical processes that influence the evolution of organic aerosol (OA) in a balanced way. The novelty of our approach is that it combines the dynamics of a convective boundary layer (BL) with a reduced gas-phase chemistry mechanism and a module for gas/particle-partitioning of semi-volatile organic species. The principles and governing equations of this modeling tool are described in Chapter 2 and in the subsequent chapters the simplified chemical reaction schemes are

presented to calculate secondary organic aerosol (SOA) formation from terpenes (Chapter 3 and 4) and from isoprene (Chapter 4).

Despite its simplicity, MXLCH-SOA is able to satisfactorily reproduce the main observed characteristics of dynamics, gas-phase chemistry and gas/particle partitioning for the two studied forest ecosystems and it enables us to explain the temporal variability of the concentrations of organic aerosol and its precursors as a function of the various processes. In short, the results show that the diurnal evolution of organic aerosol in a boreal and a tropical forest is the net result of land surface conditions, boundary layer dynamics, chemical transformations and gas/particle partitioning. In the case study for the boreal forest, the entrainment term of the background OA dominates the OA tendency, while in the tropical forest case it is the interplay of several local and large scale processes that shape the diurnal evolution of OA. A sensitivity analysis for the boreal forest case further shows that the OA concentration is sensitive to both volatile organic compound (VOC) emissions and the partitioning of the surface energy budget into a latent and a sensible heat flux. We have identified two regimes, based on which of the two studied land surface drivers dominates: one in which OA is mainly driven by SOA formation from the emitted VOCs and another in which dilution due to entrainment, as driven by the surface energy fluxes, determines the OA concentration. A background OA to fresh SOA ratio is introduced to facilitate the interpretation of this analysis and is used to quantify the contributions of both fresh and background components to the total OA concentration. One main difference between the two case studies is that in the boreal forest entrainment appears to dominate the diurnal cycle, which leads to a decreasing OA concentration during the day, while in the tropical forest the formation of SOA from both isoprene and terpenes leads to increasing OA concentrations during day time. The MXLCH-SOA framework therefore shows the need to represent all these biochemical and physical process simultaneously in order to understand the diurnal evolution of OA.

As the boundary layer dynamics-chemistry system is not a closed system, it is necessary to further study the influence of external forcings on the diurnal evolution of OA, besides the surface forcings. Two types of large-scale meteorological forcings and their effects on OA evolution through their impact on BL dynamics have been studied: subsidence due to the presence of a high pressure system and advection of relatively cool air. In Chapter 3 a theoretical sensitivity analysis is given of OA evolution to subsidence, which is applied to the tropical forest case study in Chapter 4. Subsidence has a rather counter-intuitive effect on OA concentrations: even though it suppresses the growth of the BL and consequently decreases the mixing volume for chemical species, it leads to decreased OA concentrations. The reason for this is that entrainment is strongly enhanced in case of subsidence due to thermodynamic effects, which results in a stronger dilution of OA. This knowledge is applied in the case study for the tropical forest in Chapter 4, since results from a large-scale model show subsiding air

motions over the measurement site and surroundings at Borneo.

In addition to subsidence, the advection of cool air is needed to reproduce the observed boundary layer dynamics at Borneo: only if subsidence and advection of relatively cool air are accounted for, the observed low BL height can be reconciled with the large observed surface sensible and latent heat flux. This cool air suppresses BL growth and entrainment. Consequently, the aerosol is trapped in a shallower layer, which leads to an increased concentration compared to the case without advection of cooler air. In conclusion, the large-scale meteorological forcings subsidence and advection of cool air have opposing effects on the diurnal evolution of OA, even though both suppress BL growth. These findings show the utility of our method in identifying effects that should be accounted for in large-scale chemistry transport models.

The second research question is whether recently discovered pathways of isoprene chemistry are the key to closing the gap between measured and modeled organic aerosol concentrations in tropical forests and other high isoprene environments. To address this issue, several mechanisms which may affect SOA formation from isoprene are implemented in MXLCH-SOA and discussed in Chapter 4. The hydroxyl radical (OH), the main oxidant of isoprene, is thought to be regenerated in the oxidation of isoprene. We find that for the tropical forest case study, we can not reconcile the modeled concentrations of VOCs, OH and OA with their observed concentrations and fluxes both for cases with and without OH recycling. Therefore, we conclude that the issue of recycling of the OH radical in the oxidation of isoprene has to be solved before its effect on SOA formation can be determined.

The formation of SOA from isoprene involves multiple generations of oxidation and due to this complex chemistry there is no single mechanism which can explain SOA formation from isoprene under all conditions. To gain understanding in this issue, we have implemented different pathways through which isoprene SOA is known to form, although we do not explicitly account for the detailed isoprene oxidation chain. A central aspect of this branching approach is whether the isoprene peroxy radical chemistry follows the low- or the high-NO_x pathway. We find that the latter channel dominates in our case study. For SOA formed through the high-NO_x channel, we further account for the effect of the NO_2/NO ratio on SOA yields. In the presented case study this has little effect as this ratio is low, it but could be more important in regions with slower photochemistry or higher emissions of anthropogenic pollution. In the low-NO_x regime, isoprene epoxides (IEPOX) are important intermediate gas-phase species in the formation of isoprene SOA. Even though the low-NO_x pathway is only a minor one here, the amount of IEPOX SOA formed is likely substantial, although a better understanding of the exact mechanisms for its formation is needed to confirm this.

However, as in previous studies we systematically underestimate the organic aerosol concentration in a tropical forest even though we incorporate the state-of-the-art knowledge on

isoprene SOA formation in MXLCH-SOA. Nevertheless, we advocate accounting for NO_x-regime specific chemical pathways when modeling isoprene SOA formation. As this field is rapidly evolving in terms of the development of new measurement techniques and the discovery of chemical mechanisms, we strongly recommend the intensive use of our modeling system to gain further understanding of the diurnal variability of OA and for testing new hypotheses under atmospheric conditions.

6.2 Satellite observations of cloud droplet concentration over the boreal forest

The final objective of this thesis is to understand how aerosols and meteorological factors influence cloud droplet concentration over the boreal forest. This is a first step in translating the process understanding such as addressed in the previous chapters to larger spatio-temporal scales. Since this objective considers different temporal and spatial scales, a different method is applied in Chapter 5 than in the foregoing chapters. Observations of cloud properties by the MODIS instrument onboard the Terra satellite are combined with a model that contains the microphysics and thermodynamics of a single-layered water cloud to obtain a seasonal cycle of cloud droplet number concentrations, averaged over 9 years of data. This seasonal cycle in cloud droplet concentration is compared with aerosol concentrations at the surface and meteorological fields from ECMWF reanalysis. We find that the cloud droplet number concentration is related to the potential temperature gradient in the boundary layer, a measure for the strength of convection, while it shows no clear relationship with the cloud active aerosol concentration at the surface. From this we conclude that the convective transport of the aerosols from the surface to cloud base is the limiting factor for their activation as cloud droplets. However, convection will also influence the formation of clouds from a thermodynamic perspective. Therefore, it is likely that convection, as driven by land surface conditions, regulates both transport of aerosols to cloud base and the height of the cloud base, defined as the height at which water vapor reaches its saturation pressure. To ultimately understand the effect of the boreal forest on cloud properties, the effects of aerosols and thermodynamics should be studied simultaneously.

7

Synthesis and outlook

This thesis consists of two parts, that are different in terms of both the processes and the spatiotemporal scales that are considered: Part 1 (Chapters 3 and 4) deals with the diurnal evolution of organic aerosol (OA) mass at diurnal and local scale, whereas Part 2 (Chapter 5) deals with observations of cloud droplet concentration at seasonal and regional scale. Here, I expose my view on how to close the gap between these two aspects, related to the state-of-the art literature. My strategy is to continue the line of reasoning developed in the introduction (Chapter 1) that the forested land surface is coupled with the atmosphere by regulating the sensible and latent heat fluxes on one hand and by providing volatile organic compound (VOC) emission fluxes on the other hand. Both turbulent heat fluxes are relevant in the transport of the emitted VOCs and the subsequent formation of secondary organic aerosol (SOA), and in the formation of boundary layer (BL) clouds. First, I explain which essential processes need to be addressed in future studies that aim to link the diurnal evolution of OA to the activation of aerosols as cloud droplets. To this end, I briefly review the current state of knowledge, both on biogenic aerosols from boreal and tropical forests and on the coupling of BL cloud formation to the surface (see the two branches in Fig. 7.1). Second, I analyze how to bridge the gap between the different disciplines involved in the coupling of the land surface with cloud formation.

7.1 From aerosol mass to number concentration

In Chapter 3 and 4, the diurnal evolution of the mass concentration of organic aerosol is studied by integrating the two branches of land-atmosphere coupling shown in Fig 7.1. However, to understand how aerosols affect cloud formation (as in Chapter 5), it is imperative to know the number concentration of cloud active aerosols, known as cloud condensation nuclei (CCN). To make the step from the aerosol mass concentration to aerosol number concentration and size distribution, and to complete branch that is initiated by VOC emissions in Fig. 7.1, the sources of submicron particle number have to be known. These particles provide the seed aerosols for the organic compounds to condense onto, resulting in the growth of these particles to CCN sizes. In the boreal forest, nucleation of new particles from gas-phase species is the dominating particle number source (Kulmala et al., 2001; Dal Maso et al., 2007). In tropical forests, on the other hand, nucleation has not been observed and primary particles are thought to determine the particle number (Pöschl et al., 2010; Pöhlker et al., 2012). It should be noted that observations of particle number source in tropical forests are limited to the Amazon rain forest. However, CCN concentrations at Borneo are much higher than those in the Amazon (Irwin et al., 2011), which might indicate different formation mechanisms.

Observations in boreal (Sihto et al., 2011) and tropical forests (Gunthe et al., 2009; Irwin et al., 2011) show that CCN in both environments contain a large organic fraction and therefore that organic compounds contribute to the growth of these particles. Addition of organic compounds to existing aerosols can occur by condensation onto freshly nucleated particles (O'Dowd et al., 2002; Allan et al., 2006; Laaksonen et al., 2008; Riipinen et al., 2011; Pierce et al., 2011) and by coating primary particles (Pöschl et al., 2010; Pöhlker et al., 2012).

Freshly nucleated particles have a diameter of about 1 nm and organics molecules are important in the first steps of their formation (O'Dowd et al., 2002; Metzger et al., 2010). To grow to sizes at which they can act as CCN (at least 30-100 nm (Dusek et al., 2006)), the uptake of vapors by these nanoparticles is required. Particles have been observed to grow to CCN sizes rapidly after their nucleation in forested environments (Kerminen et al., 2005; Pierce et al., 2012). In these environments, the oxidation products of biogenic VOCs are an important vapor source (Allan et al., 2006; Laaksonen et al., 2008; Riipinen et al., 2011; Pierce et al., 2012). The number of CCN that is eventually formed from nucleation depends on the competition between the growth of the freshly nucleated particles and their loss due to coagulation with other particles (Pierce and Adams, 2007). Most observed particle growth rates lie in the range from 1-10 nm h^{-1} (Kulmala et al., 2004b). Therefore, the growth of nucleated particles to CCN sizes will typically take between a few hours and a few days. However, the exact mechanisms by which organics contribute to the growth of these particles

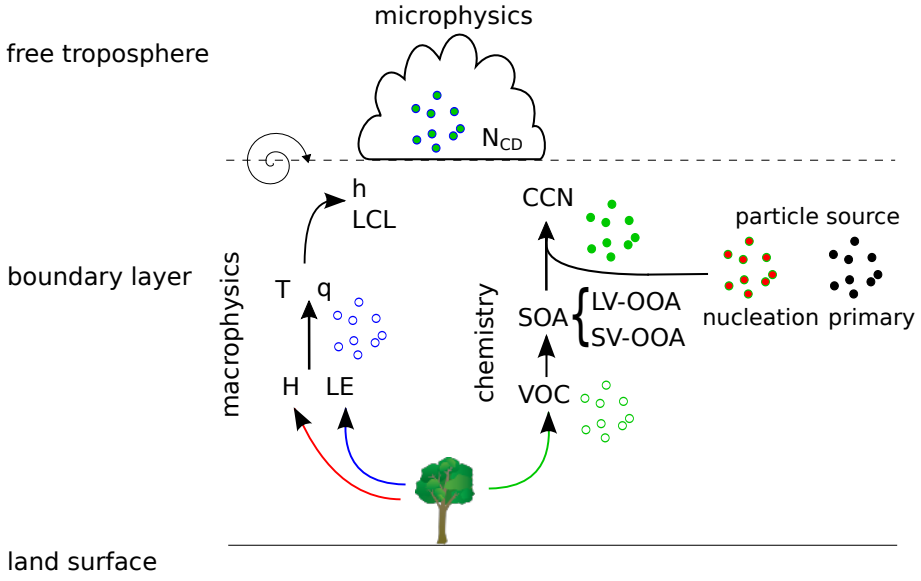

Figure 7.1: Conceptual representation of main processes and variables of the system that links the vegetated land surface, boundary layer dynamics, aerosol chemistry and dynamics, and cloud formation. Shown are the two branches through which vegetation affects clouds: heat flux partitioning into a sensible and latent heat flux, and VOC emissions. The left-hand-side branch shows how the sensible (H) and latent (LE) heat flux drive the macrophysics. The heat flux partitioning controls the temperature (T), humidity (q) and the boundary layer height (h). Therewith it determines whether saturation of water vapor occurs and at which height: the lifting condensation level (LCL). The right-hand-side branch represents the emissions of volatile organic compounds (VOC). After chemical transformation these become semi-volatile VOCs (SVOC). Dilution in the atmosphere and temperature determine whether these SVOCs condense into the secondary organic aerosol (SOA) phase. SOA consists of semi-volatile and low-volatile oxidized organic aerosol (SV-OOA and LV-OOA, respectively), depending on the degree of oxidation. The number of available particles is driven by either nucleation or primary sources. The SOA will condense onto these particles and thereby drive their growth to sizes at which they can act as cloud condensation nuclei (CCN). The physiochemical properties of the CCN and the supersaturation that is attained as driven by the macrophysics determine whether the CCN will activate as cloud droplets. In that way, both branches drive the cloud droplet number concentration (N_{CD}) and other cloud properties.

are not well understood (Riipinen et al., 2012).

Chemical aging of organics is likely an essential requirement for their condensation on existing particles, especially when these have diameters of only a few nanometers. In Chapters 3 and 4, only the formation of semi-volatile VOCs (SVOCs) and their gas/particle partitioning has been modeled and compared to the semi-volatile oxidized organic aerosol (SV-OOA) fraction as derived from AMS measurements. However, Jimenez et al. (2009) proposed to make a distinction between two subtypes of OOA: the less oxidized SV-OOA and the more oxidized low-volatile OOA (LV-OOA). SV-OOA will gradually evolve into LV-OOA due to photochemical processing. For example, SOA from α-pinene becomes similar to atmospheric SV-OOA after some aging in a reaction chamber and evolves into LV-OOA after prolonged exposure to OH (Jimenez et al., 2009). Exposure to OH leads to the further oxidation of many organic molecules that would mostly remain in the gas-phase themselves, resulting in the formation of higher generation oxidation products with lower saturation concentration (Donahue et al., 2012). Also aerosol phase reactions can be important for decreasing the volatility of organics (Riipinen et al., 2012). Aging thus leads a higher OA mass and including it in representations of SOA formation may help to close the gap between modeled and measured OA concentrations, as found in Chapter 4.

Moreover, Pierce et al. (2011) found that to condense on particles of 3 nm, organics need to have saturation concentrations of 10^{-3}-10^{-2} μg m^{-3}, which is several orders of magnitude lower than the volatilities of the SVOCs in this thesis. They suggested that reactions in both gas and aerosol phase could contribute to this decrease in volatility. Therefore, models that represent nanoparticle growth to CCN sizes due to condensation of organic vapors combine equilibrium partitioning of SV-OOA and kinetic uptake of LV-OOA (Riipinen et al., 2011; Yu, 2011).

The mechanisms governing the uptake of organics on primary particles from tropical forests have only recently begun to be studied. Pöhlker et al. (2012) proposed that in the Amazon, primary particles containing potassium salts emitted by rain forest biota are important seed aerosols for VOC oxidation products to condense onto. Specifically, they suggest that aqueous phase chemistry could be important in the growth and aging of these particles.

Regardless of the exact mechanism, addition of organic material increases both the size of a particle and the amount of hygroscopic material in it. In that way, organics influence both the Kelvin (surface tension) and Raoult (solute) terms of the Köhler equation, which describes the activation of a particle as cloud droplet (e.g. McFiggans et al., 2006). Laboratory studies show that the hygroscopicity of SOA is lower than that of inorganic salts like ammonium sulphate (King et al., 2007; Prenni et al., 2007). Similar hygroscopic properties as in lab studies are found in ambient measurements of predominantly organic CCN (Gunthe et al., 2009; Irwin et al., 2011; Sihto et al., 2011). Also here chemical aging can play an important

role, since the hygroscopicity of the OA generally increases when it becomes more oxidized (Jimenez et al., 2009).

In conclusion, organics can influence both the size and the hygroscopicity of an aerosol and therewith determine whether it will act as a CCN.

7.2 Macrophysics of cloud formation

The exact origin and type of the clouds that are included in the satellite retrievals in Chapter 5 is unknown, since their selection is based on bulk properties (i.e. cloud top pressure and optical thickness). Nevertheless, I decide to focus on shallow cumulus clouds in this description of the macrophysics of cloud formation (left-hand-side branch in Fig. 7.1), since formation of these BL clouds is strongly coupled to the land surface and consequently has a strong diurnal cycle (Freedman et al., 2001; Brown et al., 2002; Vilà-Guerau de Arellano et al., 2012). They are likely the clouds that are most directly influenced by aerosols formed from forest emissions, since the convective updrafts that transport water and heat from the surface to the height at which the cloud forms, will also transport aerosols formed near the surface. Shallow cumulus clouds play a key role in the transport of chemical species out of the BL (Vilà-Guerau de Arellano et al., 2005; Verzijlbergh et al., 2009), in reflecting and scattering incoming solar radiation (Dai et al., 1997) and in the further development of deep convective clouds (Garcia-Carreras et al., 2010; Zhang and Klein, 2010). However, their dynamics are very complex (Siebesma and Cuijpers, 1995; Jonker et al., 2008) and the effect of aerosols on their radiative and precipitation forming properties is far from being well understood (Jiang and Feingold, 2006; Stevens and Feingold, 2009).

In view of the complexity of the dynamics and microphysics in BL clouds, here I take a simple approach as a first approximation to link the two branches of Fig. 7.1. From a thermodynamic point of view, there is one clear criterion that must be met for a cloud to form: air has to be supersaturated with respect to liquid water. Since saturation of water vapor is a function of temperature and humidity, the potential for cloud formation is regulated by the dynamics of the BL, as driven by the surface forcings (Freedman et al., 2001). The height of the cloud base, known as the lifting condensation level (LCL), can be determined by comparing the specific humidity with the saturation specific humidity: where these are equal, a cloud can form (van Heerwaarden and Vilà-Guerau de Arellano, 2008). Formation of a cumulus cloud can only occur if the LCL is below the BL height, since then the large turbulent eddies rising from the surface can reach the saturation level. After reaching the LCL, water vapor starts to condense onto the CCN in the air parcel, which will then form cloud droplets. Furthermore, the updraft velocity of an ascending air parcel determines its rate of cooling and therewith the level of supersaturation that is attained. In that way, it

regulates which and how many aerosols are activated as cloud droplets (McFiggans et al., 2006).

The LCL and the updraft velocity of the air parcel thus form the link between the macro- and microphysics of cloud formation.

7.3 Outlook

In the previous two sections I have reviewed the current status of the knowledge on the aspects of organic aerosols and macrophysics related to the formation of clouds. It is necessary to further integrate the two branches of land-atmosphere coupling, initiated by surface heat flux partitioning and VOC emissions, respectively, (Fig. 7.1) to eventually determine their combined influence on cloud droplet concentration and other cloud properties.

The branch of land-atmosphere coupling initiated by the emissions of VOCs is the most challenging one. The first challenge is to accurately describe the mass (volatility) and oxidation state (aging) of OA, since both are needed to predict their contribution to the growth of existing particles and the hygroscopicity of those particles. This can be done by expanding the currently used volatility basis set (VBS) that only includes volatility to a representation that captures both the volatility and oxidation state of the OA (e.g. the 2D VBS, Jimenez et al., 2009). To further understand and quantify CCN formation, an aerosol microphysics model is needed to determine how organics affect the particle size distribution and composition both by condensational and kinetic uptake (Riipinen et al., 2011; Yu, 2011).

To finally set the step to understanding the cloud droplet concentration, micro- and macrophysics of cloud formation need to be considered simultaneously. The importance of BL dynamics in setting conditions for cloud formation by determining the LCL has been explained. A cloud parcel model that includes the microphysics of cloud droplet activation could be used to study the sensitivity of cloud droplet concentrations to aerosol concentration and properties, and updraft velocity (e.g. Reutter et al., 2009).

I recommend to further study these process interactions on diurnal time scales, because both aerosol mass and number concentration and shallow cumulus clouds have a strong diurnal cycle, so the processes that lead to their formation interact at diurnal time scales. Besides, this gives the opportunity to integrate modeling with observational data from intensive observation periods. Recent field campaigns in boreal (HUMPPA-COPEC, Williams et al., 2011), tropical (OP3, Hewitt et al., 2010), temperate (BEACHON-RoMBAS, `http://tinyurl.com/BEACHON-RoMBAS`) forests include simultaneous observations of chemistry and dynamics, and therefore provide good opportunities for gaining further understanding of the couplings between dynamics and chemistry of aerosol and cloud formation.

To eventually complete the feedback loop between vegetation and clouds, the influence of aerosols and dynamics on cloud fraction and radiative properties needs to be considered. Once activated as cloud droplets, aerosols can affect the cloud albedo (Twomey, 1977) and lifetime (Albrecht, 1989) and the formation of precipitation (Andreae and Rosenfeld, 2008). Quantifying the magnitude of these aerosol indirect effects is another great challenge (Stevens and Feingold, 2009). In principle, cloud fraction and radiative properties influence the amount of solar radiation reaching the surface. Thereby they can in turn affect the surface heat fluxes (Jiang and Feingold, 2006), on one hand, and VOC emissions (Guenther et al., 1995), on the other hand, thereby closing the feedback loop.

References

Aalto, P., Hämeri, K., Becker, E. D. O., Weber, R., Salm, J., Mäkelä, J. M., Hoell, C., O'Dowd, C. D., Karlsson, H., Hansson, H.-C., Väkevä, M., Koponen, I. K., Buzorius, G., and Kulmala, M.: Physical characterization of aerosol particles during nucleation events, Tellus B, 53, 344–358, doi:10.1034/j.1600-0889.2001.530403.x, 2001.

Albrecht, B. A.: Aerosols, cloud microphysics, and fractional cloudiness, Science, 245, 1227–1230, doi:10.1126/science.245.4923.1227, 1989.

Allan, J. D., Alfarra, M. R., Bower, K. N., Coe, H., Jayne, J. T., Worsnop, D. R., Aalto, P. P., Kulmala, M., Hyötyläinen, T., Cavalli, F., and Laaksonen, A.: Size and composition measurements of background aerosol and new particle growth in a Finnish forest during QUEST 2 using an Aerodyne Aerosol Mass Spectrometer, Atmos. Chem. Phys., 6, 315–327, doi:10.5194/acp-6-315-2006, 2006.

Andreae, M. O.: Aerosols before pollution, Science, 315, 50–51, doi:10.1126/science.1136529, 2007.

Andreae, M. O. and Rosenfeld, D.: Aerosol-cloud-precipitation interactions. Part 1. The nature and sources of cloud-active aerosols, Earth-Sci. Rev., 89, 13–41, doi:10.1016/j.earscirev.2008.03.001, 2008.

Arneth, A., Niinemets, U., Pressley, S., Bäck, J., Hari, P., Karl, T., Noe, S., Prentice, I. C., Serca, D., Hickler, T., Wolf, A., and Smith, B.: Process-based estimates of terrestrial ecosystem isoprene emissions: incorporating the effects of a direct CO_2-isoprene interaction, Atmos. Chem. Phys., 7, 31–53, doi:10.5194/acp-7-31-2007, 2007.

Arneth, A., Harrison, S. P., Zaehle, S., Tsigaridis, K., Menon, S., Bartlein, P. J., Feichter, J., Korhola, A., Kulmala, M., O'Donnell, D., Schurgers, G., Sorvari, S., and Vesala, T.: Terrestrial biogeochemical feedbacks in the climate system, Nature Geosci., 3, 525–532, doi:10.1038/ngeo905, 2010.

Atkinson, R. and Arey, J.: Atmospheric degradation of volatile organic compounds, Chem. Rev., 103, 4605–4638, doi:10.1021/cr0206420, 2003.

Bala, G., Caldeira, K., Wickett, M., Phillips, T. J., Lobell, D. B., Delire, C., and Mirin, A.: Combined climate and carbon-cycle effects of large-scale deforestation, Proc. Natl. Acad. Sci., 104, 6550–6555, doi:10.1073/pnas.0608998104, 2007.

Barth, M., McFadden, J. P., Sun, J., Wiedinmyer, C., Chuang, P., Collins, D., Griffin, R., Hannigan, M., Karl, T., Kim, S.-W., Lasher-Trapp, S., Levis, S., Litvak, M., Mahowald, N., Moore, K., Nandi, S., Nemitz, E., Nenes, A., Potosnak, M., Raymond, T. M., Smith, J., Still, C., and Stroud, C.: Coupling between land ecosystems and the atmospheric hydrologic cycle through biogenic aerosol pathways, Bull. Amer. Meteor. Soc., 86, 1738–1742, doi:10.1175/BAMS-86-12-1738, 2005.

Bennartz, R.: Global assessment of marine boundary layer cloud droplet number concentration from satellite, J. Geophys. Res., 112, D02 201, doi:10.1029/2006JD007547, 2007.

Bennartz, R., Watts, P., Meirink, J. F., and Roebeling, R.: Rainwater path in warm clouds derived from combined visible/near-infrared and microwave satellite observations, J. Geophys. Res., 115, D19 120, doi:10.1029/2009JD013679, 2010.

Bessagnet, B., Seigneur, C., and Menut, L.: Impact of dry deposition of semi-volatile organic compounds on secondary organic aerosols, Atmos. Environ., 44, 1781 – 1787, doi:10.1016/j.atmosenv.2010.01.027, 2010.

Betts, A. K. and Harshvardhan: Thermodynamic constraint on the cloud liquid water feedback in climate models, J. Geophys. Res., 92, 8483–8485, doi:10.1029/JD092iD07p08483, 1987.

Betts, R. A.: Offset of the potential carbon sink from boreal forestation by decreases in surface albedo, Nature, 408, 187–190, doi:10.1038/35041545, 2000.

Boers, R. and Rotstayn, L. D.: Possible links between cloud optical depth and effective radius in remote sensing observations, Quart. J. Roy. Meteor. Soc., 127, 2367–2383, doi:10.1002/qj.49712757709, 2001.

Boers, R. J., Acarreta, R., and Gras, J. L.: Satellite monitoring of the first indirect aerosol effect: Retrieval of the droplet concentration of water clouds, J. Geophys. Res., 111, D22 208, doi:10.1029/2005JD006838, 2006.

Bowman, F. M. and Karamalegos, A. M.: Estimated effects of composition on secondary organic aerosol mass concentrations, Environ. Sci. Technol., 36, 2701–2707, doi:10.1021/es015717g, 2002.

Brown, A. R., Cederwall, R. T., Chlond, A., Duynkerke, P. G., Golaz, J.-C., Khairoutdinov, M., Lewellen, D. C., Lock, A. P., MacVean, M. K., Moeng, C.-H., Neggers, R. A. J.,

Siebesma, A. P., and Stevens, B.: Large-eddy simulation of the diurnal cycle of shallow cumulus convection over land, Quart. J. Roy. Meteor. Soc., 128, 1075–1093, doi:10.1256/003590002320373210, 2002.

Capes, G., Murphy, J. G., Reeves, C. E., McQuaid, J. B., Hamilton, J. F., Hopkins, J. R., Crosier, J., Williams, P. I., and Coe, H.: Secondary organic aerosol from biogenic VOCs over West Africa during AMMA, Atmos. Chem. Phys., 9, 3841–3850, doi:10.5194/acp-9-3841-2009, 2009.

Cappa, C. D. and Jimenez, J. L.: Quantitative estimates of the volatility of ambient organic aerosol, Atmos. Chem. Phys., 10, 5409–5424, doi:10.5194/acp-10-5409-2010, 2010.

Carlton, A. G., Wiedinmyer, C., and Kroll, J. H.: A review of Secondary Organic Aerosol (SOA) formation from isoprene, Atmos. Chem. Phys., 9, 4987–5005, doi:10.5194/acp-9-4987-2009, 2009.

Carslaw, K. S., Boucher, O., Spracklen, D. V., Mann, G. W., Rae, J. G. L., Woodward, S., and Kulmala, M.: A review of natural aerosol interactions and feedbacks within the Earth system, Atmos. Chem. Phys., 10, 1701–1737, doi:10.5194/acp-10-1701-2010, 2010.

Cavalli, F., Facchini, M. C., Decesari, S., Emblico, L., Mircea, M., Jensen, N. R., and Fuzzi, S.: Size-segregated aerosol chemical composition at a boreal site in southern Finland, during the QUEST project, Atmos. Chem. Phys., 6, 993–1002, doi:10.5194/acp-6-993-2006, 2006.

Chan, A. W. H., Chan, M. N., Surratt, J. D., Chhabra, P. S., Loza, C. L., Crounse, J. D., Yee, L. D., Flagan, R. C., Wennberg, P. O., and Seinfeld, J. H.: Role of aldehyde chemistry and NO_x concentrations in secondary organic aerosol formation, Atmos. Chem. Phys., 10, 7169–7188, doi:10.5194/acp-10-7169-2010, 2010.

Chen, Q., Farmer, D. K., Schneider, J., Zorn, S. R., Heald, C. L., Karl, T. G., Guenther, A., Allan, J. D., Robinson, N., Coe, H., Kimmel, J. R., Pauliquevis, T., Borrmann, S., Pöschl, U., Andreae, M. O., Artaxo, P., Jimenez, J. L., and Martin, S. T.: Mass spectral characterization of submicron biogenic organic particles in the Amazon Basin, Geophys. Res. Lett., 36, L20 806, doi:10.1029/2009GL039880, 2009.

Claeys, M., Graham, B., Vas, G., Wang, W., Vermeylen, R., Pashynska, V., Cafmeyer, J., Guyon, P., Andreae, M. O., Artaxo, P., and Maenhaut, W.: Formation of secondary organic aerosols through photooxidation of isoprene, Science, 303, 1173–1176, doi:10.1126/science.1092805, 2004.

Dai, A., Del Genio, A. D., and Fung, I. Y.: Clouds, precipitation and temperature range, Nature, 386, 665–666, doi:10.1038/386665b0, 1997.

Dal Maso, M., Sogacheva, L., Aalto, P. P., Riipinen, I., Komppula, M., Tunved, P., Korhonen, L., Suur-Uski, V., Hirsikko, A., Kurtén, T., Kerminen, V.-M., Lihavainen, H., Viisanen, Y., Hansson, H.-C., and Kulmala, M.: Aerosol size distribution measurements at four Nordic field stations: identification, analysis and trajectory analysis of new particle formation bursts, Tellus B, 59, 350–361, doi:10.1111/j.1600-0889.2007.00267.x, 2007.

Dal Maso, M., Hyvärinen, A., Komppula, M., Tunved, P., Kerminen, V.-M., Lihavainen, H., Viisanen, Y., Hansson, H.-C., and Kulmala, M.: Annual and interannual variation in boreal forest aerosol particle number and volume concentration and their connection to particle formation, Tellus B, 60, 495–508, doi:10.1111/j.1600-0889.2008.00366.x, 2008.

de Bruin, H.: A model for the Priestley-Taylor parameter α, J. Appl. Meteorol., 22, 572–578, doi:10.1175/1520-0450(1983)022⟨0572:AMFTPT⟩2.0.CO;2, 1983.

Donahue, N. M., Robinson, A. L., Stanier, C. O., and Pandis, S. N.: Coupled partitioning, dilution, and chemical aging of semivolatile organics, Environ. Sci. Technol., 40, 2635–2643, doi: 10.1021/es052297c, 2006.

Donahue, N. M., Robinson, A. L., and Pandis, S. N.: Atmospheric organic particulate matter: From smoke to secondary organic aerosol, Atmos. Environ., 43, 94–106, doi:10.1016/j.atmosenv.2008.09.055, 2009.

Donahue, N. M., Henry, K. M., Mentel, T. F., Kiendler-Scharr, A., Spindler, C., Bohn, B., Brauers, T., Dorn, H. P., Fuchs, H., Tillmann, R., Wahner, A., Saathoff, H., Naumann, K.-H., Möhler, O., Leisner, T., Müller, L., Reinnig, M.-C., Hoffmann, T., Salo, K., Hallquist, M., Frosch, M., Bilde, M., Tritscher, T., Barmet, P., Praplan, A. P., DeCarlo, P. F., Dommen, J., Prévôt, A. S., and Baltensperger, U.: Aging of biogenic secondary organic aerosol via gas-phase OH radical reactions, Proc. Natl. Acad. Sci., 109, 13 503–13 508, doi:10.1073/pnas.1115186109, 2012.

Dusek, U., Frank, G. P., Hildebrandt, L., Curtius, J., Schneider, J., Walter, S., Chand, D., Drewnick, F., Hings, S., Jung, D., Borrmann, S., and Andreae, M. O.: Size matters more than chemistry for cloud-nucleating ability of aerosol particles, Science, 312, 1375–1378, doi:10.1126/science.1125261, 2006.

Dzepina, K., Volkamer, R. M., Madronich, S., Tulet, P., Ulbrich, I. M., Zhang, Q., Cappa, C. D., Ziemann, P. J., and Jimenez, J. L.: Evaluation of recently-proposed secondary organic aerosol models for a case study in Mexico City, Atmos. Chem. Phys., 9, 5681–5709, doi:10.5194/acp-9-5681-2009, 2009.

Farmer, D., Chen, Q., Kimmel, J., Docherty, K., Nemitz, E., Artaxo, P., Cappa, C., Martin, S., and Jimenez, J.: Chemically-resolved particle fluxes over tropical and temperate forests, Aerosol Sci. Technol., submitted, 2012.

Fehsenfeld, F., Calvert, J., Fall, R., Goldan, P., Guenther, A. B., Hewitt, C. N., Lamb, B., Liu, S., Trainer, M., Westberg, H., and Zimmerman, P.: Emissions of Volatile Organic Compounds from vegetation and the implications for atmospheric chemistry, Global Biogeochem. Cycles, 6, 389–430, doi:10.1029/92GB02125, 1992.

Freedman, J. M., Fitzjarrald, D. R., Moore, K. E., and Sakai, R. K.: Boundary layer clouds and vegetation-atmosphere feedbacks, J. Climate, 14, 180–197, doi:10.1175/1520-0442(2001)013⟨0180:BLCAVA⟩2.0.CO;2, 2001.

Fuentes, J. D., Gu, L., Lerdau, M., Atkinson, R., Baldocchi, D., Bottenheim, J. W., Ciccioli, P., Lamb, B., Geron, C., Guenther, A., Sharkey, T. D., and Stockwell, W.: Biogenic hydrocarbons in the atmospheric boundary layer: A review, Bull. Amer. Meteor. Soc., 81, 1537–1575, doi:10.1175/1520-0477(2000)081⟨1537:BHITAB⟩2.3.CO;2, 2000.

Ganzeveld, L., Eerdekens, G., Feig, G., Fischer, H., Harder, H., Konigstedt, R., Kubistin, D., Martinez, M., Meixner, F. X., Scheeren, H. A., Sinha, V., Taraborrelli, D., Williams, J., Vilà-Guerau de Arellano, J., and Lelieveld, J.: Surface and boundary layer exchanges of volatile organic compounds, nitrogen oxides and ozone during the GABRIEL campaign, Atmos. Chem. Phys., 8, 62236243, doi:doi:10.5194/acpd-8-11909-2008, 2008.

Garcia-Carreras, L., Parker, D. J., and Marsham, J. H.: What is the mechanism for the modification of convective cloud distributions by land surface-induced flows?, J. Atmos. Sci., 68, 619–634, doi:10.1175/2010JAS3604.1, 2010.

Goldstein, A. and Galbally, I.: Known and unexplored organic constituents in the Earths atmosphere, Environ. Sci. Technol., 40, 1514– 1521, doi:10.1021/es072476p, 2007.

Griffin, R. J., Cocker III, D., Flagan, R., and Seinfeld, J.: Organic aerosol formation from the oxidation of biogenic hydrocarbons, J. Geophys. Res., 104, 3555, doi:10.1029/1998JD100049, 1999.

Guenther, A., Hewitt, C., Erickson, D., Fall, R., Geron, C., Graedel, T., Harley, P., Klinger, L., Lerdau, M., McKay, W., Pierce, T., Scholes, B., Steinbrecher, R., Tallamraju, R., Taylor, J., and Zimmerman, P.: A global model of natural volatile organic compound emissions, J. Geophys. Res., 100, 8873–8892, doi:10.1029/94JD02950, 1995.

Guenther, A., Karl, T., Harley, P., Wiedinmyer, C., Palmer, P. I., and Geron, C.: Estimates of global terrestrial isoprene emissions using MEGAN (Model of Emissions of

Gases and Aerosols from Nature), Atmos. Chem. Phys., 6, 3181–3210, doi:10.5194/acp-6-3181-2006, 2006.

Gunthe, S. S., King, S. M., Rose, D., Chen, Q., Roldin, P., Farmer, D. K., Jimenez, J. L., Artaxo, P., Andreae, M. O., Martin, S. T., and Pöschl, U.: Cloud condensation nuclei in pristine tropical rainforest air of Amazonia: size-resolved measurements and modeling of atmospheric aerosol composition and CCN activity, Atmos. Chem. Phys., 9, 7551–7575, doi:10.5194/acp-9-7551-2009, 2009.

Hakola, H., Tarvainen, V., Laurila, T., Hiltunen, V., Hellén, H., and Keronen, P.: Seasonal variation of VOC concentrations above a boreal coniferous forest, Atmos. Environ., 37, 1623–1634, doi:10.1016/S1352-2310(03)00014-1, 2003.

Hallquist, M., Wenger, J. C., Baltensperger, U., Rudich, Y., Simpson, D., Claeys, M., Dommen, J., Donahue, N. M., George, C., Goldstein, A. H., Hamilton, J. F., Herrmann, H., Hoffmann, T., Iinuma, Y., Jang, M., Jenkin, M. E., Jimenez, J. L., Kiendler-Scharr, A., Maenhaut, W., McFiggans, G., Mentel, T. F., Monod, A., Prévôt, A. S. H., Seinfeld, J. H., Surratt, J. D., Szmigielski, R., and Wildt, J.: The formation, properties and impact of secondary organic aerosol: current and emerging issues, Atmos. Chem. Phys., 9, 5155–5235, doi:10.5194/acp-9-5155-2009, 2009.

Hao, L. Q., Romakkaniemi, S., Yli-Piril, P., Joutsensaari, J., Kortelainen, A., Kroll, J. H., Miettinen, P., Vaattovaara, P., Tiitta, P., Jaatinen, A., Kajos, M. K., Holopainen, J. K., Heijari, J., Rinne, J., Kulmala, M., Worsnop, D. R., Smith, J. N., and Laaksonen, A.: Mass yields of secondary organic aerosols from the oxidation of α-pinene and real plant emissions, Atmos. Chem. Phys., 11, 1367–1378, doi:10.5194/acp-11-1367-2011, 2011.

Hari, P. and Kulmala, M.: Station for Measuring Ecosystem-Atmosphere Relations (SMEAR II), Boreal Env. Res., 10, 315–322, 2005.

Haywood, J. and Boucher, O.: Estimates of the direct and indirect radiative forcing due to tropospheric aerosols: A review, Rev. Geophys., 38, 513–543, doi:10.1029/1999RG000078, 2000.

Heald, C. L., Coe, H., Jimenez, J. L., Weber, R. J., Bahreini, R., Middlebrook, A. M., Russell, L. M., Jolleys, M., Fu, T.-M., Allan, J. D., Bower, K. N., Capes, G., Crosier, J., Morgan, W. T., Robinson, N. H., Williams, P. I., Cubison, M. J., DeCarlo, P. F., and Dunlea, E. J.: Exploring the vertical profile of atmospheric organic aerosol: comparing 17 aircraft field campaigns with a global model, Atmos. Chem. Phys., 11, 12 673–12 696, doi:10.5194/acp-11-12673-2011, 2011.

Henry, K. M. and Donahue, N. M.: Effect of the OH radical scavenger hydrogen peroxide on secondary organic aerosol formation from α-pinene ozonolysis, Aerosol Sci. Technol., 45, 696–700, doi:10.1080/02786826.2011.552926, 2011.

Hewitt, C. N., Lee, J. D., MacKenzie, A. R., Barkley, M. P., Carslaw, N., Carver, G. D., Chappell, N. A., Coe, H., Collier, C., Commane, R., Davies, F., Davison, B., DiCarlo, P., Di Marco, C. F., Dorsey, J. R., Edwards, P. M., Evans, M. J., Fowler, D., Furneaux, K. L., Gallagher, M., Guenther, A., Heard, D. E., Helfter, C., Hopkins, J., Ingham, T., Irwin, M., Jones, C., Karunaharan, A., Langford, B., Lewis, A. C., Lim, S. F., MacDonald, S. M., Mahajan, A. S., Malpass, S., McFiggans, G., Mills, G., Misztal, P., Moller, S., Monks, P. S., Nemitz, E., Nicolas-Perea, V., Oetjen, H., Oram, D. E., Palmer, P. I., Phillips, G. J., Pike, R., Plane, J. M. C., Pugh, T., Pyle, J. A., Reeves, C. E., Robinson, N. H., Stewart, D., Stone, D., Whalley, L. K., and Yin, X.: Overview: Oxidant and particle photochemical processes above a south-east Asian tropical rainforest (the OP3 project): Introduction, rationale, location characteristics and tools, Atmos. Chem. Phys., 10, 169–199, doi:10.5194/acp-10-169-2010, 2010.

Hoyle, C. R., Boy, M., Donahue, N. M., Fry, J. L., Glasius, M., Guenther, A., Hallar, A. G., Huff Hartz, K., Petters, M. D., Petäjä, T., Rosenoern, T., and Sullivan, A. P.: A review of the anthropogenic influence on biogenic secondary organic aerosol, Atmos. Chem. Phys., 11, 321–343, doi:10.5194/acp-11-321-2011, 2010.

Irwin, M., Robinson, N., Allan, J. D., Coe, H., and McFiggans, G.: Size-resolved aerosol water uptake and cloud condensation nuclei measurements as measured above a South-east Asian rainforest during OP3, Atmos. Chem. Phys., 11, 11 157–11 174, doi:10.5194/acp-11-11157-2011, 2011.

Janssen, R. H. H., Vilà-Guerau de Arellano, J., Ganzeveld, L. N., Kabat, P., Jimenez, J. L., Farmer, D. K., van Heerwaarden, C. C., and Mammarella, I.: Combined effects of surface conditions, boundary layer dynamics and chemistry on diurnal SOA evolution, Atmos. Chem. Phys., 12, 6827–6843, doi:10.5194/acp-12-6827-2012, 2012.

Jiang, H. and Feingold, G.: Effect of aerosol on warm convective clouds: Aerosol-cloud-surface flux feedbacks in a new coupled large eddy model, J. Geophys. Res., 111, D01 202, doi:10.1029/2005JD006138, 2006.

Jimenez, J. L., Canagaratna, M. R., Donahue, N. M., Prevot, A. S. H., Zhang, Q., Kroll, J. H., DeCarlo, P. F., Allan, J. D., Coe, H., Ng, N. L., Aiken, A. C., Docherty, K. S., Ulbrich, I. M., Grieshop, A. P., Robinson, A. L., Duplissy, J., Smith, J. D., Wilson, K. R., Lanz, V. A., Hueglin, C., Sun, Y. L., Tian, J., Laaksonen, A., Raatikainen, T., Rautiainen, J., Vaattovaara, P., Ehn, M., Kulmala, M., Tomlinson, J. M., Collins, D. R., Cubison,

M. J., E, Dunlea, J., Huffman, J. A., Onasch, T. B., Alfarra, M. R., Williams, P. I., Bower, K., Kondo, Y., Schneider, J., Drewnick, F., Borrmann, S., Weimer, S., Demerjian, K., Salcedo, D., Cottrell, L., Griffin, R., Takami, A., Miyoshi, T., Hatakeyama, S., Shimono, A., Sun, J. Y., Zhang, Y. M., Dzepina, K., Kimmel, J. R., Sueper, D., Jayne, J. T., Herndon, S. C., Trimborn, A. M., Williams, L. R., Wood, E. C., Middlebrook, A. M., Kolb, C. E., Baltensperger, U., and Worsnop, D. R.: Evolution of organic aerosols in the atmosphere, Science, 326, 1525–1529, doi:10.1126/science.1180353, 2009.

Jonker, H. J. J., Heus, T., and Sullivan, P. P.: A refined view of vertical mass transport by cumulus convection, Geophys. Res. Lett., 35, L07 810, doi:10.1029/2007GL032606, 2008.

Junninen, H., Lauri, A., Keronen, P., Aalto, P., Hiltunen, V., Hari, P., and Kulmala, M.: Smart-SMEAR: on-line data exploration and visualization tool for SMEAR stations, Boreal Env. Res., 14, 447–457, 2009.

Jurányi, Z., Gysel, M., Weingartner, E., DeCarlo, P. F., Kammermann, L., and Baltensperger, U.: Measured and modelled cloud condensation nuclei number concentration at the high alpine site Jungfraujoch, Atmos. Chem. Phys., 10, 7891–7906, doi:10.5194/acp-10-7891-2010, 2010.

Karl, T., Guenther, A., Yokelson, R. J., Greenberg, J., Potosnak, M., Blake, D. R., and Artaxo, P.: The tropical forest and fire emissions experiment: Emission, chemistry, and transport of biogenic volatile organic compounds in the lower atmosphere over Amazonia, J. Geophys. Res., 112, D18 302, doi:10.1029/2007JD008539, 2007.

Karl, T., Guenther, A., Turnipseed, A., Tyndall, G., Artaxo, P., and Martin, S.: Rapid formation of isoprene photo-oxidation products observed in Amazonia, Atmos. Chem. Phys., 9, 7753–7767, doi:10.5194/acp-9-7753-2009, 2009.

Karl, T., Harley, P., Emmons, L., Thornton, B., Guenther, A., Basu, C., Turnipseed, A., and Jardine, K.: Efficient atmospheric cleansing of oxidized organic trace gases by vegetation, Science, 330, 816–819, doi:10.1126/science.1192534, 2010.

Kavouras, I. G., Mihalopoulos, N., and Stephanou, E. G.: Formation of atmospheric particles from organic acids produced by forests, Nature, 395, 683–686, doi:10.1038/27179, 1998.

Kerminen, V.-M., Lihavainen, H., Komppula, M., Viisanen, Y., and Kulmala, M.: Direct observational evidence linking atmospheric aerosol formation and cloud droplet activation, Geophys. Res. Lett., 32, L14 803, doi:10.1029/2005GL023130, 2005.

King, M. D., Platnick, S. E., Hubanks, P. A., Arnold, G. T., Wind, G., and Wind, B.: Collection 005 change summary for the MODIS cloud optical property (06 OD) algorithm, in:

Collection 005 Change Summary Documents, Level-2MODISAtmosphere Products, version 3.1, 9 May 2006, Tech. rep., NASA Goddard Space Flight Cent., Greenbelt, Md., URL http://modis-atmos.gsfc.nasa.gov/productsC005update.html, (last access: 24 March 2010), 2006.

King, S. M., Rosenoern, T., Shilling, J. E., Chen, Q., and Martin, S. T.: Cloud condensation nucleus activity of secondary organic aerosol particles mixed with sulfate, Geophys. Res. Lett., 34, L24 806, doi:10.1029/2007GL030390, 2007.

Komppula, M., Lihavainen, H., Kerminen, V.-M., Kulmala, M., and Viisanen, Y.: Measurements of cloud droplet activation of aerosol particles at a clean subarctic background site, J. Geophys. Res., 110, D06 204, doi:10.1029/2004JD005200, 2005.

Krol, M. C., Molemaker, M. J., and Vilà-Guerau de Arellano, J.: Effects of turbulence and heterogeneous emissions on photochemically active species in the convective boundary layer, J. Geophys. Res., 105, 6871–6884, doi:10.1029/1999JD900958, 2000.

Kroll, J. H. and Seinfeld, J. H.: Chemistry of secondary organic aerosol: Formation and evolution of low-volatility organics in the atmosphere, Atmos. Environ., 42, 3593 – 3624, doi:10.1016/j.atmosenv.2008.01.003, 2008.

Kroll, J. H., Ng, N. L., Murphy, S. M., Flagan, R. C., and Seinfeld, J. H.: Secondary organic aerosol formation from isoprene photooxidation, Environ. Sci. Technol., 40, 1869–1877, doi:10.1021/es0524301, 2006.

Kulmala, M., Laaksonen, A., Korhonen, P., Vesala, T., Ahonen, T., and Barrett, J. C.: The effect of atmospheric nitric acid vapor on cloud condensation nucleus activation, J. Geophys. Res., 98, 22 949–22 958, doi:10.1029/93JD02070, 1993.

Kulmala, M., Hameri, K., Aalto, P. P., Makela, J. M., Pirjola, L., Nilsson, E. D., Buzorius, G., Rannik, U., Maso, M. D., Seidl, W., Hoffman, T., Janson, R., Hansson, H. C., Viisanen, Y., Laaksonen, A., and O'Dowd, C. D.: Overview of the international project on biogenic aerosol formation in the boreal forest (BIOFOR), Tellus B, 53, 324–343, doi:10.1034/j.1600-0889.2001.530402.x, 2001.

Kulmala, M., Suni, T., Lehtinen, K. E. J., Dal Maso, M., Boy, M., Reissell, A., Rannik, U., Aalto, P., Keronen, P., Hakola, H., Bäck, J., Hoffmann, T., Vesala, T., and Hari, P.: A new feedback mechanism linking forests, aerosols, and climate, Atmos. Chem. Phys., 4, 557–562, doi:10.5194/acp-4-557-2004, 2004a.

Kulmala, M., Vehkamaki, H., Petaja, T., Dal Maso, M., Lauri, A., Kerminen, V. M., Birmili, W., and McMurry, P. H.: Formation and growth rates of ultrafine atmospheric particles: A

review of observations, J. Aerosol Sci., 35, 143–176, doi:10.1016/j.jaerosci.2003.10.003, 2004b.

Kurtén, T., Kulmala, M., Dal Maso, M., Suni, T., Reissell, A., Vehkamäki, H., Hari, P., Laaksonen, A., Viisanen, Y., and Vesala, T.: Estimation of different forest-related contributions to the radiative balance using observations in southern Finland, Boreal Env. Res., 8, 275–285, 2003.

Laaksonen, A., Kulmala, M., O'Dowd, C. D., Joutsensaari, J., Vaattovaara, P., Mikkonen, S., Lehtinen, K. E. J., Sogacheva, L., Dal Maso, M., Aalto, P., Petäjä, T., Sogachev, A., Yoon, Y. J., Lihavainen, H., Nilsson, D., Facchini, M. C., Cavalli, F., Fuzzi, S., Hoffmann, T., Arnold, F., Hanke, M., Sellegri, K., Umann, B., Junkermann, W., Coe, H., Allan, J. D., Alfarra, M. R., Worsnop, D. R., Riekkola, M. L., Hyötyläinen, T., and Viisanen, Y.: The role of VOC oxidation products in continental new particle formation, Atmos. Chem. Phys., 8, 2657–2665, doi:10.5194/acp-8-2657-2008, 2008.

Lane, T. E., Donahue, N. M., and Pandis, S. N.: Simulating secondary organic aerosol formation using the volatility basis-set approach in a chemical transport model, Atmos. Environ., 42, 7439 – 7451, doi:10.1016/j.atmosenv.2008.06.026, 2008a.

Lane, T. E., Donahue, N. M., and Pandis, S. N.: Effect of NO_x on secondary organic aerosol concentrations, Environ. Sci. Technol., 42, 6022–6027, doi:10.1021/es703225a, 2008b.

Langford, B., Misztal, P. K., Nemitz, E., Davison, B., Helfter, C., Pugh, T. A. M., MacKenzie, A. R., Lim, S. F., and Hewitt, C. N.: Fluxes and concentrations of volatile organic compounds from a South-East Asian tropical rainforest, Atmos. Chem. Phys., 10, 8391–8412, doi:10.5194/acp-10-8391-2010, 2010.

Lappalainen, H. K., Sevanto, S., Bäck, J., Ruuskanen, T. M., Kolari, P., Taipale, R., Rinne, J., Kulmala, M., and Hari, P.: Day-time concentrations of biogenic volatile organic compounds in a boreal forest canopy and their relation to environmental and biological factors, Atmos. Chem. Phys., 9, 5447–5459, doi:10.5194/acp-9-5447-2009, 2009.

Leaitch, W. R., Banic, C. M., Isaac, G. A., Couture, M. D., Liu, P. S. K., Gultepe, I., Li, S.-M., Kleinman, L., Daum, P. H., and MacPherson, J. I.: Physical and chemical observations in marine stratus during the 1993 North Atlantic Regional Experiment: Factors controlling cloud droplet number concentrations, J. Geophys. Res., 101, 29 123–29 135, doi:10.1029/96JD01228, 1996.

Lelieveld, J., Butler, T. M., Crowley, J. N., Dillon, T. J., Fischer, H., Ganzeveld, L., Harder, H., Lawrence, M. G., Martinez, M., Taraborrelli, D., and Williams, J.: Atmo-

spheric oxidation capacity sustained by a tropical forest, Nature, 452, 737 – 740, doi: 10.1038/nature06870, 2008.

Lihavainen, H., Kerminen, V.-M., Komppula, M., Hatakka, J., Aaltonen, V., Kulmala, M., and Viisanen, Y.: Production of "potential" cloud condensation nuclei associated with atmospheric new-particle formation in northern Finland, J. Geophys. Res., 108, 4782, doi: 10.1029/2003JD003887, 2003.

Lihavainen, H., Kerminen, V.-M., Komppula, M., Hyvärinen, A.-P., Laakia, J., Saarikoski, S., Makkonen, U., Kivekäs, N., Hillamo, R., Kulmala, M., and Viisanen, Y.: Measurements of the relation between aerosol properties and microphysics and chemistry of low level liquid water clouds in Northern Finland, Atmos. Chem. Phys., 8, 6925–6938, doi:10.5194/acp-8-6925-2008, 2008.

Lihavainen, H., Kerminen, V.-M., and Remer, L. A.: Aerosol-cloud interaction determined by both in situ and satellite data over a northern high-latitude site, Atmos. Chem. Phys., 10, 10 987–10 995, doi:10.5194/acp-10-10987-2010, 2010.

Lilly, D. K.: Models of cloud-topped mixed layers under a strong inversion, Quart. J. Roy. Meteor. Soc., 94, 292–309, doi:10.1002/qj.49709440106, 1968.

Lin, G., Penner, J. E., Sillman, S., Taraborrelli, D., and Lelieveld, J.: Global modeling of SOA formation from dicarbonyls, epoxides, organic nitrates and peroxides, Atmos. Chem. Phys., 12, 4743–4774, doi:10.5194/acp-12-4743-2012, 2012a.

Lin, Y.-H., Zhang, Z., Docherty, K. S., Zhang, H., Budisulistiorini, S. H., Rubitschun, C. L., Shaw, S. L., Knipping, E. M., Edgerton, E. S., Kleindienst, T. E., Gold, A., and Surratt, J. D.: Isoprene epoxydiols as precursors to secondary organic aerosol formation: Acid-catalyzed reactive uptake studies with authentic compounds, Environ. Sci. Technol., 46, 250–258, doi:10.1021/es202554c, 2012b.

Lohmann, U. and Feichter, J.: Global indirect aerosol effects: A review, Atmos. Chem. Phys., 5, 715–737, doi:10.5194/acp-5-715-2005, 2005.

Mammarella, I., Launiainen, S., Gronholm, T., Keronen, P., Pumpanen, J., Rannik, U., and Vesala, T.: Relative humidity effect on the high-frequency attenuation of water vapor flux measured by a closed-path eddy covariance system, J. Atmos. Oceanic Technol., 26, 1856–1866, doi:10.1175/2009JTECHA1179.1, 2009.

Mao, J., Ren, X., Zhang, L., Van Duin, D. M., Cohen, R. C., Park, J.-H., Goldstein, A. H., Paulot, F., Beaver, M. R., Crounse, J. D., Wennberg, P. O., DiGangi, J. P., Henry, S. B., Keutsch, F. N., Park, C., Schade, G. W., Wolfe, G. M., Thornton, J. A., and Brune, W. H.:

Insights into hydroxyl measurements and atmospheric oxidation in a California forest, Atmos. Chem. Phys., 12, 8009–8020, doi:10.5194/acp-12-8009-2012, 2012.

Martin, C. L., Fitzjarrald, D., Garstang, M., Oliveira, A. P., Greco, S., and Browell, E.: Structure and growth of the mixing layer over the Amazonian rain forest, J. Geophys. Res., 93, 1361–1375, doi:10.1029/JD093iD02p01361, 1988.

McFiggans, G., Artaxo, P., Baltensperger, U., Coe, H., Facchini, M. C., Feingold, G., Fuzzi, S., Gysel, M., Laaksonen, A., Lohmann, U., Mentel, T. F., Murphy, D. M., O'Dowd, C. D., Snider, J. R., and Weingartner, E.: The effect of physical and chemical aerosol properties on warm cloud droplet activation, Atmos. Chem. Phys., 6, 2593–2649, doi:10.5194/acp-6-2593-2006, 2006.

Metzger, A., Verheggen, B., Dommen, J., Duplissy, J., Prevot, A. S. H., Weingartner, E., Riipinen, I., Kulmala, M., Spracklen, D. V., Carslaw, K. S., and Baltensperger, U.: Evidence for the role of organics in aerosol particle formation under atmospheric conditions, Proc. Natl. Acad. Sci., 107, 6646–6651, doi:10.1073/pnas.0911330107, 2010.

Nakajima, T., Higurashi, A., Kawamoto, K., and Penner, J. E.: A possible correlation between satellite-derived cloud and aerosol microphysical parameters, Geophys. Res. Lett., 28, 1171–1174, doi:10.1029/2000GL012186, 2001.

Niinemets, U., Monson, R. K., Arneth, A., Ciccioli, P., Kesselmeier, J., Kuhn, U., Noe, S. M., Peñuelas, J., and Staudt, M.: The leaf-level emission factor of volatile isoprenoids: Caveats, model algorithms, response shapes and scaling, Biogeosciences, 7, 1809–1832, doi:10.5194/bg-7-1809-2010, 2010.

O'Dowd, C. D., Aalto, P., Hämeri, K., Kulmala, M., and Hoffmann, T.: Aerosol formation: Atmospheric particles from organic vapours, Nature, 416, 497–498, doi:10.1038/416497a, 2002.

O'Dowd, C. D., Yoon, Y. J., Junkermann, W., Aalto, P., Kulmala, M., Lihavainen, H., and Viisanen, Y.: Airborne measurements of nucleation mode particles II: Boreal forest nucleation events, Atmos. Chem. Phys., 9, 937–944, doi:10.5194/acp-9-937-2009, 2009.

Odum, J. R., Hoffmann, T., Bowman, F., Collins, D., Flagan, R. C., and Seinfeld, J. H.: Gas/particle partitioning and secondary organic aerosol yields, Environ. Sci. Technol., 30, 2580–2585, doi:10.1021/es950943+, 1996.

Ouwersloot, H. G., Vilà-Guerau de Arellano, J., van Heerwaarden, C. C., Ganzeveld, L. N., Krol, M. C., and Lelieveld, J.: On the segregation of chemical species in a clear boundary layer over heterogeneous land surfaces, Atmos. Chem. Phys., 11, 10 681–10 704, doi:10.5194/acp-11-10681-2011, 2011.

Ouwersloot, H. G., Vilà-Guerau de Arellano, J., Nölscher, A. C., Krol, M. C., Ganzeveld, L. N., Breitenberger, C., Mammarella, I., Williams, J., and Lelieveld, J.: Characterization of a boreal convective boundary layer and its impact on atmospheric chemistry during HUMPPA-COPEC-2010, Atmos. Chem. Phys., 12, 9335–9353, doi:10.5194/acp-12-9335-2012, 2012.

Pankow, J. F.: An absorption model of the gas/aerosol partitioning involved in the formation of secondary organic aerosol, Atmos. Environ., 28, 189–193, doi:10.1016/1352-2310(94)90094-9, 1994.

Pathak, R. K., Presto, A. A., Lane, T. E., Stanier, C. O., Donahue, N. M., and Pandis, S. N.: Ozonolysis of α-pinene: Parameterization of secondary organic aerosol mass fraction, Atmos. Chem. Phys., 7, 3811–3821, doi:10.5194/acp-7-3811-2007, 2007.

Paulot, F., Crounse, J. D., Kjaergaard, H. G., Kürten, A., St. Clair, J. M., Seinfeld, J. H., and Wennberg, P. O.: Unexpected epoxide formation in the gas-phase photooxidation of isoprene, Science, 325, 730–733, doi:10.1126/science.1172910, 2009.

Pearson, G., Davies, F., and Collier, C.: Remote sensing of the tropical rain forest boundary layer using pulsed Doppler lidar, Atmos. Chem. Phys., 10, 5891–5901, doi:10.5194/acp-10-5891-2010, 2010.

Petäjä, T., Mauldin III, R. L., Kosciuch, E., McGrath, J., Nieminen, T., Paasonen, P., Boy, M., Adamov, A., Kotiaho, T., and Kulmala, M.: Sulfuric acid and OH concentrations in a boreal forest site, Atmos. Chem. Phys., 9, 7435–7448, doi:10.5194/acp-9-7435-2009, 2009.

Pierce, J. R. and Adams, P. J.: Efficiency of cloud condensation nuclei formation from ultrafine particles, Atmos. Chem. Phys., 7, 1367–1379, doi:10.5194/acp-7-1367-2007, 2007.

Pierce, J. R., Riipinen, I., Kulmala, M., Ehn, M., Petäjä, T., Junninen, H., Worsnop, D. R., and Donahue, N. M.: Quantification of the volatility of secondary organic compounds in ultrafine particles during nucleation events, Atmos. Chem. Phys., 11, 9019–9036, doi:10.5194/acp-11-9019-2011, 2011.

Pierce, J. R., Leaitch, W. R., Liggio, J., Westervelt, D. M., Wainwright, C. D., Abbatt, J. P. D., Ahlm, L., Al-Basheer, W., Cziczo, D. J., Hayden, K. L., Lee, A. K. Y., Li, S.-M., Russell, L. M., Sjostedt, S. J., Strawbridge, K. B., Travis, M., Vlasenko, A., Wentzell, J. J. B., Wiebe, H. A., Wong, J. P. S., and Macdonald, A. M.: Nucleation and condensational growth to CCN sizes during a sustained pristine biogenic SOA event in a forested mountain valley, Atmos. Chem. Phys., 12, 3147–3163, doi:10.5194/acp-12-3147-2012, 2012.

Platnick, S. and Twomey, S.: Determining the susceptibility of cloud albedo to changes in droplet concentration with the Advanced Very High Resolution Radiometer, J. Appl. Meteor., 33, 334–347, doi:10.1175/1520-0450(1994)033⟨0334:DTSOCA⟩2.0.CO;2, 1994.

Platnick, S., King, M. D., Ackerman, S. A., Menzel, W. P., Baum, B. A., Riedi, J. C., and Frey, R. A.: The MODIS cloud products: Algorithms and examples from Terra, IEEE T. Geosci. Remote., 41, 459473, doi:10.1109/TGRS.2002.808301, 2003.

Pöhlker, C., Wiedemann, K. T., Sinha, B., Shiraiwa, M., Gunthe, S. S., Smith, M., Su, H., Artaxo, P., Chen, Q., Cheng, Y., Elbert, W., Gilles, M. K., Kilcoyne, A. L. D., Moffet, R. C., Weigand, M., Martin, S. T., Pöschl, U., and Andreae, M. O.: Biogenic potassium salt particles as seeds for secondary organic aerosol in the Amazon, Science, 337, 1075–1078, doi:10.1126/science.1223264, 2012.

Pöschl, U., Martin, S. T., Sinha, B., Chen, Q., Gunthe, S. S., Huffman, J. A., Borrmann, S., Farmer, D. K., Garland, R. M., Helas, G., Jimenez, J. L., King, S. M., Manzi, A., Mikhailov, E., Pauliquevis, T., Petters, M. D., Prenni, A. J., Roldin, P., Rose, D., Schneider, J., Su, H., Zorn, S. R., Artaxo, P., and Andreae, M. O.: Rainforest aerosols as biogenic nuclei of clouds and precipitation in the Amazon, Science, 329, 1513–1516, doi:10.1126/science.1191056, 2010.

Prenni, A. J., Petters, M. D., Kreidenweis, S. M., DeMott, P. J., and Ziemann, P. J.: Cloud droplet activation of secondary organic aerosol, J. Geophys. Res., 112, doi:10.1029/2006JD007963, 2007.

Pugh, T. A. M., MacKenzie, A. R., Hewitt, C. N., Langford, B., Edwards, P. M., Furneaux, K. L., Heard, D. E., Hopkins, J. R., Jones, C. E., Karunaharan, A., Lee, J., Mills, G., Misztal, P., Moller, S., Monks, P. S., and Whalley, L. K.: Simulating atmospheric composition over a South-East Asian tropical rainforest: Performance of a chemistry box model, Atmos. Chem. Phys., 10, 279–298, doi:10.5194/acp-10-279-2010, 2010.

Pugh, T. A. M., MacKenzie, A. R., Langford, B., Nemitz, E., Misztal, P. K., and Hewitt, C. N.: The influence of small-scale variations in isoprene concentrations on atmospheric chemistry over a tropical rainforest, Atmos. Chem. Phys., 11, 4121–4134, doi:10.5194/acp-11-4121-2011, 2011.

Raatikainen, T., Vaattovaara, P., Tiitta, P., Miettinen, P., Rautiainen, J., Ehn, M., Kulmala, M., Laaksonen, A., and Worsnop, D. R.: Physicochemical properties and origin of organic groups detected in boreal forest using an aerosol mass spectrometer, Atmos. Chem. Phys., 10, 2063–2077, doi:10.5194/acp-10-2063-2010, 2010.

Reutter, P., Su, H., Trentmann, J., Simmel, M., Rose, D., Gunthe, S. S., Wernli, H., Andreae, M. O., and Pöschl, U.: Aerosol- and updraft-limited regimes of cloud droplet formation: influence of particle number, size and hygroscopicity on the activation of cloud condensation nuclei (CCN), Atmos. Chem. Phys., 9, 7067–7080, doi:10.5194/acp-9-7067-2009, 2009.

Riipinen, I., Pierce, J. R., Yli-Juuti, T., Nieminen, T., Häkkinen, S., Ehn, M., Junninen, H., Lehtipalo, K., Petäjä, T., Slowik, J., Chang, R., Shantz, N. C., Abbatt, J., Leaitch, W. R., Kerminen, V.-M., Worsnop, D. R., Pandis, S. N., Donahue, N. M., and Kulmala, M.: Organic condensation: a vital link connecting aerosol formation to cloud condensation nuclei (CCN) concentrations, Atmos. Chem. Phys., 11, 3865–3878, doi: 10.5194/acp-11-3865-2011, 2011.

Riipinen, I., Yli-Juuti, T., Pierce, J. R., Petaja, T., Worsnop, D. R., Kulmala, M., and Donahue, N. M.: The contribution of organics to atmospheric nanoparticle growth, Nature Geosci., 5, 453–458, doi:10.1038/ngeo1499, 2012.

Rinne, J., Taipale, R., Markkanen, T., Ruuskanen, T. M., Helln, H., Kajos, M. K., Vesala, T., and Kulmala, M.: Hydrocarbon fluxes above a Scots pine forest canopy: measurements and modeling, Atmos. Chem. Phys., 7, 3361–3372, doi:10.5194/acp-7-3361-2007, 2007.

Robinson, N. H., Hamilton, J. F., Allan, J. D., Langford, B., Oram, D. E., Chen, Q., Docherty, K., Farmer, D. K., Jimenez, J. L., Ward, M. W., Hewitt, C. N., Barley, M. H., Jenkin, M. E., Rickard, A. R., Martin, S. T., McFiggans, G., and Coe, H.: Evidence for a significant proportion of Secondary Organic Aerosol from isoprene above a maritime tropical forest, Atmos. Chem. Phys., 11, 1039–1050, doi:10.5194/acp-11-1039-2011, 2011a.

Robinson, N. H., Newton, H. M., Allan, J. D., Irwin, M., Hamilton, J. F., Flynn, M., Bower, K. N., Williams, P. I., Mills, G., Reeves, C. E., McFiggans, G., and Coe, H.: Source attribution of Bornean air masses by back trajectory analysis during the OP3 project, Atmos. Chem. Phys., 11, 9605–9630, doi:10.5194/acp-11-9605-2011, 2011b.

Robinson, N. H., Allan, J. D., Trembath, J. A., Rosenberg, P. D., Allen, G., and Coe, H.: The lofting of Western Pacific regional aerosol by island thermodynamics as observed around Borneo, Atmos. Chem. Phys., 12, 5963–5983, doi:10.5194/acp-12-5963-2012, 2012.

Roebeling, R. A., Placidi, S., Donovan, D. P., Russchenberg, H. W. J., and Feijt, A. J.: Validation of liquid cloud property retrievals from SEVIRI using ground-based observations, Geophys. Res. Lett., 35, L05 814, doi:10.1029/2007GL032115, 2008.

Rosenfeld, D. and Feingold, G.: Explanation of the discrepancies among satellite observations of the aerosol indirect effects, Geophys. Res. Lett., 30, 1776, doi:10.1029/2003GL017684, 2003.

Ruuskanen, T. M., Taipale, R., Rinne, J., Kajos, M. K., Hakola, H., and Kulmala, M.: Quantitative long-term measurements of VOC concentrations by PTR-MS: annual cycle at a boreal forest site, Atmos. Chem. Phys. Discuss., 9, 81–134, doi:10.5194/acpd-9-81-2009, 2009.

Seinfeld, J. H. and Pandis, S. N.: Atmospheric chemistry and physics: From air pollution to climate change, John Wiley & Sons, Inc., New York, 2nd edn., 2006.

Sheehan, P. E. and Bowman, F. M.: Estimated effects of temperature on secondary organic aerosol concentrations, Environ. Sci. Technol., 35, 2129–2135, doi:10.1021/es001547g, 2001.

Siebesma, A. P. and Cuijpers, J. W. M.: Evaluation of parametric assumptions for shallow cumulus convection, J. Atmos. Sci., 52, 650–666, doi:10.1175/1520-0469(1995)052⟨0650:EOPAFS⟩2.0.CO;2, 1995.

Sihto, S.-L., Mikkilä, J., Vanhanen, J., Ehn, M., Liao, L., Lehtipalo, K., Aalto, P. P., Duplissy, J., Petäjä, T., Kerminen, V.-M., Boy, M., and Kulmala, M.: Seasonal variation of CCN concentrations and aerosol activation properties in boreal forest, Atmos. Chem. Phys., 11, 13 269–13 285, doi:10.5194/acp-11-13269-2011, 2011.

Sjostedt, S. J., Slowik, J. G., Brook, J. R., Chang, R. Y.-W., Mihele, C., Stroud, C. A., Vlasenko, A., and Abbatt, J. P. D.: Diurnally resolved particulate and VOC measurements at a rural site: Indication of significant biogenic secondary organic aerosol formation, Atmos. Chem. Phys., 11, 5745–5760, doi:10.5194/acp-11-5745-2011, 2011.

Slowik, J. G., Stroud, C., Bottenheim, J. W., Brickell, P. C., Chang, R. Y.-W., Liggio, J., Makar, P. A., Martin, R. V., Moran, M. D., Shantz, N. C., Sjostedt, S. J., van Donkelaar, A., Vlasenko, A., Wiebe, H. A., Xia, A. G., Zhang, J., Leaitch, W. R., and Abbatt, J. P. D.: Characterization of a large biogenic secondary organic aerosol event from eastern Canadian forests, Atmos. Chem. Phys., 10, 2825–2845, doi:10.5194/acp-10-2825-2010, 2010.

Sogacheva, L., Saukkonen, L., Nilsson, E. D., Dal Maso, M., Schultz, D. M., De Leeuw, G., and Kulmala, M.: New aerosol particle formation in different synoptic situations at Hyytiälä, Southern Finland, Tellus B, 60, 485–494, doi:10.1111/j.1600-0889.2008.00364.x, 2008.

Spirig, C., Guenther, A., Greenberg, J. P., Calanca, P., and Tarvainen, V.: Tethered balloon measurements of biogenic volatile organic compounds at a Boreal forest site, Atmos. Chem. Phys., 4, 215–229, doi:10.5194/acp-4-215-2004, 2004.

Spracklen, D. V., Bonn, B., and Carslaw, K. S.: Boreal forests, aerosols and the impacts on clouds and climate, Phil. Trans. R. Soc. A, 366, 4613–4626, doi:10.1098/rsta.2008.0201, 2008.

Spracklen, D. V., Jimenez, J. L., Carslaw, K. S., Worsnop, D. R., Evans, M. J., Mann, G. W., Zhang, Q., Canagaratna, M. R., Allan, J., Coe, H., McFiggans, G., Rap, A., and Forster, P.: Aerosol mass spectrometer constraint on the global secondary organic aerosol budget, Atmos. Chem. Phys., 11, 12 109–12 136, doi:10.5194/acp-11-12109-2011, 2011.

Stevens, B. and Feingold, G.: Untangling aerosol effects on clouds and precipitation in a buffered system, Nature, 461, 607–613, doi:10.1038/nature08281, 2009.

Stone, D., Evans, M. J., Edwards, P. M., Commane, R., Ingham, T., Rickard, A. R., Brookes, D. M., Hopkins, J., Leigh, R. J., Lewis, A. C., Monks, P. S., Oram, D., Reeves, C. E., Stewart, D., and Heard, D. E.: Isoprene oxidation mechanisms: Measurements and modelling of OH and HO_2 over a South-East Asian tropical rainforest during the OP3 field campaign, Atmos. Chem. Phys., 11, 6749–6771, doi:10.5194/acp-11-6749-2011, 2011.

Surratt, J. D., Chan, A. W. H., Eddingsaas, N. C., Chan, M., Loza, C. L., Kwan, A. J., Hersey, S. P., Flagan, R. C., Wennberg, P. O., and Seinfeld, J. H.: Reactive intermediates revealed in secondary organic aerosol formation from isoprene, Proc. Natl. Acad. Sci., 107, 6640–6645, doi:10.1073/pnas.0911114107, 2010.

Szczodrak, M., Austin, P. H., and Krummel, P. B.: Variability of optical depth and effective radius in marine stratocumulus clouds, J. Atmos. Sci., 58, 2912–2926, doi:10.1175/1520-0469(2001)058⟨2912:VOODAE⟩2.0.CO;2, 2001.

Taraborrelli, D., Lawrence, M. G., Crowley, J. N., Dillon, T. J., Gromov, S., Grosz, C. B. M., Vereecken, L., and Lelieveld, J.: Hydroxyl radical buffered by isoprene oxidation over tropical forests, Nature Geosci., 5, 190–193, doi:10.1038/ngeo1405, 2012.

Tennekes, H.: A model for the dynamics of the inversion above a convective boundary layer, J. Atmos. Sci., 30, 558–567, doi:10.1175/1520-0469(1973)030⟨0558:AMFTDO⟩2.0.CO;2, 1973.

Thunis, P. and Bornstein, R.: Hierarchy of mesoscale flow assumptions and equations, J. Atmos. Sci., 53, 380–397, doi:10.1175/1520-0469(1996)053⟨0380:HOMFAA⟩2.0.CO;2, 1996.

Tsimpidi, A. P., Karydis, V. A., Zavala, M., Lei, W., Molina, L., Ulbrich, I. M., Jimenez, J. L., and Pandis, S. N.: Evaluation of the volatility basis-set approach for the simulation of organic aerosol formation in the Mexico City metropolitan area, Atmos. Chem. Phys., 10, 525–546, doi:10.5194/acp-10-525-2010, 2010.

Tunved, P., Hansson, H. C., Kerminen, V. M., Strom, J., Maso, M. D., Lihavainen, H., Viisanen, Y., Aalto, P. P., Komppula, M., and Kulmala, M.: High natural aerosol loading over boreal forests, Science, 312, 261–263, doi:10.1126/science.1123052, 2006.

Tunved, P., Ström, J., Kulmala, M., Kerminen, V.-M., Dal Maso, M., Svenningson, B., Lunder, C., and Hansson, H.-C.: The natural aerosol over Northern Europe and its relation to anthropogenic emissions: Implications of important climate feedbacks, Tellus B, 60, 473–484, doi:10.1111/j.1600-0889.2008.00363.x, 2008.

Twomey, S.: The influence of pollution on the shortwave albedo of clouds, J. Atmos. Sci., 34, 1149–1152, doi:10.1175/1520-0469(1977)034⟨1149:TIOPOT⟩2.0.CO;2, 1977.

van Heerwaarden, C. C. and Vilà-Guerau de Arellano, J.: Relative humidity as an indicator for cloud formation over heterogeneous land surfaces, J. Atmos. Sci., 65, 3263–3277, doi:10.1175/2008JAS2591.1, 2008.

van Heerwaarden, C. C., Vilà-Guerau de Arellano, J., Moene, A. F., and Holtslag, A. A. M.: Interactions between dry-air entrainment, surface evaporation and convective boundary-layer development, Quart. J. Roy. Meteor. Soc., 135, 1277–1291, doi:10.1002/qj.431, 2009.

Várnai, T. and Marshak, A.: View angle dependence of cloud optical thicknesses retrieved by Moderate Resolution Imaging Spectroradiometer (MODIS), J. Geophys. Res., 112, D06 203, doi:10.1029/2005JD006912, 2007.

Verzijlbergh, R. A., Jonker, H. J. J., Heus, T., and Vilà-Guerau de Arellano, J.: Turbulent dispersion in cloud-topped boundary layers, Atmos. Chem. Phys., 9, 1289–1302, doi:10.5194/acp-9-1289-2009, 2009.

Vilà-Guerau de Arellano, J., Kim, S.-W., Barth, M. C., and Patton, E. G.: Transport and chemical transformations influenced by shallow cumulus over land, Atmos. Chem. Phys., 5, 3219–3231, doi:10.5194/acp-5-3219-2005, 2005.

Vilà-Guerau de Arellano, J., van den Dries, K., and Pino, D.: On inferring isoprene emission surface flux from atmospheric boundary layer concentration measurements, Atmos. Chem. Phys., 9, 3629–3640, doi:10.5194/acp-9-3629-2009, 2009.

Vilà-Guerau de Arellano, J., Patton, E. G., Karl, T., van den Dries, K., Barth, M. C., and Orlando, J. J.: The role of boundary layer dynamics on the diurnal evolution of isoprene and the hydroxyl radical over tropical forests, J. Geophys. Res., 116, D07 304, doi:10.1029/2010JD014857, 2011.

Vilà-Guerau de Arellano, J., van Heerwaarden, C. C., and Lelieveld, J.: Modelled suppression of boundary-layer clouds by plants in a CO_2-rich atmosphere, Nature Geosci., 5, 701–704, doi:10.1038/ngeo1554, 2012.

Went, F. W.: Blue hazes in the atmosphere, Nature, 187, 641–643, doi:10.1038/187641a0, 1960.

Williams, J., Crowley, J., Fischer, H., Harder, H., Martinez, M., Petäjä, T., Rinne, J., Bäck, J., Boy, M., Dal Maso, M., Hakala, J., Kajos, M., Keronen, P., Rantala, P., Aalto, J., Aaltonen, H., Paatero, J., Vesala, T., Hakola, H., Levula, J., Pohja, T., Herrmann, F., Auld, J., Mesarchaki, E., Song, W., Yassaa, N., Nölscher, A., Johnson, A. M., Custer, T., Sinha, V., Thieser, J., Pouvesle, N., Taraborrelli, D., Tang, M. J., Bozem, H., Hosaynali-Beygi, Z., Axinte, R., Oswald, R., Novelli, A., Kubistin, D., Hens, K., Javed, U., Trawny, K., Breitenberger, C., Hidalgo, P. J., Ebben, C. J., Geiger, F. M., Corrigan, A. L., Russell, L. M., Ouwersloot, H. G., Vilà-Guerau de Arellano, J., Ganzeveld, L., Vogel, A., Beck, M., Bayerle, A., Kampf, C. J., Bertelmann, M., Köllner, F., Hoffmann, T., Valverde, J., González, D., Riekkola, M.-L., Kulmala, M., and Lelieveld, J.: The summertime Boreal forest field measurement intensive (HUMPPA-COPEC-2010): An overview of meteorological and chemical influences, Atmos. Chem. Phys., 11, 10 599–10 618, doi:10.5194/acp-11-10599-2011, 2011.

Yu, F.: A secondary organic aerosol formation model considering successive oxidation aging and kinetic condensation of organic compounds: Global scale implications, Atmos. Chem. Phys., 11, 1083–1099, doi:10.5194/acp-11-1083-2011, 2011.

Zhang, Y. and Klein, S. A.: Mechanisms affecting the transition from shallow to deep convection over land: Inferences from observations of the diurnal cycle collected at the ARM Southern Great Plains site, J. Atmos. Sci., 67, 2943–2959, doi:10.1175/2010JAS3366.1, 2010.

Samenvatting

Boreale en tropische bossen vormen een belangrijke bron van organische aerosolen (OA), die het klimaat kunnen beïnvloeden op een directe manier door inkomende straling te verstrooien of indirect door het veranderen van de capaciteit van wolken om zonlicht te weerkaatsen. Daarmee beïnvloeden ze de stralingsbalans aan het landoppervlak, en vormen op die manier een koppeling tussen bossen, aerosolen en het klimaat. In dit proefschrift wordt de evolutie van organische aerosolen in de atmosferische grenslaag bestudeerd en hoe deze geactiveerd worden als wolkendruppels, met een speciale nadruk op de rol die land-atmosfeer interacties hierin spelen. Bossen spelen hierin een dubbele rol: ze sturen de dynamica van de atmosferische grenslaag aan door het verdelen van de beschikbare energie aan het oppervlak in een voelbare en een latente warmtestroom en ze drijven de formatie van secundaire organische aerosolen (SOA) doordat ze vluchtige organische componenten (VOC) uitstoten, die SOA kunnen vormen na oxidatie in de atmosfeer. Het doel van dit onderzoek is het begrijpen van de evolutie van organische aerosol concentraties in de atmosfeer boven bossen en hoe deze aerosolen activeren als wolkendruppels. Hiertoe bestuderen we het gekoppelde landoppervlak-grenslaagdynamica-VOC chemie systeem op een geïntegreerde manier.

Als eerste onderzoeken we de evolutie van OA in de atmosfeer op de tijdschaal van een dag. Daarvoor ontwikkelen we een modelopzet met als doel het representeren van de essentie van alle relevante componenten in het gekoppelde grenslaagdynamiek-VOC chemie systeem, met inbegrip van de formatie van semi-volatiele organische componenten (SVOC) en hun splitsing tussen de gas- en de aerosolfase (Hoofdstuk 2). Dit model is gebruikt om de dagelijkse gang van OA in een boreaal bos in Finland te analyzeren als functie van landoppervlaktecondities, grenslaagdynamiek en chemie (Hoofdstuk 3). We analyseren wat de bijdrage is van de verschillende processen aan de waargenomen OA concentraties. Vervolgens voeren we systematische numerieke experimenten uit om uit te zoeken hoe gevoelig OA concentraties zijn voor landoppervlaktecondities en meteorologische forceringen. Onze belangrijkste bevinding is dat in het boreale bos de uitwisseling tussen de atmosferische grenslaag en de vrije troposfeer (een proces dat entrainment wordt genoemd) een belangrijke bijdrage levert aan de dagelijkse gang van OA die niet genegeerd kan worden in de interpretatie van metingen

en in grootschalige modellen.
In Hoofdstuk 4 breiden we de vorige studie uit naar het tropische regenwoud (op Borneo), omdat dit het ecosysteem is dat de grootste hoeveelheden VOC's uitstoot, met name isopreen. We onderzoeken het effect op het OA budget van zowel meteorologische forceringen als van onlangs ontdekte chemische reactiepaden in de formatie van SOA van isopreen. We vinden dat subsidentie en advectie van relatief koele lucht een tegengesteld effect hebben op OA concentraties, terwijl ze beiden de groei van de grenslaag onderdrukken. De recycling van het hydroxyl radicaal in de oxidatie van isopreen heeft een effect op de hoeveelheid SOA die wordt gevormd, maar dient beter begrepen te worden voordat dit effect daadwerkelijk gekwantificeerd kan worden. SOA formatie van isopreen is verder sterk afhankelijk van de precieze reactiepaden die leiden tot de formatie van SVOC's. We implementeren daarom parameterisaties voor isopreen SOA formatie onder hoge en lage concentraties stikstofoxiden (NO_x). Ondanks het meenemen van deze nieuwe inzichten in de formatie van SOA uit isopreen onderschatten we de OA concentratie met ruwweg een factor 2.

In Hoofdstuk 5 maken we gebruik van satellietwaarnemingen om te bestuderen hoe de seizoensgang in wolkendruppelconcentraties boven het boreale bos afhangt van aerosolen en meteorologische factoren. Deze druppelconcentratie vertoont geen duidelijke relatie met concentraties van wolkencondensatiekernen aan het oppervlak. Dit leidt tot de hypothese dat het convectieve transport van deze condensatiekernen van het oppervlak naar de wolkenbasis de limiterende factor is voor hun activatie als wolkendruppels. Dit onderstreept de integrerende rol van de atmosferische grenslaag in het tot stand brengen van de verbinding tussen processen aan het landoppervlak en wolkenvorming.

Dankwoord / Acknowledgments

Het lijkt een eeuwigheid geleden dat ik aan dit proefschrift begon. Eind 2007 was de belangstelling voor klimaatverandering op een hoogtepunt, had nog niemand van de crisis gehoord en was ESS-CC net vanuit Lumen naar Atlas verhuisd. Ook al heb ik de meeste tijd in Wageningen achter een beeldscherm doorgebracht, ik heb in deze jaren ontzettend veel geleerd en de mensen beter leren kennen. Het begon als een worsteling met de materie, die werd gevolgd door een kantelpunt waarna de zaak ineens begon te rollen. Daarna was het een kwestie van hard doorwerken om het allemaal af te krijgen. Het feit dat het nu af is, zou nooit mogelijk geweest zijn zonder de bijdrage van velen.

Als eerste wil ik mijn (co-)promotoren bedanken: Pavel Kabat, Jordi Vilà en Laurens Ganzeveld. Pavel, jij hebt me de mogelijkheid geboden een promotieonderzoek te doen en me toegang gegeven tot je uitgebreide netwerk. Dank voor het vertrouwen dat je in mij gesteld hebt en dat je me altijd mijn eigenwijze gang hebt laten gaan. Jordi, thank you for everything you did to help me finish this thesis! I really enjoyed every minute we have been working together. You brought the clarity that I was searching for and helped me to keep things as simple as possible (but not simpler than that!). Working with you has confirmed my belief that aiming for quality will always pay off in the end. Laurens, je hebt me geleerd op mijn eigen ideeën te vertrouwen en deze scherp te formuleren. Ik bewonder je niet-aflatend enthousiasme; ooit komt er een dag dat ik droge depositie interactief ga berekenen!

I am also grateful to the persons who contributed to my work as co-authors of one or more chapters of this thesis. First, I would like to thank Jose-Luis Jimenez. Jose, your contribution to the work in this thesis has been crucial! Thank you very much for sharing your insights on organic aerosol formation and for thinking along in the analysis and the writing of two papers. I think we have been able to establish a truly interdisciplinary collaboration, in which the result is more than the sum of the parts. I hope we will be able to continue this work! Delphine Farmer, I greatly appreciate the very useful input you gave on important aspects of gas-phase chemistry and SOA formation. Markku Kulmala, thank you very much for sharing your terrific knowledge and insights on aerosols with me, especially during the period that

I had the opportunity to visit your group in Helsinki. It is a great honor to have you in my committee. Tuomo Nieminen, thanks for your help with the analysis of the Hyytiälä data and the writing of the cloud droplet paper! Rob Roebeling, op een dag klopte ik bij jou aan om advies over satellietwaarnemingen van wolken. Mijn totale onwetendheid op dat gebied was gelukkig geen belemmering voor jou om hier tijd in te willen steken. Jouw bijdrage aan het wolkendruppelpaper heeft tot significante verbeteringen geleid die ongetwijfeld hebben bijgedragen aan de vlotte acceptatie van het paper. Dank hiervoor!
Niall Robinson, James Allan, Hugh Coe and Thomas Pugh, I am thankful to you for your willingness to share the data from the OP3 campaign and for discussing their interpretation.
Chiel, knakker, als er iemand is die me er de afgelopen vijf jaar doorheen heeft gesleept, ben jij het wel. Alleen al inhoudelijk door mij de elegantie van het mixed-layer model te laten inzien, wat een groot voordeel bleek toen ik het zelf ging gebruiken. Maar door alleen dat te benoemen zou ik je zwaar tekort doen. Ik dank je voor alle fietstochten die we in de loop der jaren hebben ondernomen, voor de broodnodige vakanties, voor de tijdelijke werkplek in HH en bovenal voor het eindeloze gezwets over de dingen des levens. Leuk dat je m′n paranimf wil zijn!

Dan zijn er collega′s van ESS en MAQ wiens bijdrage ik erg waardeer. Ik wil Petra, Robbert, Obbe, Marleen, Emma en Saskia bedanken voor de vele kilometers die we gelunchwandeld hebben. Ook al hadden we de nodige moeite om vakinhoudelijke overeenkomsten te vinden, deze wandelingen waren erg nuttig voor het uitwisselen van ervaringen wat betreft het omgaan met de, om het eens eufemistisch uit te drukken, uitdagingen die het doen van een promotieonderzoek met zich meebrengt. Joel, ik ken weinig mensen die zo′n groot analytisch vermogen combineren met een even grote creativiteit en als ik mijn werk met jou besprak, snapte ik daarna vaak veel beter waar ik zelf mee bezig was. Huug, dank je voor het meedenken over het mixed-layer model! Maarten, jouw opmerkingen waren erg nuttig voor het verder aanscherpen van het paper dat hoofdstuk 3 vormt. Rik, hartelijk dank voor je belangstelling voor mijn werk en het administratief veilig stellen van de tijd om in relatieve rust dit proefschrift af te kunnen maken.

En dan heb ik ook nog enkele goede vrienden, die op een indirecte –maar niet minder belangrijke– wijze hebben bijgedragen aan het tot stand komen van dit boekje. Reurt en Wiebe, broeders, wij hebben de tand des tijds doorstaan. We hadden geen verre reizen nodig om elkaar tegen te komen, maar ook als dat wel zo zal zijn hoop ik jullie nog vaak te verwelkomen in een of ander nederig onderkomen. Dankbaar ben ik ook de mèn van de band: Bart, Frank, Jeroen, Marco. Merci voor alle uren die ik met jullie in oefenhok en opnamestudio heb mogen doorbrengen. Wij komen er wel, zolang we maar gaan waar we willen en doen wat we leuk vinden! Marian, er is niemand met wie ik zo goed bellen kan als met jou!

Bram, laat ons rap weer eens fietsen.

En tot slot wil ik mijn familie danken, gewoon, omdat ze er zijn. En voor alles wat vanzelfsprekend lijkt, maar dat niet per se is. Suzanne, oneindig bedankt voor het ontwerpen van het sjieke omslag: ik ben er heel blij mee! Thijs, fijn dat je paranimf wil zijn. Bij mijn ouders kon ik altijd terecht voor een luisterend oor en frisse lucht. Pap en mam: dieke merci!

Hij stak z′n arm uit en wees in de ruimte. Dáár waren de dingen. Hij sloeg met z′n vuist tegen z′n voorhoofd. En *daar* waren ze. Er uit wilden ze, maar ze deden ′t niet. Stapelgek werd je ervan.

Nescio, Titaantjes

List of journal publications

Janssen, R. H. H., Meinders, M. B. J., van Nes, E. H. and Scheffer, M.: Microscale vegetation-soil feedback boosts hysteresis in a regional vegetation-climate system. Global Change Biology, 14, 1104-1112, doi:10.1111/j.1365-2486.2008.01540.x, 2008.

Janssen, R. H. H., Ganzeveld, L. N., Kabat, P., Kulmala, M., Nieminen, T., and Roebeling, R. A.: Estimating seasonal variations in cloud droplet number concentration over the boreal forest from satellite observations, Atmos. Chem. Phys., 11, 7701-7713, doi:10.5194/acp-11-7701-2011, 2011.

Janssen, R. H. H., Vilà-Guerau de Arellano, J., Ganzeveld, L. N., Kabat, P., Jimenez, J. L., Farmer, D. K., van Heerwaarden, C. C., and Mammarella, I.: Combined effects of surface conditions, boundary layer dynamics and chemistry on diurnal SOA evolution, Atmos. Chem. Phys., 12, 6827-6843, doi:10.5194/acp-12-6827-2012, 2012.

Janssen, R. H. H., Vilà-Guerau de Arellano, J., Jimenez, J. L., Ganzeveld, L. N., Robinson, N. H., Allan, J. D., Coe, H., and Pugh, T. A. M.: Influence of meteorological forcings and isoprene chemistry on the organic aerosol budget in a tropical forest, submitted to J. Geophys. Res., 2012.

Netherlands Research School for the
Socio-Economic and Natural Sciences of the Environment

C E R T I F I C A T E

The Netherlands Research School for the
Socio-Economic and Natural Sciences of the Environment
(SENSE), declares that

Ruud Henricus Hubertus Janssen

born on 7 September 1983 in Roggel, The Netherlands

has successfully fulfilled all requirements of the
Educational Programme of SENSE.

Wageningen, 1 March 2013

the Chairman of the SENSE board	the SENSE Director of Education
Prof. dr. Rik Leemans	Dr. Ad van Dommelen

The SENSE Research School has been accredited by the Royal Netherlands Academy of Arts and Sciences (KNAW)

KONINKLIJKE NEDERLANDSE
AKADEMIE VAN WETENSCHAPPEN

The SENSE Research School declares that **Mr. Ruud Janssen** has successfully fulfilled all requirements of the Educational PhD Programme of SENSE with a work load of 33 ECTS, including the following activities:

SENSE PhD Courses

- Environmental Research in Context
- Research Context Activity: Co-organizing WIMEK Water Cycle Symposium, 29 January 2009, Wageningen

Other PhD and Advanced MSc Courses

- Formation and Growth of Atmospheric Aerosols
- Biogeochemistry and -physics of the lower atmosphere
- Clouds and climate

Oral Presentations

- *Combined effects of surface conditions, boundary layer dynamics and chemistry on diurnal SOA evolution.* SENSE PhD symposium: Water and energy cycles at multiple scales, 1 March 2012, Wageningen

SENSE Coordinator PhD Education

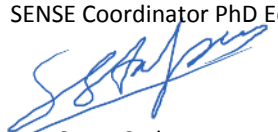

Drs. Serge Stalpers

Cover design by Suzanne Janssen

Printed by GVO drukkers & vormgevers B.V. | Ponsen & Looijen

Financial support from Wageningen University for printing this thesis
is gratefully acknowledged.